Metasurface based MIMO Microstrip Antenna with Reduced Mutual Coupling

A dissertation submitted in fulfilment of the requirements for the degree

of

Master of Science in Electronic Engineering

by

Sthembile Dubazane

COLLEGE OF AGRICULTURE, ENGINEERING AND SCIENCE,
UNIVERSITY OF KWAZULU-NATAL,
DURBAN-4041 SOUTH AFRICA

STUDENT NO: 213526437

March 2022

Metasurface based MIMO Microstrip Antenna with Reduced Mutual Coupling

Student:

Sthembile Dubazane

Supervisor

Dr. Pradeep Kumar

Co-Supervisor

Prof. Thomas Afullo

This dissertation is submitted in fulfilment of the requirements for the degree of

Masters of Science: Electronic Engineering

in

The Department of Electronic Engineering, Howard College

University of KwaZulu-Natal. Durban

South Africa

As the candidate's supervisor I agree to the submission of this dissertation.

Signed:  Date: 24 March 2022

Name: Dr. P Kumar

Declaration 1-Plagarism

I, **Sthembile Dubazane** with student number **213526437** and thesis titled **Metasurface base MIMO Microstrip Antenna with Reduced Mutual Coupling** hereby declare that:

(i) The research reported in this thesis, except where otherwise indicated is my original work.

(ii) This thesis has not been submitted for any degree or examination at any other university.

(iii) This thesis does not contain other persons' data, pictures, graphs or other information, unless specifically acknowledged as being sourced from other persons.

(iv) This thesis does not contain other persons' writing, unless specifically acknowledged as being sourced from other researchers. Where other written sources have been quoted, then:

a. Their words have been re-written but the general information attributed to them has been referenced

b. Where their exact words have been used, then their writing has been placed in italics and inside quotation marks and referenced.

(v) This thesis does not contain text graphics or tables copied and pasted from the internet. Unless specifically acknowledged with the source being detailed in the thesis and in the references section.

[redacted]

Sthembile Dubazane Date: 24 March 2022

Declarations 2 – Publications

Details of contribution to publications that form part of the research presented in this thesis include publications in preparation, already submitted, in press and published. They give details of the contributions of each author to the experimental work, simulation and writing of each publication.

List of Publications

1 **S. Dubazane, P. Kumar, and T. J. O. Afullo, "Metasurface based MIMO microstrip antenna with reduced mutual coupling**," *IEEE AFRICON Conf.*, vol. 2021-September, pp. 1–7, 2021, doi: 10.1109/AFRICON51333.2021.9570916, (**3rd prize winner**).

[IEEE]

2 **S. Dubazane, P. Kumar and T.J.O Afullo, "Metasurface superstrate based MIMO patch antenna with Reduced Mutual Coupling for 5G communication",** Applied Computational Electromagnetics Society Journal, 2021 (under review).

[redacted]

Sthembile Dubazane

Date: 24 March 2022

ACKNOWLEDGEMENTS

First and foremost, I am thankful to the almighty God for granting me this life, where I have been able to learn, grow mentally and physically. His guidance and acceptance has led me to meet great people who have been mentoring, supervising and advising me through my studying journey. Without his grace and love, this work would have impossible to accomplish.

Secondly, I would like to thank the University of Kwazulu Natal, for its world-class education, resources, tools and finally fair and kind educators. Through this university, I was able to meet Dr. P Kumar who has been my supervisor since 2020. I am truly grateful to Dr. P Kumar for his supervision, guidance, support, kindness, motivation and his availability when needed most. I am also most grateful and thankful to my co-supervisor prof. T Affulo for his support. I am thankful to Transnet Port Terminal for allowing me the time I needed to complete my work. I am also thankful to my colleagues for their support and cheering when I was down and needed it the most. Lastly, I am thankful to my late mother Xoli Khumalo who always told me to keep my head up, look forward, and work hard to be the best version of myself. My friends and family, who motivated me, to further pursue my studies in engineering.

ABSTRACT

In this thesis, a negative permeability (μ) metasurface is used to reduce the mutual coupling of a 2-port Multiple-Input Multiple-Output (MIMO) rectangular inset fed microstrip antenna. That was designed using the transmission model of analysis, simulated and optimized using CST microwave studio. The microstrip antenna that operates at the (5.9-6.1) *GHz* band is designed for 5G applications, at the extended 6 *GHz* band (5.925-7.125) *GHz*. The extended band was chosen because of its new additional spectrum, which results in less noise interference. Three metasurface wall based antenna designs and two metasurface superstrate based antenna designs are conducted. The metasurface wall based antenna designs are formulated by placing a metasurface wall vertically between the two radiating antenna elements. The metasurface superstrate based antenna designs are formulated by suspending a metasurface superstrate above the 2-port microstrip antenna. Both the metasurface wall and superstrate are made up metasurface unit cells, which are formulated by periodic split ring resonators printed on a FR-4 dielectric substrate. The metasurface cells are responsible for introducing a negative permeability medium, which converts the electromagnetic propagating waves into evanescent hence rejecting mutual coupling.

In the first metasurface based antenna design, a single metasurface wall is vertically placed between the two microstrip antenna elements. A slight increase of 0.5 *dB* in mutual coupling is observed. In the second design, a double metasurface wall is vertically placed between the two antenna elements. A mutual coupling reduction of 11 *dB* is achieved. In the third design a triple metasurface wall is also placed between the two antenna elements, a mutual coupling reduction of 25 *dB* and up to 17 % bandwidth enhancement is achieved. In the fourth design a single metasurface superstrate is suspended above the 2-port microstrip antenna. A mutual coupling reduction of 32 *dB* is achieved. Lastly, in the fifth design a metasurface superstrate is also suspended above the 2-port microstrip antenna. A mutual coupling reduction of 22 *dB*, a 38% bandwidth enhancement and a 2.09 *dB* gain enhancement is achieved.

Contents

List of Abbreviations

DPS	Double positive
DGS	Defected ground structure
DNG	Double negative
EBG	Electromagnetic gap
ENG	Epsilon negative
FNBW	First null beamwidth
FEM	Finite-element method
FDTD	Finite difference time domain
FSRR	Folded split ring resonator
FCC	Federal communication commission
GPS	Global positioning system
GSM	Global system for mobile communications
HPBW	Half power beamwidth
LS	Least Squares Estimator
MISO	Multiple Input Single Output
MIMO	Multiple Input Multiple Output
MNM	Multi port network method
MoM	Method of Moments
MMSE	Minimum Mean Squared Error Estimator
MNG	Mu-negative

M-coupling	Mutual coupling
M-antenna	Microstrip antenna
RPA	Rectangular probe fed microstrip antenna
RIA	Rectangular inset fed microstrip antenna
SISO	Single Input Single Output
SIMO	Single Input Multiple Output
STD	Spectral Domain Technique
SNR	Signal to noise ratio
SRR	Split ring resonator
TIA	Triangular inset fed microstrip antenna
VSWR	Voltage standing wave ratio
WI-FI	Wireless fidelity
5G	Fifth generation
2D	Two-dimensional
3D	Three-dimensional
3GGP	3rd Generation Partnership Project

List of Symbols

a	Side length
C	Speed of light
dB	Decibels
ε_r	Dielectric constant of the substrate
ε_{reff}	Effective dielectric constant
f_r	Resonant frequency
h	Substrate height
L	Length of Patch
L_{eff}	Effective length
Lg	Ground length
t	Patch thickness
Wg	Ground width
Ws	Width of transmission line
W	Width of patch
Yo	Inset length
Z_L	Load impedance
Z_o	Characteristic impedance
λ_0	Free space wavelength
Γ	Reflection coefficient

List of Figures

List of Tables

Chapter 1 : Introduction

The thesis is introduced in this chapter. It first discusses the background, which highlights the importance of MIMO systems in 5G applications. It then discusses the problem statement, which highlights the mutual coupling issues in MIMO systems. Followed by literature review that looks into details, different mutual coupling reduction methods currently being used in antenna design. Finally, it discusses research aims and objectives, research significance, methodological approach and the thesis structure.

1.1. Background

Fifth-generation (5G) applications require high gain and higher directivity, which is hard to achieve using single element antenna systems. MIMO antenna systems provide higher data rates without any increase in power or bandwidth. Hence it is anticipated that MIMO antenna systems will be the building block of 5G systems. In a traditional wireless communication system, one antenna is used at the transmitter and one antenna is used at the receiver this system arrangement is known as the Single-Input Single-Output (SISO) system. It often gives problems with multipath fading or multipath effects. Where multipath can be defined as the propagation phenomenon that causes the electromagnetic signal to reach the intended receiver by more than one path. This is mainly due to obstructions such as buildings and hills. [1]. As a result, they will be multiple superposed copies of the transmitted signal reaching the intended receiver by different paths. Each signal copy will experience time delays, frequency shifts and angle spread. This fluctuation in signal level is known as fading and it causes reduced data speed and increase in errors [2,3]. According to Shannon-Nyquist criterion, the SISO system arrangement suffers major drawbacks from low channel capacity.

Shannon's capacity model is used to compute an achievable transmission rate for a given channel. In a digital communication system, capacity is used as performance measure. It is the maximum transmission rate of which communication can be achieved [4]. The channel capacity of a SISO system is given by the equation below [5].

$$C = \log_2(1 + SNR\,|h|^2) \tag{1.1}$$

Where h is the channel gain and SNR is the signal to noise ratio at the receiving antenna.

The limitation of a SISO communication system is that capacity increases very slowly with the log of *SNR* and hence remains low.

The total MIMO capacity from the sum of individual sub channels capacities is given by the equation below.

$$C = \sum_{k=1}^{n} \log_2(1 + p_k \, \varepsilon_k{}^2) \quad (1.2)$$

Where p_k is the power allocated to *k*th sub channel and $\varepsilon_k{}^2$ is the gain.

A capacity comparison for SISO and MIMO systems in terms of *SNR* for several values of M_T transmitting antennas and M_R receiving antennas, is depicted in Figure 1.1 below. For the SISO case where there is $M_T = 1$ and $M_R = 1$, the capacity ranges from 1 to 17 *bps*. It increases slowly with the log of *SNR* and hence remains low. This illustrates the limitations of the SISO systems despite the modern techniques to improve its capacity. For a MIMO case where there is $M_T = 4$ and $M_R = 4$ the capacity ranges from 3 to 48 *bps*. It increases rapidly with *SNR* resulting in higher performance that can be seen to be three times larger than that of the SISO system.

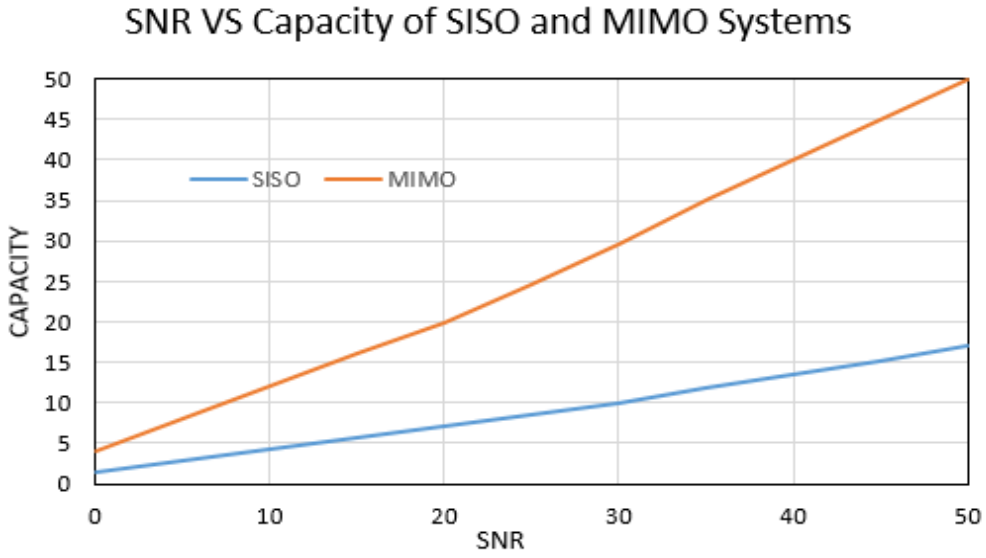

Figure 1:1 Comparison between SISO and MIMO channel capacity [4].

Greater channel capacity is a requirement in modern wireless communication systems, as it supports higher data rates. Increasing the bandwidth or transmission power of a SISO system can improve its channel capacity. This unfortunately increases the total cost of the system [6]. MIMO systems are employed to close gaps by SISO systems.

MIMO technology is the antenna technology for wireless communication, which uses several antennas at the receiver and at the transmitter. A MIMO system is one of the several forms of smart antenna systems. It is a combination of Multiple-Input Single-Output (MISO) system and Single-Input Multiple-Output (SIMO) system hence has the advantages of both [7,8]. MIMO systems utilise multiple antennas to increase the transmitted data rates, this is done by using the reflected signals to provide gains. They result in significant increases in channel capacity, higher spectral efficiencies, and reduced fading without requiring additional bandwidth and transmission power. Figure 1.2 depicts a typical MIMO system. In a MIMO system, at the transmitter a digital signal is first fed to a serial to parallel splitter. It is then coded for error control, and mapped into complex modulation symbols [9-12]. The parallel splitter produces multiple separate data streams, which are mapped to one of the several transmitting antennas. This may include antenna spatial weighting or space-time precoding. Signals are then received by multiple antennas at the receiver, where they are demodulated and de-mapped.

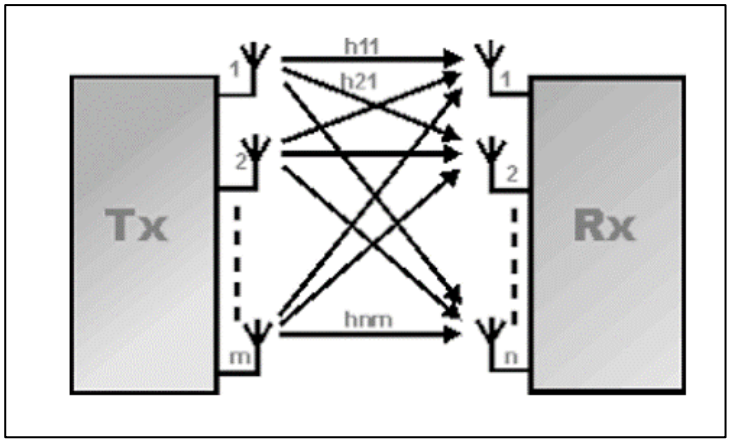

Figure 1:2: General Outline of a MIMO system [2].

1.2. Problem statement

Due to space limitations in all modern wireless devices, compact and dense MIMO systems are preferred. This results in smaller distances between antenna elements, which leads to strong mutual coupling(m-coupling) between the antenna elements. Where mutual coupling can be defined as an electromagnetic wave interaction between antenna elements in a MIMO system. It is generally a result of two phenomena, the first being radio leakage received through space between the antenna elements, the second being signal leakage from currents on the ground or surface waves from the substrate. Mutual coupling degrades the performance of antennas such

that it causes high side lobes, which reduces the beam scanning capacity of the array system. It also results in gain and efficiency reduction, additional to that it deteriorates the signal-to-noise-ratio [13-16]. Several decoupling methods have been used, these include but are not limited to meta-materials [17], photonic band gap structure [18], electronic band-gap structure [19], and these methods are discussed in literature review below.

1.3. Literature Review

The fifth-generation (5G) mobile network is the recent generation of wireless communication system. It has been created due to the limitations of the existing fourth generation (4G) mobile network. The limitations include but are not limited to, limited bandwidth, restricted channel capacity e.tc. 5G is an improvement to 4G such that it offers higher data rates, large bandwidth, reduced latency, energy saving, cost reduction, larger system capacity and it caters for full potential of the Internet of Things [20,21]. 5G technology is expected to operate in three frequency bands, which are the low frequency band, mid frequency band and the new high frequency band [22]. The low frequency band (600 – 700 *MHz*) has a frequency band that is similar to 4G, hence has data rates that are also similar to the 4G mobile network. It offers the advantage of a wider coverage area and the disadvantage of low downloads speeds of 30 to 250 megabits per second (Mbps). The mid frequency bands covers radio frequencies from 2 *GHz* – 6 *GHz*, offers the advantage of both a good coverage area and good data speeds. The high frequency band is unique to 5G network; it offers the advantages of providing greater data speeds of up to 20 Gbps, and greater bandwidth. It unfortunately offers the disadvantages of a smaller area coverage, hence cannot be used for long distances. The millimeter waves also faces difficulty penetrating solid structures i.e. walls, mountains, cars e.tc. The high frequency band is also known as frequency range 2 (FR2) it covers the frequency band (24.45 *GHz* – 52.6 *GHz*) [22- 25]. The combination of the low frequency band and the mid frequency band is also known as frequency range 1 (FR1) or Sub-6 *GHz* band. Recently the 3rd Generation Partnership Project (3GGP) extended it from the frequency range of (410 *MHz* – 6 *GHz*) to the frequency range of (410 *MHz* -7.125 *GHz*). Hence introducing 1200 *MHz* additional spectrum. The sub-6 *GHz* band is used for wider area coverage and hence is used in traditional cellular phone applications. In this thesis a microstrip antenna (m-antenna) operating at the sub -6 *GHz* band is designed.

As mentioned previously, various methods have been proposed to reduce mutual coupling between multiple antenna elements. One of the techniques that have been used is the

employment of electromagnetic gap (EBG) structures; they generally consist of a periodic order of dielectric and metallic elements. One of the most commonly used EBG structure to reduce mutual coupling is the mushroom-like EBG structure [26-30]. In [26], an EBG structure is introduced between microstrip antenna array elements, which have an edge-to-edge separation of $0.75\lambda_o$ (where $\lambda_o$is the free space wavelength at the operating frequency) at 5.8 *GHz* and achieves a mutual coupling reduction of 8 *dB*. In [28], an altered slotted mushroom-like three-dimensional EBG structure is introduced between two microstrip patches that are $0.19\lambda_o$ apart to achieve a maximum mutual coupling reduction of 8 *dB*. EBG structures can largely be associated with fabrication difficulties because of their vertical vias placement, additionally they require thicker dielectric materials or substrates which results in an increased antenna structure.

Another widely used mutual coupling reduction technique is the usage of defected ground structure (DGS). It can be explained as etching of a periodic or non-period gap on the ground plane, to introduce current distribution disturbance in the antenna. Different DGS configurations have been employed to reduce mutual coupling between multiple antenna elements [31-36]. In [31], a DGS comprising of concentric circular rings in multiple arrangements is used to reduce mutual coupling of an antenna array with center-to-center distance of $0.5\lambda_o$ at 10 *GHz*. Achieving maximum mutual coupling reduction of 8 *dB*. In [36], a dumb-bell-like pattern is carved on the ground plane amongst two parallel planar inverted F antennas (PIFAs). Achieving, mutual coupling reduction of 20 *dB*. In [34], a dumb-bell-like shaped DGS is inserted in the E-plane between a four-antenna element array. The antenna array has a separation distance of $0.47\lambda_o$ that suppress surface waves; a mutual coupling reduction of 20 *dB* was achieved. The major drawbacks of using DGS to reduce mutual coupling is that, it leaks a segment of the propagating energy that causes electromagnetic interference with the neighboring circuitry. Additionally, the introduced gap may result in a distorted radiation pattern of the antenna structure.

Employment of decoupling networks (DN) is one of the methods that have been highly utilized for m-coupling reduction. They work on the basis of transforming cross-admittance to a completely imaginary value by utilizing discrete elements and step up transmission lines [37-42]. In [38], a coupled resonator decoupling method is used to decouple two coupled dual band antennas. In the lower band (2.4-2.48 *GHz*) a maximum m-coupling reduction 7 *dB* was achieved, while for the upper band (5.15-5.135 *GHz*) the m-coupling remains the same and is

not reduced. In [40], an LTE700/WWAN MIMO antenna system is decoupled using a DN which is formed by two terminals shorted to the ground with a capacitor in the center of the line and a suspended transmission line. In the lower band (704-960 *MHz*) the m-coupling was reduced by 9 *dB*, while in the upper band (1710-2170 *MHz*) the m-coupling is not reduced and remains the same.

Metamaterials structures have also grown popular over years. This is due to their unique properties not found in nature, like electric and magnetic resonance, cloaking and negative refractive index. Metamaterials structures are widely used in enhancing antenna performance i.e. reduction of antenna size, improvement of radiated power, improvement of gain, enhancement of bandwidth and creation of multiband antennas. The usage of metamaterials to reduce mutual coupling between antenna elements is another technique that is widely employed [43-49]. In [43], a three-dimensional metamaterial structure consisting of an m-shaped patch and two U-shaped patches that are linked by two shorted pins is used to reduce mutual coupling between the antenna array elements. A mutual coupling reduction of 18 *dB* was achieved. In [44], a 3-D (three-dimensional) dual band metamaterial array is suspended on top of a dual band microstrip antenna array to reduce mutual coupling. A mutual coupling reduction of 3 *dB* was obtained. In [46], a negative permeability thin wire metamaterial array structure is positioned between two radiating antenna elements to reduce their mutual coupling. A mutual coupling reduction of 12 *dB* was achieved. Metamaterial structures can be used to attain excellent results when it comes to mutual coupling reduction. Their major drawback is that they are mostly used as three-dimensional structures, which present problems in terms of fabrication cost and complexity.

The usage of spit ring resonator (SRR) structures both as metamaterials and metasurface for mutual coupling reduction has also grown popular over the years [50-52]. In [50], low-profile folded Split ring resonators (FSRRs) are etched in the ground plane between two probe fed patch antennas. Due to the disturbed surface current distribution on the ground plane, a mutual coupling reduction of 30 *dB* can be seen. However, a number of drawbacks can also be seen i.e. reduction of bandwidth, enhancement of backward radiation, reduction of gain, reduction of radiation efficiency and a decrease in front-to-back ratio. In [51], a split ring resonator is printed between two planar inverted F antennas; a mutual coupling reduction of only 6 *dB* is achieved. In [52], a (1-D EBG) structure and a split ring resonator is inserted between two monopole antennas achieving an m-coupling reduction of 42 *dB*. However, a number of

drawbacks can also be observed since the EBG and SRR structure are printed directly on the substrate. A larger surface area is required in-between the radiating antennas to fit both structures. The EBG structure only achieves a minor mutual coupling reduction of 4.7 *dB* out of 42 *dB*, while it is made up of eight periodic cells patterned on two columns. This increases fabrication complexity and costs. Additionally, a 27% reduction in -10 *dB* impedance bandwidth can be seen.

Metasurface superstrate based antenna designs have been previously utilized. In [1], a metasurface superstrate is suspended above an antenna array for m-coupling reduction purposes. A mutual coupling reduction of 19 *dB* is achieved. In [2], a metasurface superstrate is also utilized to reduce the m-coupling of an antenna array. Maximum m-coupling reduction of 25 *dB* is achieved. In both designs, the employment of metasurface superstrates results in significant antenna mismatches. In [1], when the metasurface superstrate is employed the refection coefficient is significantly increased from -30 *dB* to -9 *dB*. In [2], the reflection coefficient is increased from -20 *dB* to -5*dB*. To combat the antenna mismatches, a U-shaped slot was etched on all elements of the antenna array. However introducing the slots to an antenna changes the path of the current distribution .This results in changes in radiation patterns and impedance. Additionally, the introduction of the U-slot increases fabrication costs and complexities. The design conducted in this dissertation achieves significant mutual coupling reduction of 22 *dB,* a 38% bandwidth enhancement and a 2.09 *dB* gain enhancement. It achieves all this without requiring additional matching methods. This means that it is inexpensive to fabricate and less complex. Hence, this design can also be implemented in already existing antenna designs because it does not change the original structure of the antenna.

1.4. Research Aim and Objectives

Mutual coupling is a major issue in MIMO antenna systems as it drastically degrades the antenna performance. This research seeks to reduce mutual coupling of a 2-port MIMO microstrip antenna using metasurface technology. A metasurface is a two-dimensional structure with properties equivalent to the metamaterials. Researchers in various fields are currently exploring its capabilities. Therefore, this research also seeks to make a substantial contribution in literature. By increasing the knowledge of metasurface usage in improving antenna performance. The generated research outputs of this research will also be a stepping-

stone for future techniques, in MIMO microstrip antenna performance improvement. In summary this research aims to:

- To design and investigate the microstrip patch MIMO antenna system using metasurface technology.
- To decrease or reduce the m-coupling of the MIMO m-antenna system utilising metasurface technology.
- To improve or increase the overall performance of the MIMO m-antenna system utilisng metasurface technology.

1.5. Research significance

The work conducted in this research utilizes a two-dimensional metasurface structure for mutual coupling reduction. Metasurface structures are planar in structure, hence they are less complex to fabricate and less costly. The work conducted in this research offers major advantages when compared to other mutual coupling reduction methods mentioned previously. That, mostly utilize three-dimensional structures, that are difficult to fabricate for practical use and much more expensive. Additionally, the work conducted can be seen to significantly reduce the m-coupling of the MIMO m-antenna when compared to other work. It does not only reduce mutual coupling but it also improves other antenna performance parameters like gain and bandwidth without requiring additional antenna matching methods. Unlike the other m-coupling reduction methods, no changes were made to the original antenna structure. This means that this work can be merged with already existing antenna structures without changing the original design of the antenna. Since no work was done to the original structure of the antenna, the radiation pattern of the microstrip antenna is highly preserved.

1.6. Methodological approach

The research is to follow an approach of performing theoretical design as guided by chapter 2 and chapter 3. This is to ensure that the designs are sensible and are agreeing with the theoretical expectations. The use of the CST microwave studio approach will assist in the design and optimization of the formulated theoretical studies such that any necessary adjustments are made to better the overall antenna performance. The last approach is the prototype fabrication and measurements taking, this is to ensure that a better performance of

the antenna is achieved and its parameters are improved. This approach will help generate a validation of the theoretical aspect with respect to the practical implementation.

1.7. Thesis Structure

This dissertation is categorised into seven different chapters. The first four chapters outline the design theory of the metasurface-based microstrip MIMO antenna. The last three chapters outline the antenna design, simulation, results analyses, fabrication, measurements and conclusion.

Chapter 1: This chapter is the introduction to the thesis. It discusses the research background, the problem statement, literature review (which discuses different existing mutual coupling reduction methods). It also covers aims and objective of the research, motivation and the methodology.

Chapter 2: This chapter discusses microstrip antenna design theory. Included in this chapter are different types of microstrip antennas, different microstrip antenna feeding methods and different microstrip antenna analysis methods. It also outlines different microstrip antenna matching methods and important antenna design parameters. The matching methods include an inset feed and a quarter-wavelength transmission line. The design parameters include, voltage standing wave ratio (VSWR), return loss(r-loss), directivity, gain input impedance, radiation pattern, polarization and bandwidth.

Chapter 3: This chapter discusses metamaterial and metasurface design theory. This includes metamaterial and metasurface classification and application.

Chapter 4: This chapter outlines the design, simulation and analysis of three single element microstrip antennas with different radiating geometries and different feeding techniques. These three antenna designs are then compared for the best performing antenna.

Chapter 5: This chapter outlines the design of the 2-port microstrip antenna and five metasurface-based antenna designs that are applied to reduce the m-coupling of the 2-port antenna. The five metasurface-based antenna designs are simulated, analysed and discussed. The metasurface antenna that best reduces the mutual coupling of the two port antenna is fabricated and measured.

Chapter 6: This chapter discusses the conclusion of this thesis and proposes future work that can be conducted for mutual coupling reduction.

1.8. Chapter Summary

5G applications require high gain and higher directivity, which can be achieved by utilizing MIMO antenna systems. However due to space limitations in modern wireless devices, compact MIMO systems are employed. This unfortunately results in strong mutual coupling between antenna elements. That degrades the antenna performance drastically, it results in high side lobes, gain reduction and efficiency reduction. Various mutual coupling reduction methods have been used; these methods include but are not limited to electromagnetic gap structures, decoupling networks, defected ground structures, metamaterials and split ring resonators. However, these methods are mostly 3D structures hence they are complex to fabricate. They also have major drawbacks that include electromagnetic interference and distorted radiation pattern. This research aims to reduce the m-coupling and improve the overall m-antenna performance by utilizing metasurface structures. It also seeks to make a substantial contribution in literature by improving the knowledge of the usage of metasurfaces in improving antenna performance. The work conducted in this thesis is significant because it uses metasurfaces structures to reduce mutual coupling, which are 2D structures that are easy to fabricate. Additionally other antenna performance parameters such as gain and bandwidth are significantly improved; the radiation pattern is also highly maintained.

Chapter 2 : Microstrip Antenna Design Theory

The microstrip antenna design fundamentals are given in this chapter. Included in this chapter are different microstrip antenna applications in various fields. Different microstrip antenna patch geometries and their applications. Different microstrip antenna feeding methods with their advantages and disadvantages. Microstrip antenna methods of analysis and their mathematical models. Finally, it discusses important antenna design parameters and the main two microstrip antenna matching methods.

2.1. Introduction

M-antennas are one of the latest technology in antenna and electromagnetic applications. They having been evolving with the growth of internet, growth of portable devices (Mobile cellular phones, laptops and Wi-Fi.) [53]. The m-antenna concept was first theorised by Deschamps in the year 1953, Gutton and Baissinot presented a patent of the antenna in the year 1955 [54]. Due to the unavailability of printed circuit board technology at the time, microstrip antennas were not practical until the late 1970s. Since then microstrip antennas have grown to be one of the most commonly utilised antennas across various microwave field applications. Microstrip antennas are highly used to create communication links in different wireless applications like aircrafts, satellites, spacecraft, missile applications, mobile communication. Table 2.1 lists different applications of microstrip antennas in different fields. They are preferred in the above mentioned applications due to their smaller sizes, lighter weight, inexpensive cost, simplicity of installation, ability to conform to various structures, ability to provide both circular and linear polarization, ability to provide dual as well as triple frequency operation and their ease of integration to microwave integrated circuitry [55]. Additional to that the different patch shapes and modes of design allow microstrip antennas to be very versatile to resonant frequencies, impedance, polarization and radiation pattern [56].

Table 2.1: Microstrip antenna applications in various systems [57].

System	**Applications**
Aircraft and spacecraft	Communication, navigation, altimiters and landing systems
Satellites	Vehicle based antennas, TV broadcasts, communication and GPS
Missile Applications	Radar, telemetry and proximity fuses
Mobile Radio	Mobile vehicle, hand telephones, GPS, GSM
Biomedical Applications	Applications in microwave hyperthermia

In its basic form, an m-antenna has a thin metallic patch or strip ($t << \lambda_0$), positioned a fraction of wavelength on top of the ground plane ($h << \lambda_0$). Where, t is the thickness of a metallic strip, λ_0 is free space wavelength, h is the substrate height and is usually such that ($0.003\lambda_0 \leq h \leq 0.05\ \lambda_0$).

The dielectric substrate is responsible for separating the patch and ground plane of an m-antenna. The patch or metallic strip material is commonly selected to be conducting metals such as Copper (Cu) or Gold (Au). This is because these metals have desired properties like low resistance, ease of soldering and resistance to oxidation [58]. A m-antenna can be designed for frequencies from 1 *GHz* to 100 *GHz.* Figure 2.1 depicts a rectangular m-antenna.

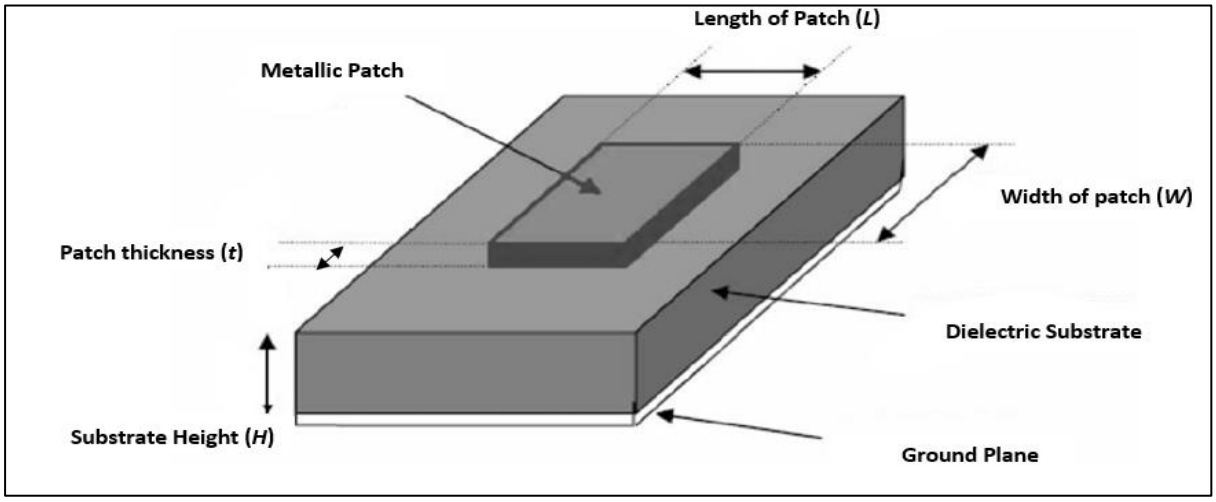

Figure 2:1: Rectangular m- antenna [56].

The m-antenna's radiating patch can be of several geometries or shapes, which includes but is not limited to square, dipole, rectangular, circular, elliptical and triangular. Figure 2.2 depicts different m-antenna patch geometries. Amongst the mentioned, the frequently used radiating patches are square, rectangular, circular and dipole. This is because they have low cross polarization and they are easy to analyse and fabricate. The other patch geometries are intricate to analyse and they involve heavy numerical simulations or computations. Dipole m-antennas tend to be ideal for arrays because they occupy less space and possess a large bandwidth [56].

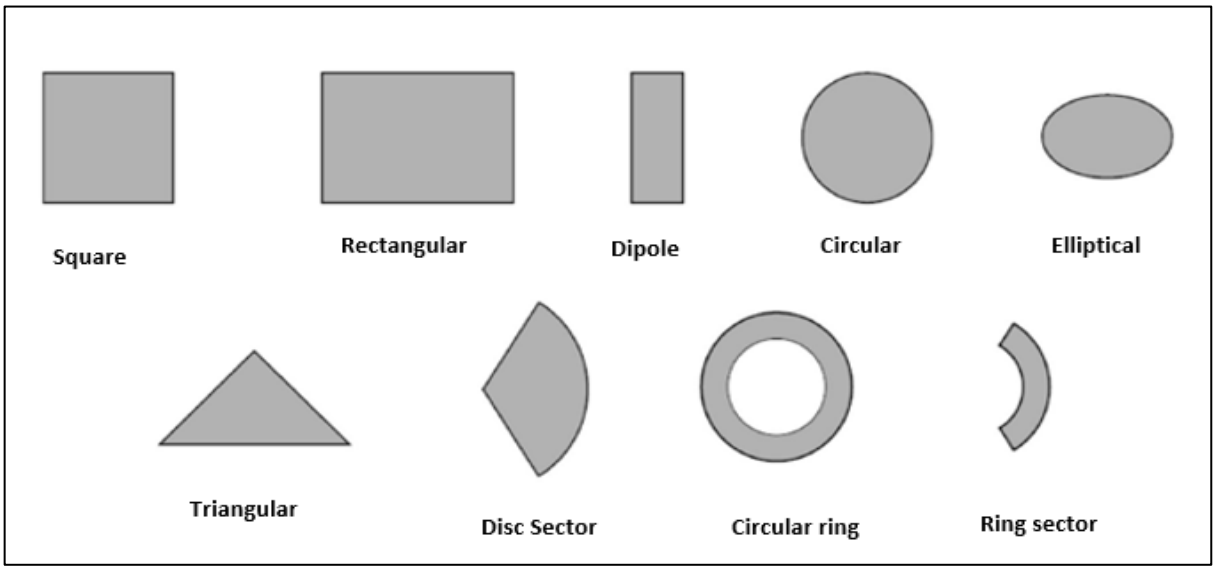

Figure 2:2: Different patch geometries of a microstrip antenna [57].

The basic m-antenna element is a strip conductor of width (W), thickness *(t),* length *(L)* placed above a dielectric substrate with a dielectric constant of ε_r and a height of value *h* positioned above of the ground plane. In a rectangular patch, the length of the strip is given by ($\lambda_0/3 < L < \lambda_0/2$), where λ_0 is free space wavelength. There are countless dielectric substrates that may be utilised for the design of m-antennas with dielectric constant in the range of ($2.2 \leq \varepsilon_r \leq 12$) [56, 57]. Dielectric substrates play a crucial role in determining, electrical properties of an m-antenna. The choice of dielectric substrates is entirely dependent on antenna applications, i.e. conformal m-antennas require substrates that are flexible in nature. Low frequency m-antenna applications require high dielectric substrates to keep the size of the antenna small [59]. Thin substrates with larger dielectric constants are usually undesired because they result in reduced radiation efficiency and bandwidth. Thicker substrates with lower dielectric constants are preferred, as they result in better radiation efficiency and bandwidth.

The plot of bandwidth and efficiency at different substrate heights, for two dielectric substrates is shown in Figure 2.3 below [59]. It can be observed from the figure, that an increase in dielectric constant results in a decrease in bandwidth. However, an increase in substrate height results in an increase in bandwidth. Efficiency can also be seen to decrease with an increase in dielectric constant. From this, it can be concluded that a dielectric material with low dielectric constant yields higher bandwidth and efficiency.

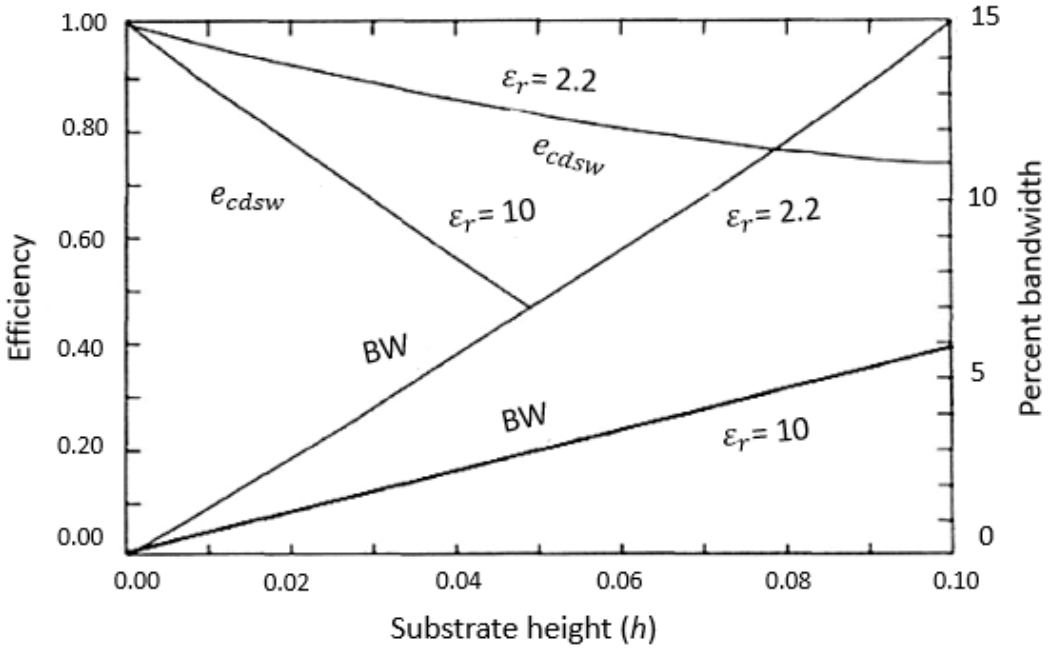

Figure 2:3: Plot of efficiency and bandwidth at different substrate heights and different dielectric constants.

2.2. Microstrip Antenna Feeding Methods

Feeding techniques are of great importance in m-antenna design as they directly influence the input impedance and characteristics of an antenna [57]. M-antennas can be fed by different methods or techniques that can be categorized into two. They are the, contacting method and the non-contacting method. The contacting method, directly feds the electromagnetic energy to the patch via a contacting element like a microstrip line (m-line). The non-contacting method feds the electromagnetic energy to the patch by electromagnetic field coupling [58, 60]. The two commonly used contact-feeding methods are the m-line and coaxial probe (coaxial-p). The two commonly used non-contact, feeding methods are the proximity coupling and aperture coupling.

2.2.1. Microstrip Line

The microstrip line (m-line) feeding method is the first; of the most commonly, used contacting feed methods. In an m-line feed, the conducting metallic strip or line is connected or linked directly to the microstrip patch edge. The conducting metallic strip has a smaller width, than the microstrip patch. This feeding technique is the easiest to fabricate, because the feed line and the radiating patch are etched on one dielectric substrate so as to provide a planar structure. This planar structure is highly preferred when designing large array structures because of its ease of fabrication [58].

The microstrip feed line technique; can also have an insert cut in the patch of the m-antenna. This is done to achieve impedance matching between the patch and the feed line, without the necessity of any further matching methods. This impedance matching is achieved by accurately controlling the insert position [61]. The major advantages offered by this feeding technique are, it is planar in structure, it is simple to model, it is easy to fabricate, and simple to match (by insert feed). The major drawbacks offered by this feeding technique are the increase in substrate height results in an increase in spurious radiation and surface waves, which also limits the antenna bandwidth. Additional to that, the feed line radiation can result in an increase of antenna cross polarization. Finally, in the millimetre - wave region of the spectrum the feed line and patch sizes become comparable. This, leads to an increase in undesired radiation [57]. Figure 2.4 depicts the microstrip line fed microstrip antenna.

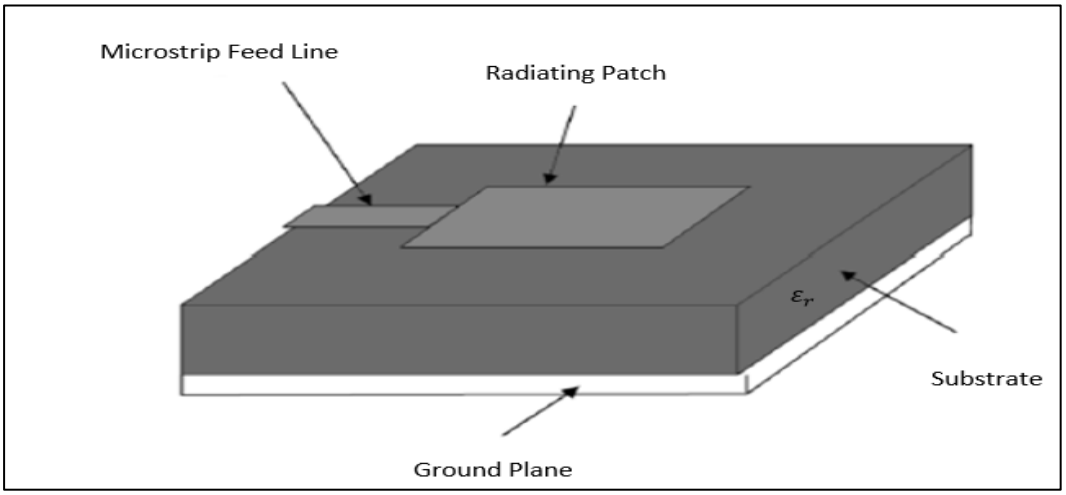

Figure 2:4: Microstrip line fed rectangular antenna.

2.2.2. Co-axial Feed

The co-axial feed which is also known as the probe feed, it is the second most commonly used contact feeding method. In the co-axial line feed method the microstrip patch is linked to the coaxial connector via the inner coaxial conductor that extends through the dielectric substrate, while the outer coaxial conductor connects to the ground plane. The major advantages offered by this feeding technique are that, the point of feed can be moved to any anticipated position or location inside the patch to achieve impedance matching, additionally it has low spurious radiation. The major disadvantages offered by this feeding technique are that, it results in a narrow antenna bandwidth. Additional to that it is complex to model and fabricate due to the hole that must be drilled, the connector protrudes outside the bottom ground plane hence resulting in a non-planar structure for thick substrates with ($h > 0{,}02\lambda_0$) [55]. Figure 2.5 depicts the co-axial fed microstrip antenna.

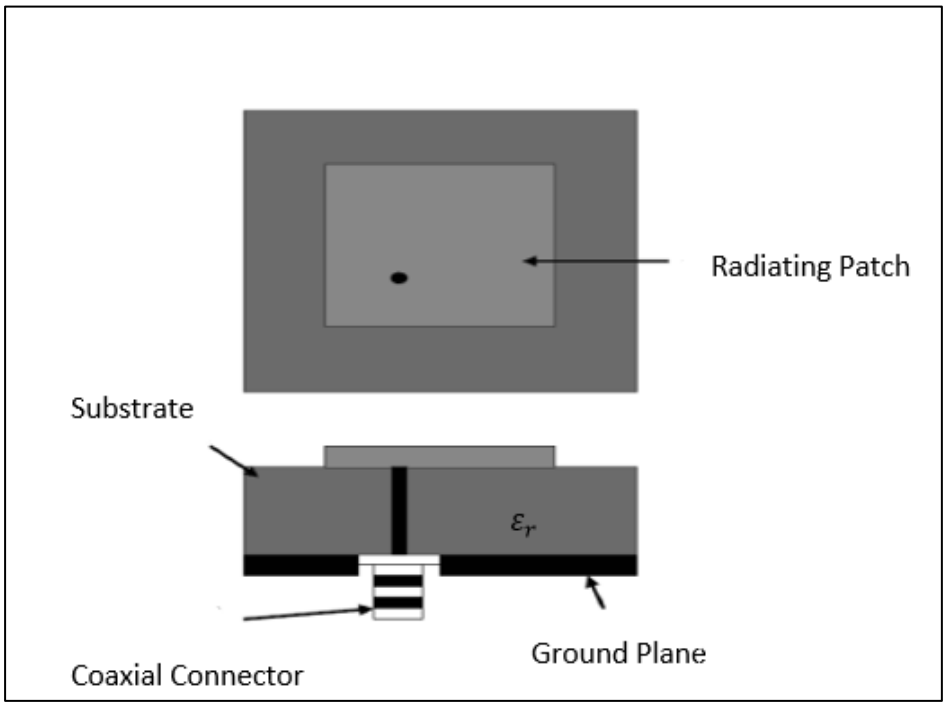

Figure 2:5: Coaxial fed rectangular m-antenna.

2.2.3. Aperture Coupled Microstrip Feed

An aperture coupled (a-coupled) feed method, is one of the two most commonly used non-contact type of feeds. In an a-coupled microstrip feed, the ground plane is positioned in-between two dielectric substrates. Where the bottom dielectric substrate contains the microstrip line and the upper dielectric substrate contains the radiating patch. The feed line is electromagnetically coupled to the patch via an electrical slot or aperture slot cut in the ground plane. To lower cross polarization, the coupling electrical slot is placed at the centre under the radiating patch. Generally, the top substrate utilises a low dielectric material, while the bottom substrate utilises a high dielectric material [56]. Another purpose of the ground plane between the two substrates is to isolate the feed line from the patch and minimise the interference from spurious radiation. The level of coupling between the feed line and the patch is determined by, the shape and location of the electrical slot relative to the patch and size of the aperture [58].

The electrical slot can be either resonant or non-resonant. When the slot is resonant, it provides additional resonance to the already existing patch resonance hence increasing the bandwidth. Unfortunately, that results in unwanted back radiation therefore a non-resonant slot aperture is preferred. The key advantage of this feeding technique is that it eradicates the problem of cross-polarisation, which resulted from the contacting feeding methods mentioned previously. The major disadvantages of this method are that, it is complex to fabricate due to the multilayer substrates; it results in increased antenna thickness and narrow bandwidth. Figure 2.6 depicts the aperture coupled microstrip antenna.

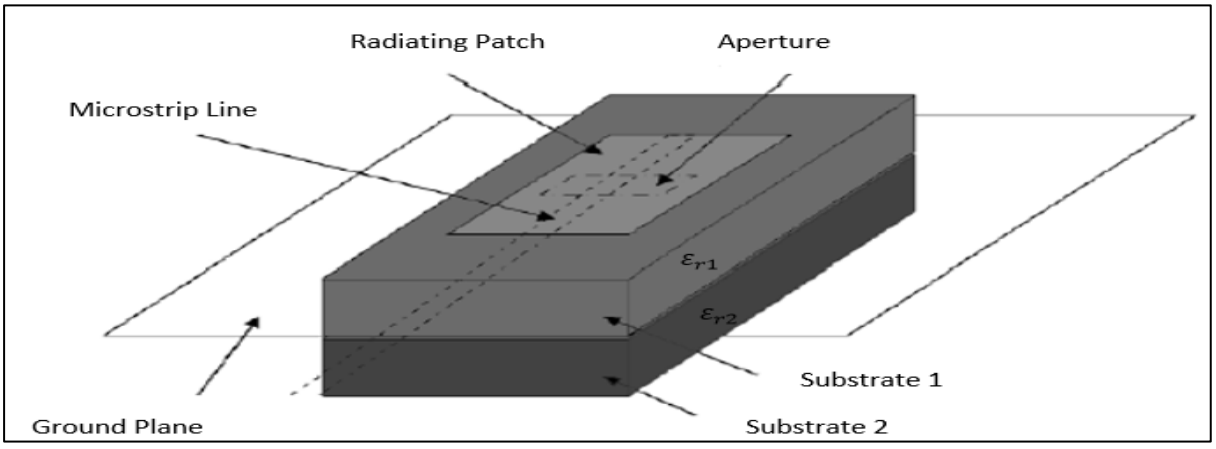

Figure 2:6: Aperture coupled microstrip fed antenna.

2.2.4. Proximity Coupled Microstrip Feed

Proximity or electromagnetic coupled microstrip feed is the second of the two commonly used non-contacting feeding methods. In proximity coupling the feed line is positioned in-between two dielectric substrate, while the patch is placed above the upper dielectric substrate. A thick layer with low dielectric material is utilised for the upper substrate, to increase the radiation of the microstrip patch. A thin layer with high dielectric material is utilised for the bottom substrate to reduce radiation from the feed line [59]. The major advantages offered by this feeding method are, it offers the largest bandwidth when compared to the other feeding methods. It also eliminates spurious radiation and cross polarization. The disadvantages offered by this feeding method are, it results in an increase in antenna thickness and its fabrication process is complex due to the two dielectric substrates that need alignment. Figure 2.7 depicts the proximity coupled microstrip antenna.

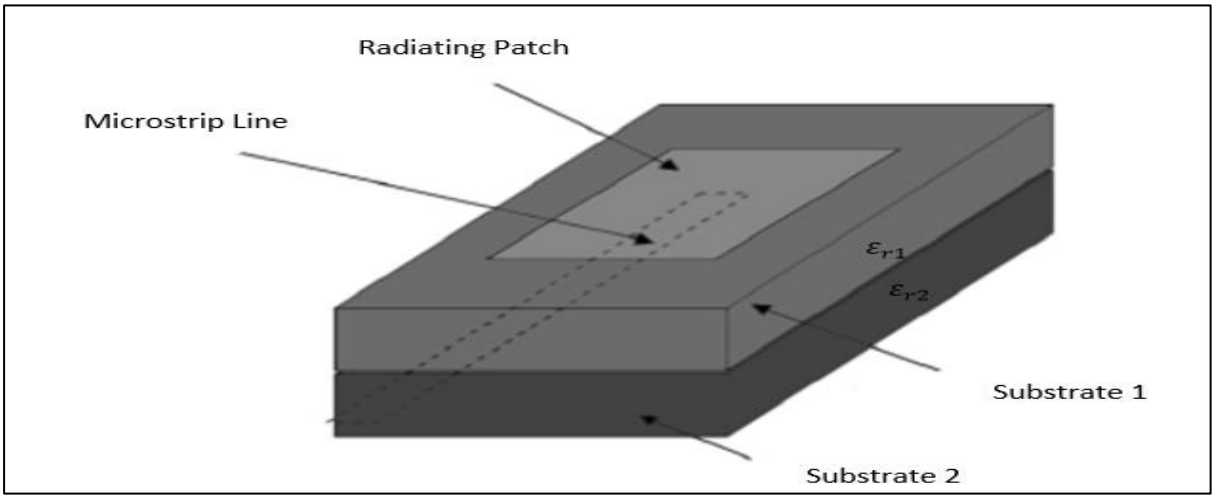

Figure 2:7: Proximity coupled microstrip fed antenna.

2.3. Microstrip Methods of Analysis

Microstrip methods of analysis can be divided into two groups. Both analysis groups use the fact that, an m-antenna is formed by 2D radiating patch printed above a thin dielectric substrate. Hence may be categorised as a 2D planar structure for analysis purpose [55]. In the first group, analysis is done based on an equivalent current distribution around the edges of the patch. Generally, three analysis methods are utilised from this group and they are cavity model, transmission line model and multi-port network method (MNM). These three methods provide

good physical insight, they are easy to implement for a single antenna element but they are less accurate when compared to the other group.

On the second group, analysis is done based on the electrical current distribution on the ground plane and on the patch conductor. The most popular numerical methods used are finite difference time domain (FDTD), finite-element method (FEM), spectral domain technique (STD) and method of moments (MoM) method [57]. These numerical methods offer the advantage of more accuracy when compared to the first group but they are complex and they take longer simulation time. The main purpose of the analysis methods is to determine and design the radiation characteristics of the microstrip antenna. The different analysis methods, allow for antenna design parameters to be determined.

2.3.1. Transmission Line Model

The transmission line (t-line) technique of analysis has great physical insight, it is simple to analyse and is effective in understanding the m-antenna. In this model the m-antenna's radiating patch is taken as a transmission line resonator with no transverse field variations. The radiation mostly occurs from the fringing fields at the open circuited ends [62-64]. It represents the radiating patch as two different slots of height (*h)* and width (*W)*, with a transmission line of length (*L)* between them. Initially this model was designed for a rectangular radiating patch but has since been adapted for different patch geometries as well. It is the simplest model yet, but not all configuration types can use it. Since it does not take into consideration, the variations of orthogonal fields in the propagation direction. Figure 2.8 depicts the microstrip antenna's transmission model.

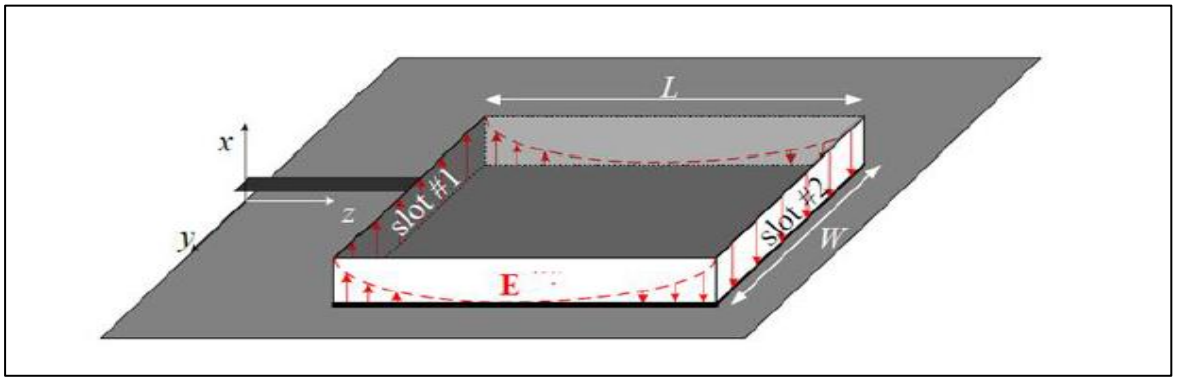

Figure 2:8: Microstrip antenna's transmission model [56].

2.3.1.1. Fringing Effect

The fields along the patch of the m-antenna experience fringing, because of the finite width (*W*) and length (*L*) of the antenna. The height of the dielectric substrate and the dimensions of the patch determined the amount of fringing in the m-antenna [59]. Since fringing has an effect on the resonant frequency (r-frequency) of the m-antenna, it should be taken into account. Figure 2.9 depicts the fringing effect of a rectangular microstrip antenna. From the figure, it can be seen that the microstrip has a non-homogeneous line of two dielectrics, one being the substrate the second one being the air. One can also clearly see that, most electric field lines of the patch are located inside the dielectric substrate and few in the air. Hence fringing makes the line look electrically wider than its physical dimensions [55]. Due to this, the t-line will not support pure transverse electric-magnetic mode of transmission. It will rather support the quasi-TEM mode of transmission [59]. To take account of wave propagation and fringing effect in the line an effective dielectric constant is introduced.

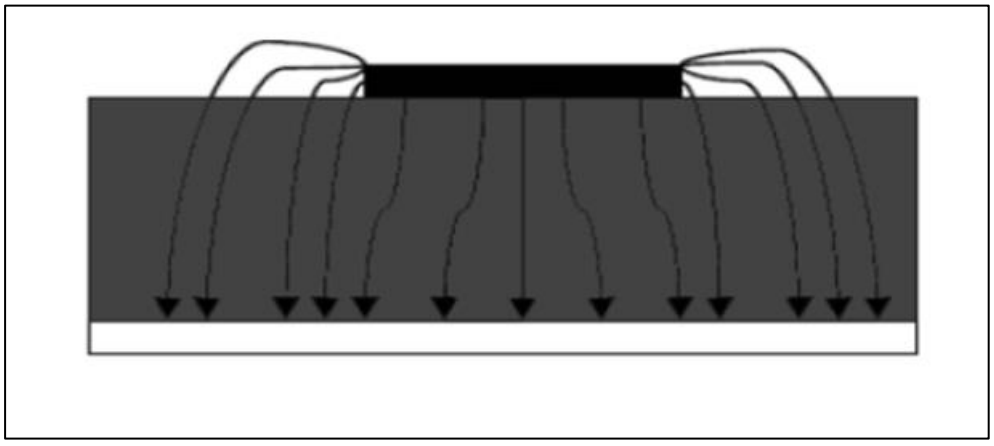

Figure 2:9: Fringing effect of the transmission line method [60].

The effective dielectric constant of the line with air above the substrate becomes in the range of $1 < \varepsilon_{reff} < \varepsilon_r$. The value of the effective dielectric constant can be calculated using equation (2.1) expressed below [53].

$$\varepsilon_{reff} = \frac{\varepsilon_r + 1}{2} + \frac{\varepsilon_r - 1}{2} \left[1 + 12\frac{h}{w}\right]^{-1/2} \quad (2.1)$$

Where: ε_{reff} is the effective dielectric constant, ε_r is the dielectric constant of the substrate, h is the height of the dielectric substrate and w is the width of the radiating patch.

2.3.1.2. Effective Length

Due to fringing effect, the electrical length of the patch becomes larger than its actual dimensions. The length of the microstrip patch becomes extended by a distance of ΔL on each side. Figure 2.10 depicts a microstrip antenna with extended length.

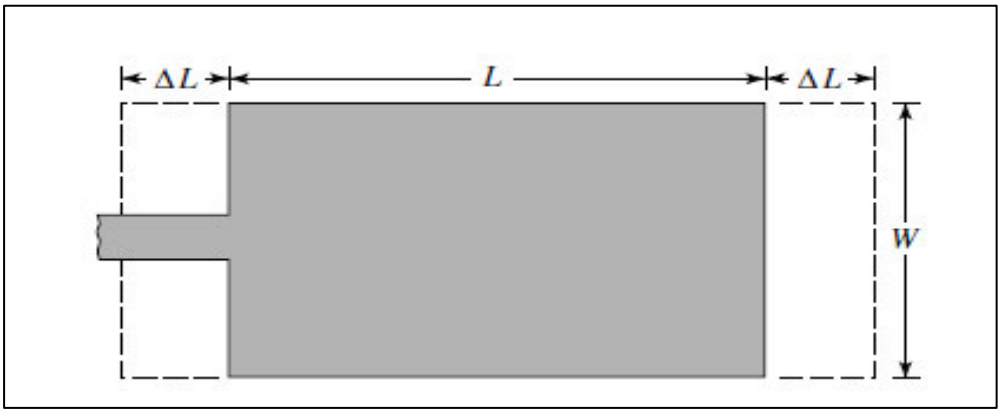

Figure 2:10: Microstrip antenna with extended length (ΔL) [56].

The length extension (ΔL) can be calculated as a function of the height of the substrate (h), the width of the patch (W) and the effective dielectric constant of the substrate (ε_{reff}), it can be calculated using equation (2.2) below [55, 59].

$$\Delta L = 0.412h \frac{(\varepsilon_{reff}+0.3)(\frac{W}{h}+0.264)}{(\varepsilon_{reff}-0.258)(\frac{W}{h}+0.8)} \quad (2.2)$$

As mentioned the patch length has been extended by ΔL on each side; hence it can be expressed as $L = \lambda/2$ for dominant TM_{010} mode with no fringing effect. The effective length can be calculated by equation (2.3) [59].

$$L_{eff} = L + 2\Delta L \quad (2.3)$$

2.3.1.3. Resonant Frequency

For a given resonant frequency (f_r), the length can be calculated by equation (2.4) below [60].

$$L = \frac{c}{f_r\sqrt{\varepsilon_{reff}}} - 2\Delta L \quad (2.4)$$

Substituting equation (2.4) into the above equation (2.3), the effective length can be expressed by equation (2.5).

$$L_{eff} = \frac{c}{2f_r\sqrt{\varepsilon_{reff}}} \quad (2.5)$$

For any TM_{mn} mode, the resonant or centre frequency of a rectangular m-antenna can be expressed by equation (2.6) [59].

$$f_r = \frac{c}{2\sqrt{\varepsilon_{reff}}} \left[\left(\frac{m}{L}\right)^2 + \left(\frac{n}{w}\right)^2\right]^{1/2} \quad (2.6)$$

Where *n* and *m* are modes along *W* and *L*, respectively.

For the dominant mode TM_{01}, the resonant frequency can be expressed by equation (2.7).

$$(f_r)_{01} = \frac{1}{2L\sqrt{\varepsilon_o \mu_0}\sqrt{\varepsilon_r}} \quad (2.7)$$

2.3.1.4. Effective Width

The width of the microstrip patch that results in great radiation efficiencies is given by equation (2.8) [55].

$$W = \frac{1}{2f_r\sqrt{\varepsilon_o \mu_0}}\sqrt{\frac{2}{\varepsilon_r+1}} = \frac{C}{2f_r}\sqrt{\frac{2}{\varepsilon_r+1}} \quad (2.8)$$

2.3.2. Cavity Model

The transmission line method of analysis is the simplest modelling technique to utilize, but it suffers numerous drawbacks. It is more useful for a patch antenna of rectangular shape as it disregards the varying fields along the radiating edge of the patch and it cannot be adapted to include these fields [59]. The cavity method of analysis offers improvements to the drawbacks from the transmission line. The microstrip cavity model treats the area between the ground plane and the patch as a cavity bounded by perfect electric conductor on the top side and bottom side. The area along periphery is treated as a perfect magnetic conductor (to simulate an open circuit). Figure 2.11 depicts the microstrip cavity model.

Since the substrate of the microstrip antenna is thin, the fields inside the cavity along the thickness of the dielectric substrate is uniform. For regular geometrical patch shapes i.e. circular, triangular and rectangular, the fields beneath the patch can be written as a summation of numerous resonant modes of the 2D resonator [64]. The fringing field around the edges are encountered, for by extending the boundary of the patch outwards so that the actual physical dimensions are smaller than the effective dimensions of the patch [57]. The conductor loss, antenna radiation loss, tangential loss of the dielectric substrate and sky wave loss are responsible for the total radiation of the antenna [54]. These losses are taken into account by being added to the tangential loss of the dielectric substrate.

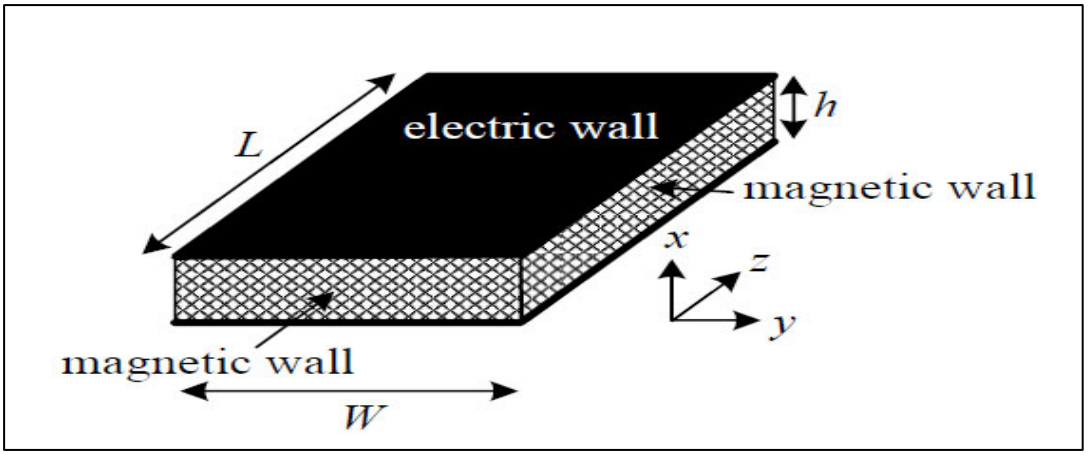

Figure 2:11: Microstrip antenna cavity model [56].

2.3.2.1. Field Configuration Modes

The cavity model of analysis assumes that the E-field is purely tangential to the formed slots between the patch edges and the ground plane. This is because of the assumption that the edges of the microstrip patch are perfect magnetic conductors. The cavity model also considers only TM^x modes (field configurations), which are modes with no H_x component [64].The field configuration within the cavity may obtained by employing the vector potential approach. The vector potential approach treats the volume underneath the patch as a cavity of rectangular shape loaded with dielectric material, of dielectric constant ε_r [55]. The vector potential A_x must satisfy the homogeneous wave equation, as seen in equation (2.9).

$$\nabla A_x + K^2 A_x = 0 \tag{2,9}$$

Using the separation of variables A_x can be expressed by equation (2.10).

$$A_x = [A_1 \cos(k_x x) + B_1 \sin(k_x x)]\,[A_2 \cos(k_y y) + B_2 \sin(k_y y)]\,[A_3 \cos(k_z z) + B_3 \sin(k_z z)] \tag{2.10}$$

Where k_x , k_y , k_z are wave numbers along the x, y and z direction.

Subjected to the boundary condition of the electric field and magnetic field within the cavity, the vector potential A_x within the cavity can be expressed as equation (2.11).

$$A_x = A_{mnp} \cos(k_x x') \cos(k_y y') \cos(k_z z') \tag{2.11}$$

Where A_{mnp} is the amplitude coefficient of each *mnp* mode. The wave numbers k_x , k_y , k_z can be expressed as equation (2.12), equation (2.13) and equation (2.14), respectively.

$$K_x = (\frac{m\pi}{h}),\ m = 0,1,2,\ldots. \tag{2.12}$$

$$K_y = (\frac{n\pi}{L}),\ n = 0,1,2,\ldots. \qquad m = n = p\ \neq 0 \tag{2.13}$$

$$K_z = (\frac{p\pi}{W}),\ p = 0,1,2,\ldots. \tag{2.14}$$

Where m, n, p represent the number of half cycle field variations along the x , y, z directions, respectively.

The frequency of the different modes can be calculated from the wave numbers as expressed in equation (2.15) below.

$$(K_x)^2 + (K_y)^2 + (K_y)^2 = (\frac{m\pi}{h})^2 + (\frac{n\pi}{L})^2 + (\frac{p\pi}{W})^2 = {K_r}^2 = {\omega_r}^2 \mu\varepsilon \tag{2.15}$$

The resonant frequencies for the cavity can then be expressed by equation (2.16) [55].

$$(f_r)_{mnp} = \frac{1}{2\pi\sqrt{\mu\varepsilon}} \sqrt{(\frac{m\pi}{h})^2 + (\frac{n\pi}{L})^2 + (\frac{p\pi}{W})^2} \tag{2.16}$$

Using the vector potential as calculated in equation (2.11) the electric and magnetic field within the cavity can be expressed by the equations below [65-66].

$$E_x = -j \frac{(k^2 - {k_x}^2)}{\omega\mu\varepsilon} A_{mnp} \cos(k_x x') \cos(k_y y') \cos(k_z z') \tag{2.17}$$

$$E_y = -j \frac{K_x K_y}{\omega\mu\varepsilon} A_{mnp} \sin(k_x x') \sin(k_y y') \cos(k_z z') \tag{2.18}$$

$$E_z = -j \frac{K_x K_y}{\omega\mu\varepsilon} A_{mnp} \sin(k_x x') \cos(k_y y') \sin(k_z y') \tag{2.19}$$

$$H_x = 0 \tag{2.20}$$

$$H_y = -\frac{K_z}{\mu} A_{mnp} \cos(k_x x') \cos(k_y y') \sin(k_z z') \tag{2.21}$$

$$H_z = -\frac{K_z}{\mu} A_{mnp} \cos(k_x x') \sin(k_y y') \cos(k_z z') \tag{2.22}$$

2.3.2.2. Far Field Evaluation

To calculate far field, the aperture technique is used. The total field is the sum of the two elements array. Where, each slot is represented by one of the elements. Since the slots are the same, the total field is calculated as an array factor for two slots.

2.3.2.2.1. Radiating Slots

The electric far field region radiated by each slot, using the equivalent current densities can be expressed by the equations below [55, 65, 66].

$$E_\phi = j\frac{k_o hWE_o e^{-jk_o r}}{2\pi r}\{\sin\theta\frac{\sin X}{X}\frac{\sin Z}{Z}\} \quad (2.23)$$

Where

$$X = \frac{K_o h}{2}\sin\theta\cos\phi \quad (2.24)$$

$$Z = \frac{K_o W}{2}\cos\theta \quad (2.25)$$

The array factor, for the two elements that are of identical magnitude and identical phase separated by a distance L_e along the y direction, can be expressed by equation (2.26).

$$(AF)_y = 2\cos(\frac{K_o L_e}{2}\sin\theta\ \sin\phi) \quad (2.26)$$

The total electric field for the two radiating slots is then given by, multiplying the array factor given by equation (2.26) with electric field radiated by each slot given by equation (2.23) above.

$$E_\phi{}^t = j\frac{k_o hWE_o e^{-jk_o r}}{2\pi r}\left\{\sin\theta\frac{\sin X}{X}\frac{\sin Z}{Z}\right\}\ x\ (AF)_y \quad (2.27)$$

This is then equivalent to equation (2.28) below.

$$E_\phi{}^t = j\frac{k_o hWE_o e^{-jk_o r}}{2\pi r}\left\{\sin\theta\frac{\sin X}{X}\frac{\sin Z}{Z}\right\}\ x\ 2\cos(\frac{K_o L_e}{2}\sin\theta\ \sin\phi) \quad (2.28)$$

The cavity model can be seen to be more complex than to the transmission line model of analysis, but it is more accurate. It does not ignore field variation along the radiating edge and it can be used for more patch antenna geometries.

2.4. Microstrip Antenna Design Parameters

In this section different m-antenna, matching methods and important antenna design parameters are studied. The matching methods include an inset feed and a quarter-wavelength t-line. The design parameters include VSWR, return loss (r-loss), gain, directivity, input impedance, radiation pattern, polarization and bandwidth.

2.4.1. Return Loss

Return loss is used to measures a degree of impedance mismatch between the antenna and the t-line. It is the ratio between the incident power and the reflected power; it is measured in *dB* [65]. It is related to both the reflection (Γ) coefficient VSWR. A perfect t-line will have a VSWR of 1:1, where all the incident power reaches the antenna and no power is reflected back. Return loss can be calculated from quation (2.29) [75].

$$RL = -20\log|\Gamma|\ dB \tag{2.29}$$

Where Γ is the reflection coefficient given by equation (2.30).

$$\Gamma = S_{11} = \frac{V_o^-}{V_o^+} = \frac{Z_L - Z_o}{Z_L + Z_o} \tag{2.30}$$

Where V_o^- is the reflected voltage, V_o^+ is the incident voltage, Z_L is the load impedance and Z_o is the characteristic impedance.

VSWR can be written as a function of reflection coefficient as shown in equation (2.31).

$$VSWR = \frac{1+|\Gamma|}{1-|\Gamma|} \tag{2.31}$$

A perfectly matched antenna will have Γ = 0 and $RL = \infty$, this indicates that there is no reflected power. However, for real life applications a VSWR value of two equates to a return loss value of - 10 *dB* which is acceptable [68,69].

2.4.2. Gain and Directivity

Gain is the radiation intensity (r-intensity) ratio in a specific direction, to the r-intensity of an isotropic antenna. It is frequently used to measure the antenna performance since it takes into account occurred losses. Directivity can be described as the r-intensity ratio in a specific direction, to the r-intensity averaged in all directions. If the direction is not specified then the direction of maximum r-intensity is utilised [57]. Gain can be expressed by, equation (2.32) below [56, 69].

$$G = 4\pi\ \frac{U(\theta,\phi)}{P_{in}} \tag{2.32}$$

Where $U(\theta,\phi)$ is the r-intensity in a given direction and P_{in} is the input power.

Directivity can be expressed by equation (2.33) below [56, 69].

$$D = \frac{U}{U_0} = 4\pi \frac{U}{P_{rad}} \tag{2.33}$$

Where U is the r-intensity, U_0 is the r-intensity of an isotropic source and P_{rad} is the total radiated power.

The relationship between antenna gain and directivity can be written as seen in equation (2.34).

$$G = \eta D \tag{2.34}$$

Where, η is the radiation efficiency of the antenna.

2.4.3. Radiation Pattern

Radiation pattern illustrates radiation properties of an antenna in far field region as a function of space coordinates [56]. It can also be described as an illustration or a mathematical model of how power is radiated or received power by an antenna in space. There are several radiation parameters of concern and they are directivity, gain, power flux density, polarization, field strength and radiation intensity. A radiation pattern has three lobes which are the main lobe, back lobe and side lobe . The main lobe represents the direction of maximum antenna radiation. Any other lobes are referred to as the minor lobes and they consist of side lobes and back lobes. The side lobe is the lobe that adjacent to the main lobe and is the same hemisphere of the main lobe. The back lobe is in the opposite hemisphere as the main lobe. Minor lobes are radiation in unwanted locations and must be minimised. Figure 2.12 depicts a typical radiation pattern.

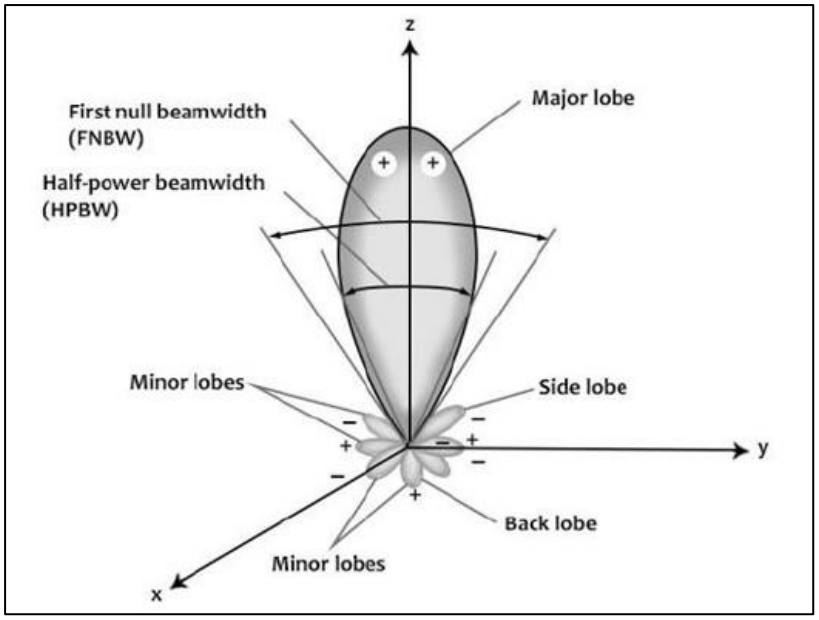

Figure 2:12: Antenna radiation pattern showing lobes and beam width [70].

Beamwidth can be described as, an angular separation between two points where maximum radiated power is measured. The First null beamwidth (FNBW) can be described as, an angular separation between first null points of the radiation pattern. The half-power beamwidth (HPBW) can be describes as, an angular width at half power of the antenna radiation pattern. Half power occurs where the signal power is $^1/_2$ of the peak power.

2.4.4. Input Impedance and Impedance Matching

Input impedance can be defined as "*the impedance presented by an antenna at its terminals or the ratio of voltage to current at a pair of terminals or the ratio of the appropriate components of the electric to magnetic field at a point*" [56]. Figure 2.13 depicts a thevenin equivalent of an antenna during transmission, the input terminals of the antenna are denoted as **a** and **b.** The antenna impedance is made up of, the resistance which is the real part and reactance which is the imaginary part and it is expressed by equation (2.35) [56, 68, 69].

$$Z_A = R_A + jX_A \tag{2.35}$$

Where Z_A is the antenna impedance at terminals a-b, R_A is the antenna resistance at terminals a-b and X_A is the antenna reactance at terminals a-b.

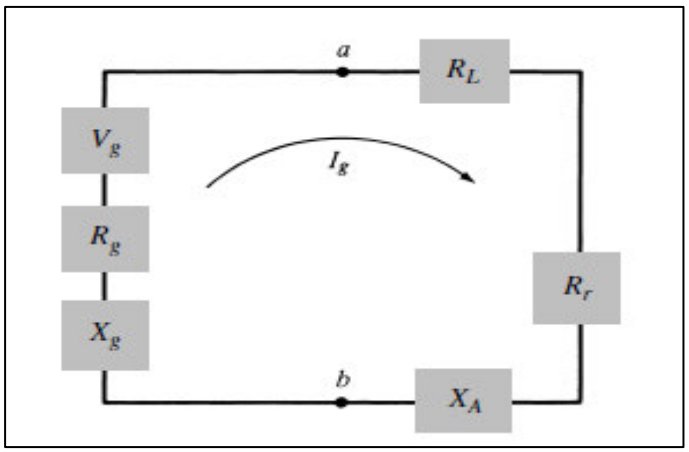

Figure 2:13: Thevenin equivalent of an antenna in transmission mode [56].

The resistance of the antenna $(R_A)$is a sum of loss resistance and radiation resistance. It can be expressed by equation (2.36).

$$R_A = R_L + R_r \tag{2.36}$$

Where R_L is the loss resistance and R_r is the radiation resistance.

If we assume that the antenna is attached to a generator with an internal impedance, then the impedance of the generator can be expressed by equation (2.37) [56].

$$Z_g = R_g + jX_g \tag{2.37}$$

Where, R_g is the resistance of the generator and X_g is the reactance of the generator.

Maximum power is delivered to the antenna when, there is conjugate matching (impedance matching) which occurs when,

$R_A = R_g$ and $X_A = -X_g$

2.4.4.1. Impedance Matching using Inset Feed

One of the ways to achieve impedance matching when using a microstrip feedline is by adding an inset distance. Figure 2.14 depicts an inset fed m-antenna. It has been shown that the input impedance of the patch is very high (150-300 ohms) at the edge, but decreases as the inset distance is increased towards the centre of the patch [70]. Hence, impedance matching can be achieved by notching the feedline by an inset distance of y_o. Using modal expansion analysis, the input resistance of the inset feed can be approximated to be given by equation (2.38) [70].

$$R_{in}(y = y_o) = R_{in}(y = 0) = cos^2\left(\frac{\pi}{L}y_o\right) \quad (2.38)$$

Where y_o is the inset length and L is the length of the microstrip antenna.

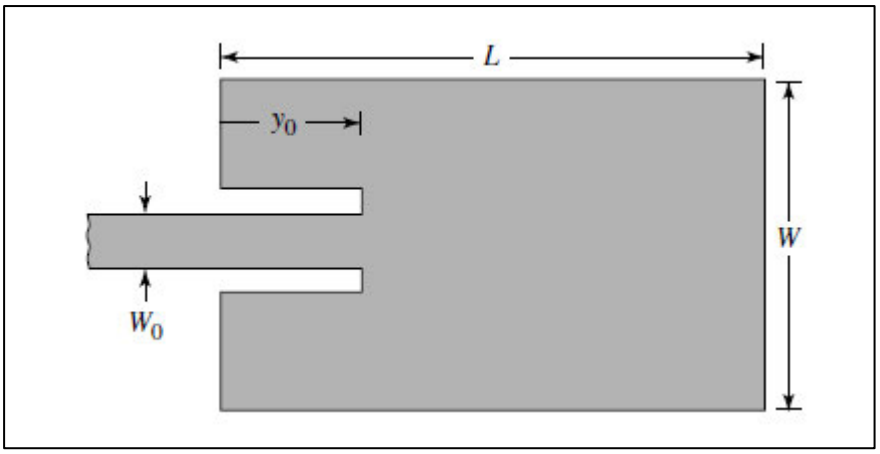

Figure 2:14: Rectangular inset fed microstrip antenna [56].

2.4.4.2. Impedance Matching using Quarter-Wavelength T-Line

A microstrip t-line of characteristic impedance Z_O can be matched to, the microstrip patch antenna with impedance Z_A. By utilizing a quarter wavelength t-line with a characteristic impedance of Z_1. Figure 2.15 depicts an m-antenna with a quarter-wavelength transmission line. The input impedance seen from the start of the quarter-wavelength t-line can be expressed by equation (2.39) [56].

$$Z_{in} = Z_o = \frac{{Z_1}^2}{Z_A} \quad (2.39)$$

Where

$$Z_1 = \sqrt{(Z_O \times Z_A)} \quad (2.40)$$

The input impedance ($Z_{in} = Z_o$) can be altered to match Z_A, by changing the width of the quarter wave transmission line. This also changes the characteristic impedance Z_1.

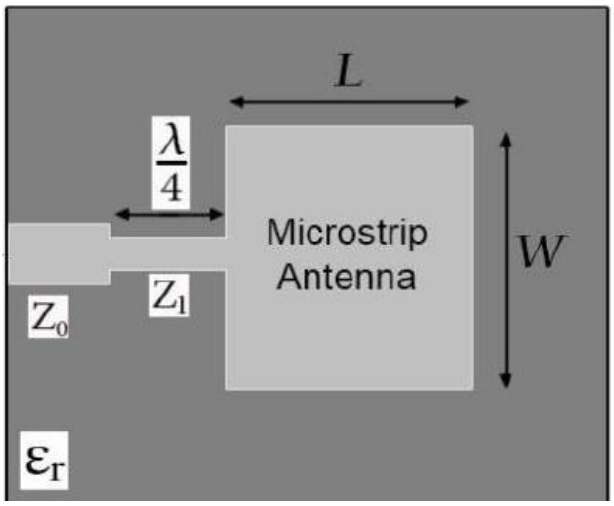

Figure 2:15: Rectangular microstrip patch antenna with a quarter-wavelength section [56].

The quarter-wavelength transmission line is only effective at a specific frequency. Hence, this matching technique can only be used for narrow band microstrip antennas.

2.4.5. Bandwidth

The bandwidth of an antenna is the frequency ranges over which an antenna satisfies certain specified performance. This performance is measured in terms of gain, VSWR, input impedance, radiation pattern and radiation efficient. Bandwidth can be calculated by using equations (2.41) and (2.42) below [62].

$$BW_{broadband} = \frac{f_H}{f_L} \tag{2.41}$$

$$BW_{narrowband}(\%) = \left[\frac{f_H - f_L}{f_C}\right] \times 100\% \tag{2.42}$$

Where f_H is the higher frequency, f_L is the lower frequency and f_C is the centre frequency.

When the ratio $\frac{f_H}{f_L} > 2$, the antenna is said to be broadband.

2.4.6. Antenna Polarization

Antenna polarization is the direction of radiated electromagnetic fields produced by an antenna, as the energy radiates away from it observed in far field. It can be described as "*The property of an electromagnetic wave describing the time varying direction and relative magnitude of the electric field vector*" [56]. The magnetic field and electric field propagate perpendicular to

one another and to the direction of propagation in free space. The direction of oscillation in free space of the electric field component is referred to as the polarization of an antenna.

The antenna can be polarized in three different ways, which are circular polarization, linear polarization and elliptical polarization. Linear polarization is when the electric field vector varies along a line (horizontal or vertical direction). Elliptical polarization is when the two perpendicular waves are of unequal amplitude, and differ in phase by 90°. Circular polarization is when the two perpendicular waves are of equal amplitude, and differ in phase by 90° [71]. The basic microstrip patch antenna is frequently designed to radiate mainly in linear polarisation. A single patch with proper excitation can also achieve circular polarisation in a microstrip antenna. If it supports orthogonal fields of equal magnitude that are 90°out of phase. Figure 2.16 depicts different polarization styles.

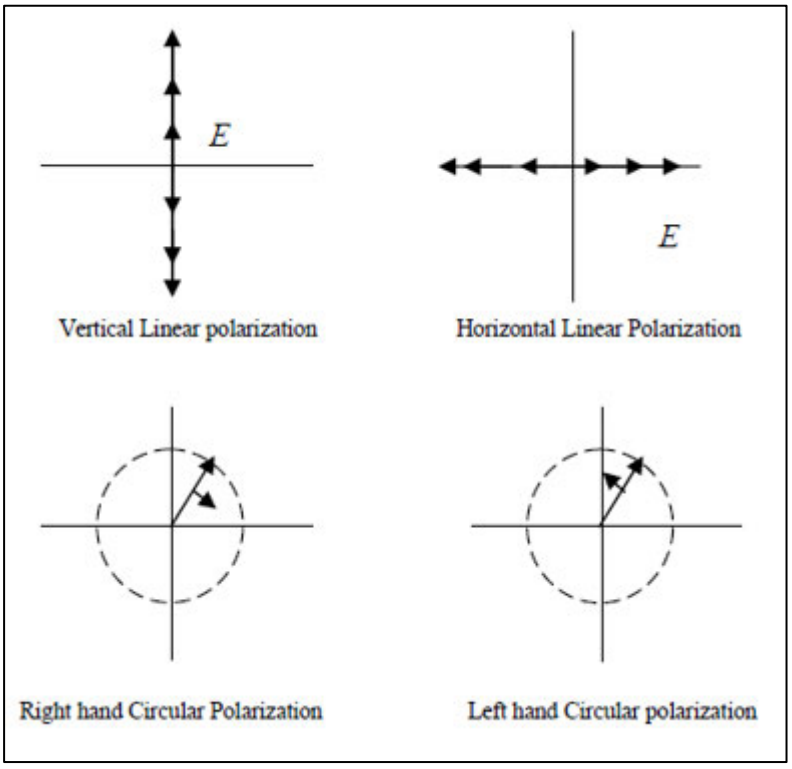

Figure 2:16: Different antenna polarization styles [62].

2.4.7. Substrate Properties

In microstrip antenna design, substrates are used to separate the ground plane from the radiating antenna patches. When an antenna is designed to resonate at a certain fundamental mode, the properties of the substrate are of sugnificant importance. The patch dimensions and the r-frequency are primarily dependent on the thickness and permittivity of the substrate. The properties of substrate frequently studied during the design of microstrip antenna include, permittivity (ε_r), loss tangent, temperature coefficient of the resonant frequency and chemical compatibility [72].

Thick substrates with low dielectric constants offer great antenna performance due to the advantages they offer, which include better antenna efficiency and larger bandwidth. However, they have major drawbacks as well i.e. the increase in substrate height generates undesirable surface waves and results in larger element size. This is highly undesirable in microstrip antennas. Thin dielectric materials with higher dielectric constants, are highly preferred for microwave circuitry due to their small element sizes. However, they also have major drawbacks that include smaller bandwidths, greater losses and low efficiencies. The frequently

used substrate materials are honeycomb ($\varepsilon_r = 1.07$), duroid ($\varepsilon_r = 2.32$), quartz ($\varepsilon_r = 3.8$), FR-4 ($\varepsilon_r = 4.4$) and aluminia ($\varepsilon_r = 10$) [73].

2.4.8. Effect of Finite Ground Plane

The microstrip methods of analysis mentioned previously only consider infinite ground plane but for practical purposes like antenna manufacturing, the ground plane size must be finite. The effect of finite ground plane is taken into consideration by various numerical methods. Unfortunately, this increases simulation time because both the ground plane and patch must be analysed. It has been seen that when the ground plane's dimensions are six times larger than that of the radiating patch, the results obtained are comparable to those of the infinite ground plane [64].

2.5. Chapter Summary

M-antennas are one of the latest technology in antenna and electromagnetic applications. M-antennas are used to create communication links in various wireless applications such as aircraft, satellites, spacecraft, missile applications and mobile applications. They are preferred in these various field due to their lightweight, inexpensive costs and ability to conform to various structures. They have different patch geometries such as rectangular patch, triangular, dipole, elliptical, circular e.tc. These different patch geometries allow the m-antenna to be versatile in terms of resonant frequency, polarization and radiation pattern. Feeding techniques are of great importance in m-antenna design as they directly influence the input impedance and characteristics of an antenna. The m-antenna's feeding technique can be categorised into two sub methods, which are the contacting method and non-contacting method. The contact feeding method offers the advantages of being simple to model and easy to fabricate, however it also suffers from cross polarization . The non-contact feeding method eliminates the problem of cross polarization, but it is complex to fabricate. The m-antenna's methods of analysis can be divided into two groups. In the first group, analysis is done on the basis of an equivalent current distribution around the edges of the radiating patch. The analysis methods from this group provide great physical insight, they are easy to implement but are less accurate. In the second group, analysis is done on the basis of electrical current distribution on the ground plane and on the patch conductor. These numerical methods offer the advantage of more accuracy when compared to the first group but they are complex and they take longer simulation time. Antenna

design parameters such as VSWR, return loss, gain, directivity, radiation pattern are important in measuring the antenna performance and hence they also need to be studied carefully.

Chapter 3 : Metamaterial and Metasurface Design Theory

Metamaterial and metasurface design fundamentals are outlined in this chapter. This includes metamaterial classification based on their electromagnetic properties. Metasurface classification, which include high impedance metasurfaces, active impedance metasurfaces, Huygens metasurfaces and dielectric metasurfaces with their applications.

3.1. Introduction

In this thesis, a metasurface-based MIMO microstrip patch antenna system will be designed. Antenna parameters will be improved by utilizing metasurface technology. A metasurface is two-dimensional structure with properties equivalent to metamaterials. Metasurface structures are planar, thin and practical for implementation. Hence, they have been getting antenna researchers attention in recent years.The word metamaterial is deduced from Greek it combines two words, meta and material. Where meta can be descried as something unnatural, modified and advanced. It is synthetic material, engineered to have physical properties that are not naturally occurring. The metamaterial term, was first used in 1999 by Rodger M. Walser in University of Texas. He described metamaterials as – "*Macroscopic composites having a synthetic, three dimensional, periodic cellular architecture designed to produce an optimized combination not available in nature, of two or more responses*" [74]. There is a wide range of materials that fit the definition of being metamaterials. Hence, any engineered material with sub-wavelength dimensions that exhibit unnatural properties can be classified as a metamaterial [75-78].

Different types of metamaterials can manipulate different types of waves (radio, microwave, optical and acoustic.). Hence, there is a vast number of possible metamaterial applications. Examples of these applications include metamaterial-based antennas, which are antennas that use metamaterials to enhance the parameters of an antenna. Metamaterial-based super lenses, which are lenses that use metamaterials to go beyond the diffraction limit. Metamaterial-based super lenses offer major advantages, because they improve the resolution of the lenses and miniaturize their sizes [79, 80]. Metamaterial-based acoustic, which are acoustic materials engineered to direct, regulate and manipulate sound in a form of ultrasonic waves [79].

Metamaterial-based cloaking device, which can be accomplished by deflecting microwave beams such that they flow around the cloaking object. Hence altering the electromagnetic field inside the cloaking device to zero, making the region covered by the device invisible.

3.2. Metamaterial Classification

The behaviour of any material towards the applied electromagnetic radiation can be categorized by two electromagnetic parameters, which are magnetic permeability (μ).and electrical permittivity (ε). The two parameters are combined to define a square refractive index. That determines how fast the material transmit light and how lights bends in the material. Higher refraction index results in slower propagation and stronger deflection.

The electromagnetic characteristics of materials are in general categorized to four different types, which are epsilon negative (ENG), double positive (DPS), double negative (DNG) and mu negative (MNG). The DPS materials are also known as right-handed medium (RHM) materials, they exist when the permittivity (ε) and permeability (μ) are both positive. They are naturally occurring materials i.e. dielectric materials. The epsilon negative (ENG) materials, occur when $\varepsilon < 0$ and $\mu > 0$, they are also naturally occurring materials i.e. plasmas. The double negative (DNG) or left-handed medium (LHM) materials occur when $\varepsilon < 0$ and $\mu < 0$ (permittivity and permeability are both negative), they are not naturally occurring materials i.e. metamaterials. The mu negative (MNG) materials occur when $\varepsilon > 0$ and $\mu < 0$, they are naturally occurring materials i.e. ferrite materials [76, 81]. Figure 3.1 depicts the four types of material classification.

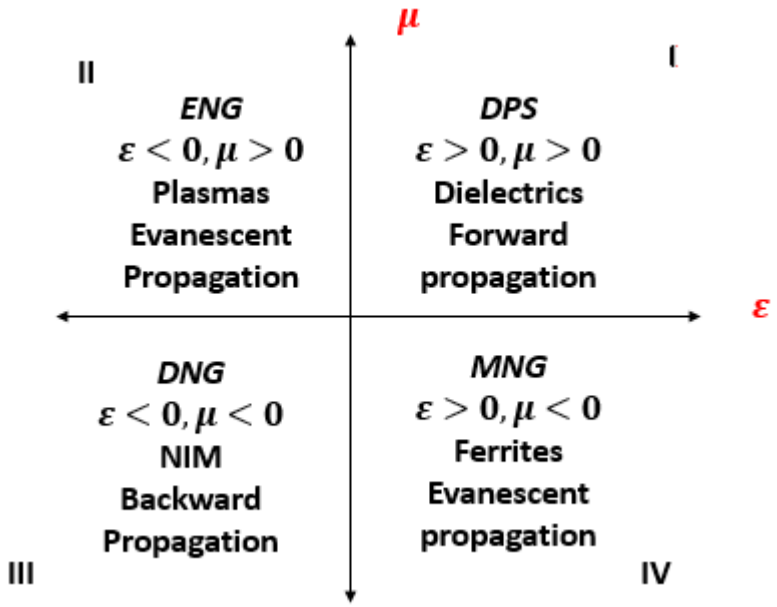

Figure 3:1: Classification of materials based on their electromagnetic properties.

They are a vast number of metamaterials that exist and that are currently being researched, in this thesis only two types will be considered.

3.2.1. Single Negative Metamaterials

Single Negative metamaterials (SNG) are materials, with either negative permeability or negative permittivity, at an instance. This includes epsilon negative (ENG) and mu negative (MNG) materials. The ENG metamaterials utilise a mesh of thin metallic wires to obtain, negative permittivity (ε). This is achieved by periodically arranging thin wires of copper, silver, aluminium, gold e.tc. The effective permittivity becomes negative when the frequency of operation is below plasma frequency [83, 84]. The MNG metamaterial uses periodically arranged split ring resonators (SRRs) to obtain, negative permeability (μ). Each SRR unit cell is made of concentric metallic loops or rings placed a small gap apart. Each ring has a slim slot, which is 180 degrees apart from the other slots. The gap between the two rings acts as a capacitor, while the rings acts as an inductor. This combination then results in an LC resonant circuit [80, 82].

3.2.2. Double Negative Metamaterials

The double negative metamaterial (DNG) simultaneously have negative permeability and negative permittivity, which results in a negative refraction index. Victor Veselago, who was a Russian physicist first predicted the concept of a negative index material to exist in 1968 [78]. This prediction was not proved until early 2000's, where the properties of the DNG material were realized by combing the SRR based MNG metamaterial with the thin metallic wire based ENG metamaterial. This material is also referred to as the left-handed material, because if follows the left hand rule. Such that the propagation of waves takes place in the backward direction. This property is the opposite of (DPS) material that follows the right hand thumb rule, with forward wave the propagation. The usage of negative refraction index in Snell's law results in, the incident wave to face the negative refraction at the interface. Figure 3.2 depicts the first DNG metamaterial.

Figure 3:2: Conventional DNG metamaterial [76].

3.3. Metasurfaces

Metasurfaces are planner 2D equivalents of metamaterials, they are utilized to manipulate or alter wave propagation in microwave and optical frequencies. For the purposes of creating new optical guiding properties and new radiation properties [85]. Metasurfaces are constituted of planar arrays, of resonant sub-wavelength elements printed on grounded dielectric substrate. They can be arranged in a quasi-periodic fashion or aperiodic manner, depending on the wave-fronts to be manipulated [86]. Metamaterials use propagation effect to manipulate electromagnetic waves; this unfortunately results in complicated bulky 3D structures that are difficult to fabricate [87]. The 2D properties of metasurfaces enables them to be lightweight,

less bulky, less costly and easy to fabricate using planar tools. This makes them preferred over metamaterials for m-antenna, performance enhancement. They are also easier to integrate into the existing microstrip antenna circuitry.

Subwave-length thickness introduces minimal propagation phase. Hence, the effective permeability, permittivity, and refractive index are of no great interest in metasurface behaviour. It is rather the interface reflection and transmission resulting from tailored surface impedance that are of great interests [88]. By using appropriately tailored metasurface structures, the subwave-length thickness can greatly supress undesirable losses.

3.3.1. Metasurfaces Classification and Applications

There are different types of metasurfaces available in the market; these different types are used for different applications ranging from antenna enhancement application to cloaking applications. In this section, we will look at the classifications and applications of impedance metasurfaces, Huygens metasurfaces and dielectric metasurface.

3.3.1.1. Impedance Metasurfaces

When a propagating wave in space hits a surface. The resulting transmission and reflection outcomes are determined by the properties or characteristics of the surface, which can be defined in terms of impedance. Impedance metasurfaces provide ways in which the impedance of the surface can be, manipulated and designed for different applications. These applications include but are not limited to polarisation control, absorption, leaky wave radiation and cloaking.

3.3.1.1.1. High Impedance Metasurface

In many antenna systems, close proximity of metal planes to the radiating antenna is highly unwanted due to the out of phase reflection from the metal plane that causes destructive interference. Destructive interference results in power inefficiency, reduced gain and a degraded radiation pattern in an antenna [89]. In addition to that, if the distance between conducting ground plane and the radiating patch or element is less than a quarter wavelength. Then the image currents radiation will interfere destructively with the radiating antenna, resulting in an impedance mismatch. The above mentioned issues can be resolved by using a

high impedance metasurface. That can reflect all the incident plane waves in phase, resulting in constructive interference in the normal direction.

A high impedance metasurface is made up of subwavelength metallic patches and a conductor at the centre of each unit cell, printed on a dielectric substrate placed above ground. They are related to corrugated surfaces (which are metal slabs with periodic vertical slot, and subwavelength spacing), in a way that they both provide ways of controlling scattering and surface wave propagation. The construction of a high impedance metasurface can be explained in this manner. Each patch is coupled to the patch next to it, which forms a capacitance. The patches are coupled to each other with a conductive path that has a vias and a ground plane, which forms an inductance. Hence, a parallel LC circuit is formed. Where the values of L and C are determined by the geometry of the metallic patches and substrate thickness [90]. At resonant frequency, the parallel LC circuit is equivalent to an open circuit with infinite impedance. This results in a reflection phase that is equal to zero at normal incidence. This behaviour is similar to that of an artificial magnetic conductor (AMC), hence high impedance metasurface are sometimes referred to as AMC [91].

In an AMC the tangential magnetic field at the surface is zero, this property is useful for antenna miniaturization. The surface image currents add in phase with the antenna currents, eliminating the requirement for a quarter-wavelength distance between the radiating patch and the antenna [92]. Additional to that high impedance metasurfaces supress any propagating surface waves where the equivalent surface impedance is high. This property is referred to as the electromagnetic bandgap and is useful for decoupling of antenna arrays or close antennas. Other applications of high impedance metasurfaces include magnetic walls for waveguides, absorbers, scattering reduction, field enhancement e.tc. Figure 3.3 depicts a high impedance metasurface.

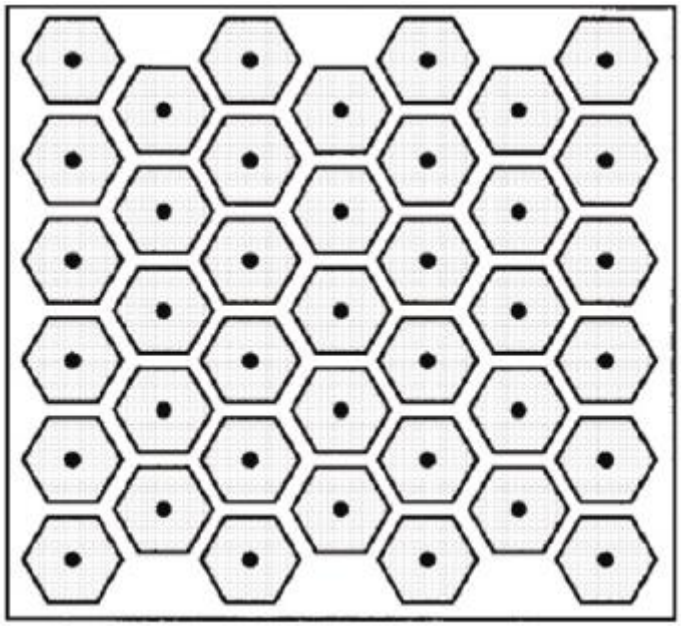

Figure 3:3: High impedance metasurface.

3.3.1.1.2. Active Impedance Metasurface

Even though high impedance metasurfaces have plenty of applications, they still have certain limitations like angular dependence and limited bandwidth [93]. Other limitation of high passive impedance metasurfaces include a fixed or permanent operating frequency and a linear response. Active impedance metasurfaces overcome the drawbacks inherited from high passive impedance metasurfaces by, loading the metasurface with electronic devices like transistors, varactor diodes and pin diodes [94]. Diodes offer capacitance that is voltage dependent, which can be applied at the unit cell gaps to change capacitance. A steerable electronic reflector can be designed by applying a reflection phase gradient that is programmed to tune the varactor diode's bias voltage, hence controlling the reflected beam. Another example on usage of active impedance metasurfaces is a reconfigurable antenna printed on a high impedance graphene metasurface. The graphene conductivity is controlled by changing the bias voltage of the diode, hence changing the radiation properties of the antenna positioned above it.

3.3.1.2. Huygens Metasurface

Huygens principle states that, every point on a wave front acts as a secondary source by creating its own wave front. Huygens metasurfaces have an ability to produce different field patterns for different types of incident illumination; they are electrically and magnetically tuneable. Their properties include, reflection control, beam steering and polarization manipulation [90, 95]. Huygens metasurfaces have an ability to induce magnetic and electric dipole moments when illuminated by electromagnetic wave. The induced dipole moments correspond to the magnetic and electric surface current densities. When these surface currents are properly excited, they can be matched to the surrounding media's impedance to eliminate reflection, increase coupling efficiency and manipulate polarization. [88, 96].

Figure 3.4 depicts an incident electromagnetic field ($\overrightarrow{E_1}, \overrightarrow{H_1}$) that gets converted to a transmitted field ($\overrightarrow{E_2}, \overrightarrow{H_2}$), through a field discontinuity sustained by induced orthogonal electric and magnetic current ($\overrightarrow{J_S}, \overrightarrow{M_S}$) [64]. When fields $\overrightarrow{E_1}, \overrightarrow{H_1}$ and $\overrightarrow{E_2}, \overrightarrow{H_2}$ are specified or designed into two half spaces, the electric ($\overrightarrow{J_S}$) and magnetic current densities ($\overrightarrow{M_S}$) needed to transform the field from one field to the other can be determined from equation (3.1) below [97-99].

$$\overrightarrow{J_S} = \hat{n}\, x\, (\overrightarrow{H_2^+} - \overrightarrow{H_1^+})\,,\ \overrightarrow{M_S} = -\hat{n}\, x\, (\overrightarrow{E_2^+} - \overrightarrow{E_1^+}) \tag{3.1}$$

Where $\overrightarrow{E_1^+}, \overrightarrow{H_1^+}, \overrightarrow{E_2^+}, \overrightarrow{H_1^+}$ are the values of $\overrightarrow{E_1}, \overrightarrow{H_1}$ and $\overrightarrow{E_2}, \overrightarrow{H_2}$ at the boundary of the field, respectively.

In Huygens metasurfaces the greatest achievement is to produce the required surface current densities for different field transformation [100, 101]. One method of achieving this is by; external excitation of surface current densities instead of internally inducing them. This happens when the radiated fields of the externally induced sources collide with the incident field to produce the wanted output fields.

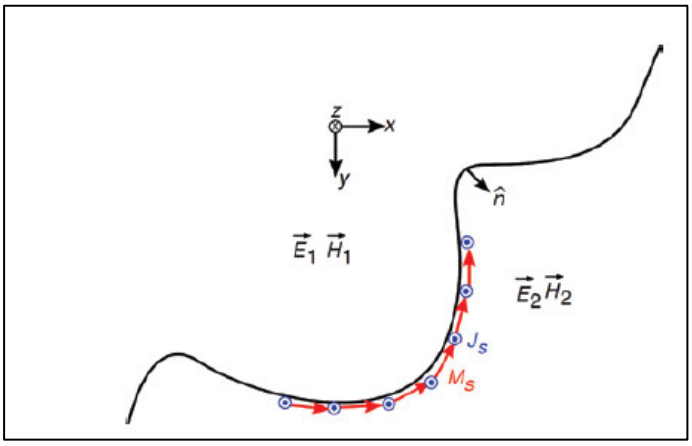

Figure 3:4: Incident electromagnetic field $(\overrightarrow{E_1}, \overrightarrow{H_1})$ *being converted to transmitted electromagnetic field* $(\overrightarrow{E_2}, \overrightarrow{H_2})$ *[97].*

3.3.1.3. Dielectric Metasurface

Dielectric metasurfaces are periodic planar arrays of sub-wavelength dielectric particles printed on a surface. They are used for controlling the properties of optical wave fronts propagating through them. Examples of their applications include dispersion control, imaging, spectrometry, conformal optics e.tc. In optical applications, dielectric metasurfaces are preferred. Due to the fact that they have lower absorption coefficients, high transmission efficiency and dissipate less than metallic metasurfaces in the visible or near infrared region [67].

3.4. Chapter Summary

Metamaterials are 3D synthetic materials, engineered to have physical properties that are not naturally occurring. They are utilised for different applications in different fields, which include microwaves, optics, and acoustics e.tc. Like all other materials, they can be categorised by two electromagnetic parameters, which are magnetic permeability (μ).and electrical permittivity (ε).The most commonly used metamaterials in antenna design and improvement are the single negative metamaterials (SNG) and the double negative metamaterial (DNG). SNG are materials, with either negative permeability or negative permittivity, at an instance.. The double negative metamaterial (DNG) simultaneously have negative permeability and negative permittivity, resulting in a negative refraction index. . A metasurface is two-dimensional structure with properties equivalent to metamaterials, hence can be used in the same fields as metamaterial structures. The 2D properties of metasurfaces enables them to be

lightweight, less bulky, less costly and easy to fabricate using planar tools. This makes them preferred over metamaterials for m-antenna, performance enhancement. They can be classified into three sub categories, which are impedance metasurface, Huygens metasurface and dielectric metasurface. Impedance metasurfaces provide ways in which the impedance of the surface can be, manipulated for different applications. Huygens metasurfaces have an ability to produce different field patterns for different types of incident illumination; they are electrically and magnetically tuneable. Dielectric metasurfaces are periodic planar arrays of sub-wavelength dielectric particles printed on a surface. In this thesis a high impedance metasurface is utilised due to its ability to manipulate surface wave propagation.

Chapter 4 : Design of Microstrip Antenna for SISO Systems

This chapter outlines the design, simulation and discussion of, three single element microstrip antennas with different radiating geometries and different feeding techniques. The first design is formulated by a triangular inset fed m-antenna, the second design is formulated by a probe fed rectangular m-antenna. The third design is formulated by a rectangular inset fed m-antenna. The results obtained from these three-microstrip antenna designs will be evaluated and compared. The best performing antenna will be used for the 2-port microstrip antenna design.

4.1. Introduction

All three designs are designed with the radiating frequency of 6 *GHz* in the sub-6 *GHz* band. 5G frequency bands are regularly updated, when new bands are availed in different countries. Recently the 3rd Generation Partnership Project (3GGP) extended the 5G FR1 band from (410 *MHz* – 6 *GHz*) to (410 *MHz* -7.125 *GHz*). Hence introducing 1200 *MHz* additional spectrum [102]. In 2020, the federal communication commission (FCC) also permitted the usage of 6 *GHz* band (5.925-7.125) *GHz* for unlicensed use. This was done with certain regulations and standards to protect incumbent licensed services from interference [103-106]. The approval of 6 *GHz* for unlicensed use, has introduced a new market for 6 *GHz* wireless solutions. Like the new WI-FI 6E, which is an extension of WI-FI 6 that operates at the (2.4 *GHz* and 5 *GHz*) bands [103].

The simulation software used in this design is CST microwave design studio, which is part of the CST design studio suite. It offers several solvers for various applications, because no solver can provide accurate results for all different applications. The solvers offered are the frequency domain solver, transient solver, integral equation solver and eigen mode solver. The transient solver can be utilised for most applications, as it can obtain the entire broadband frequency behaviour of the simulated item from a single simulation run. It can also be used for other high frequency applications like different antennas, different filters and various transmission lines. It is based on the finite integration technique [107].

4.2. Triangular Microstrip Antenna

The conducting patch of the m-antenna can be of different geometrical shape. Circular and rectangular patches are the most frequently utilised patches in m-antenna design. The triangular shaped conducting patch is one of the shapes that has recently attracted attention [61]. This is due to the fact that it occupies less metalized space on the substrate, has similar radiating properties to the rectangular patch and has low radiation loss [73]. The recent applications of the triangular patch microstrip antenna include but are not limited to broadband radiators, multiband antennas, circular polarized antennas and array antennas [109]. In this section, an equilateral triangular microstrip patch (ETMP) antenna is designed. The ETMP antenna can be analysed and modelled using different analysis techniques, which include the cavity resonator model, geometrical theory, method of moments and the generic algorithm. The cavity resonator model is used in this design due to its simple computer aided formulas, which can be used to determine the antenna parameters.

4.2.1. Antenna Substrate

As discussed in the previous chapter, an antenna substrate has a huge impact on the antenna size and the overall antenna performance. The important substrate properties that must be focused on in the m-antenna design process are the dielectric constant (ε_r), loss tangent ($\tan\delta$), substrate thickness (h) and the cladding thickness (t).

4.2.1.1 Dielectric Constant and Loss Tangent

The dielectric material that has been selected in this design is, FR-4 with $\varepsilon_r = 4.4$. This dielectric material has a thick substrate with low dielectric constant. It has been chosen to achieve greater antenna efficiency and larger bandwidth; it has a loss tangent of $tan\,\delta = 0.002$.

4.2.1.2. Substrate Height and Thickness

The height of the substrate must be such that $0.0030\lambda_0 \leq h \leq 0.05\lambda_0$. The height of the substrate was selected to be *1.5mm* and the cladding thickness was chosen to be *0.035.*

The set of equations used to calculate the ETMP parameters are discussed below.

4.2.2. Resonant Frequency

Assuming perfect magnetic sidewalls, the resonant frequency of an equilateral triangular microstrip patch for various $TM_{m,n}$ modes is given by equation (4.1) [73].

$$f_{m,n,l} = \frac{2c}{3a\sqrt{\varepsilon_r}} \sqrt{m^2 + mn + n^2} \tag{4.1}$$

Where a is the length of the microstrip patch and c is the speed of light.

m, n, l cannot be zero at the same time, they must satisfy the condition that $m + n + l \neq 0$.

4.2.3. Effective Side Length

The side length of a triangular m-antenna for dominant mode TM_{10} is given by.

$$a = \frac{2c}{3f_r\sqrt{\varepsilon_r}} \tag{4.2}$$

Where a is the triangle's side length.

Taking into consideration the effect of spurious radiation, the side length is calculated as the effective side length, which is given by the equation below.

$$a_e = a\left[1 + 2.199\frac{h}{a} - 12.853\frac{h}{a\sqrt{\varepsilon_r}} + 16.436\frac{h}{a\varepsilon_r} + 6.182\left(\frac{h}{a}\right)^2 - 9.802\frac{1}{\sqrt{\varepsilon_r}}\left(\frac{h}{a}\right)^2\right] \tag{4.3}$$

Where a_e is the effective side length.

4.2.4. Results

Figure 4.1 depicts the CST model of the triangular microstrip inset feed antenna. This design utilises a resonant frequency (fr) of 6 *GHz*. An FR-4 dielectric substrate with a dielectric constant of 4.4 ($\varepsilon_r = 4.4\ F/m$) and a substrate height of 1.5 *mm* was selected.

Substituting fr = 6 *GHz*, $C = 3 \times 10^9$ and ($\varepsilon_r = 4.4\ F/m$) into equation (4.2), the side length of a triangular antenna is obtained to be.

$a = \frac{2(3\times10^9)}{3(6GHz)\sqrt{(4.4)}} = 15.89\ mm$.

The ground length and width can be obtained using equation (4.4) and equation (4.5), respectively. Substituting $a = 15.89\ mm$ and $h = 1.5mm$ into the equations below gives

$$L_g = 6 \times h \times a = 6 \times 1.5 \times 15.89 = 24.89\, mm \quad (4.4)$$

$$W_g = 6 \times h \times a = 6 \times 1.5 \times 15.89 = 24.89 mm \quad (4.5)$$

The results obtained include the effective side length, effective dielectric constant, they are listed in Table 4.1. These calculated parameters were then optimised using CST microwave studio. It can be seen that the side length, ground width and ground length were the only parameters that were changed due to optimisation.

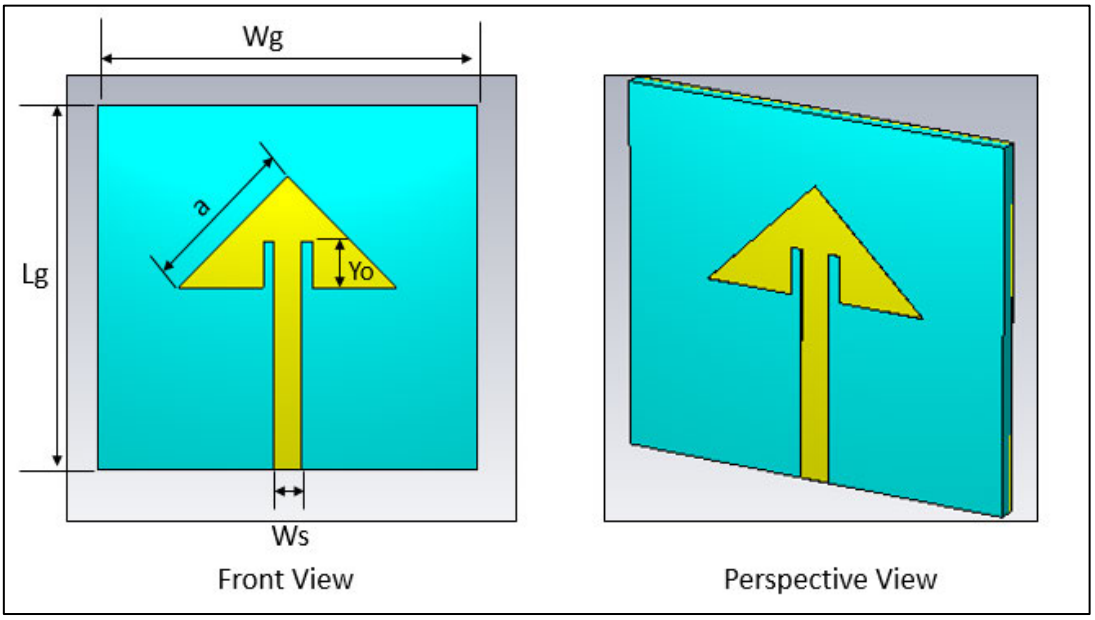

Figure 4:1: Triangular inset feed microstrip antenna.

Table 4.1: Calculated and optimised design parameters of the triangular microstrip antenna.

Antenna Parameters(*mm*)	**Calculated Parameter**	**Optimised Parameter**
Side Length (a)	15.891	10.55
Ground width (Wg)	24.89	35
Ground Length (Lg)	24.89	33
Inset Length (Yo)	4.2112	4.2112
Substrate Height (h)	1.5	1.5
Width of transmission line (Ws)	2.89	2.89

Inset Width (Gf)	1	1

Figure 4.2 depicts the return loss (r-loss) of the triangular microstrip antenna at different values of the side length $\boldsymbol{a}$ which are (11.5*mm*, 11.0*mm*, 10.55*mm*, 10.1*mm* ,9.50*mm*, and 9.00*mm*). It can be observed from the figure that the only side length value which resonates at the desired resonant frequency is 10.55*mm* , it resonates at 6 *GHz* with a return loss of -17,30dB. The values greater than 10.55*mm* (11.5*mm* and 11*mm*) can be observed to be shifted away from the resonant frequency towards the left. They resonate at smaller frequencies to the desired resonant frequency (5.6 *GHz* and 5.8 *GHz*), they also have a greater return loss of (-10 dB, -14.8 dB) when compared to the optimised side length. The values less than 10.55*mm* (10.1*mm*, 9.50*mm* and 9.00*mm*) can be observed to be shifted away from the resonant frequency towards the rigth and they resonate at greater frequencies to the desired resonant frequency (6.195*GHz*, 6.45*GHz*).

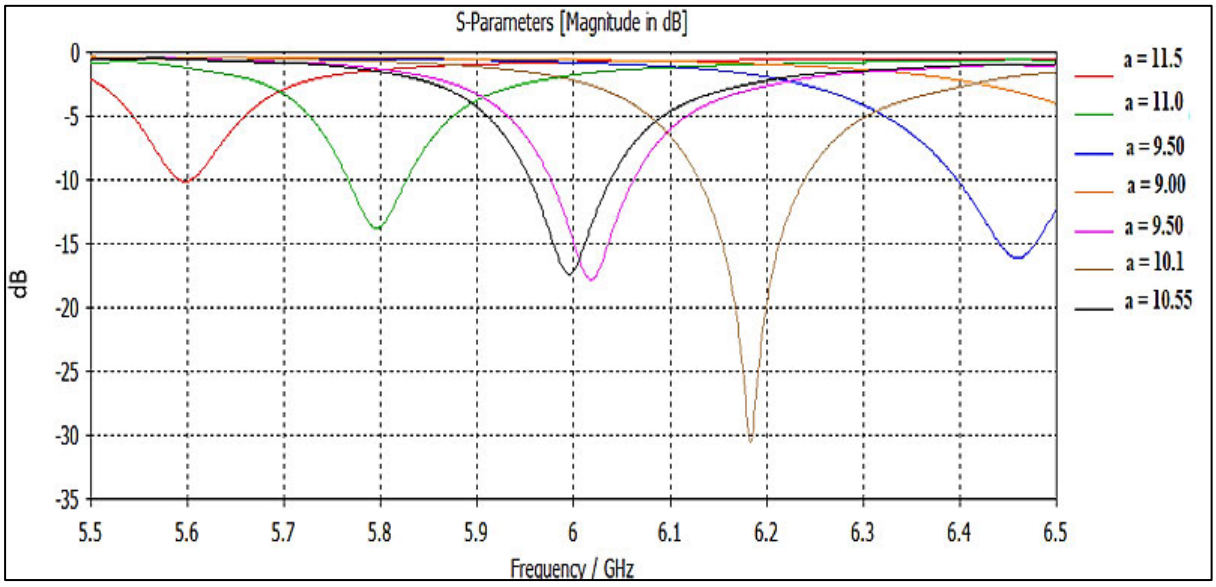

Figure 4:2: Return loss of different side lengths (a).

Figure 4.3 depicts the return loss of the optimised sidelength. It can be seen from the figure that antenna resonates at of 5.99 *GHz*. This resonant frequency (r-frequency) is acceptably similar to the desired r-frequency.The return loss that was obtained is -17.30 dB and the bandwidth is 87.7 *MHz*. Figure 4.4 depicts the directivity and gain of the inset fed triangular m-antenna, it can be observed from the figure that gain and directivity were obtained to be 5.66

dB and 6.1 *dBi*, respectively. Figure 4.5 depicts the VSWR of the m-antenna, from the figure it can be seen that the VSWR was obtained to be 1.31.

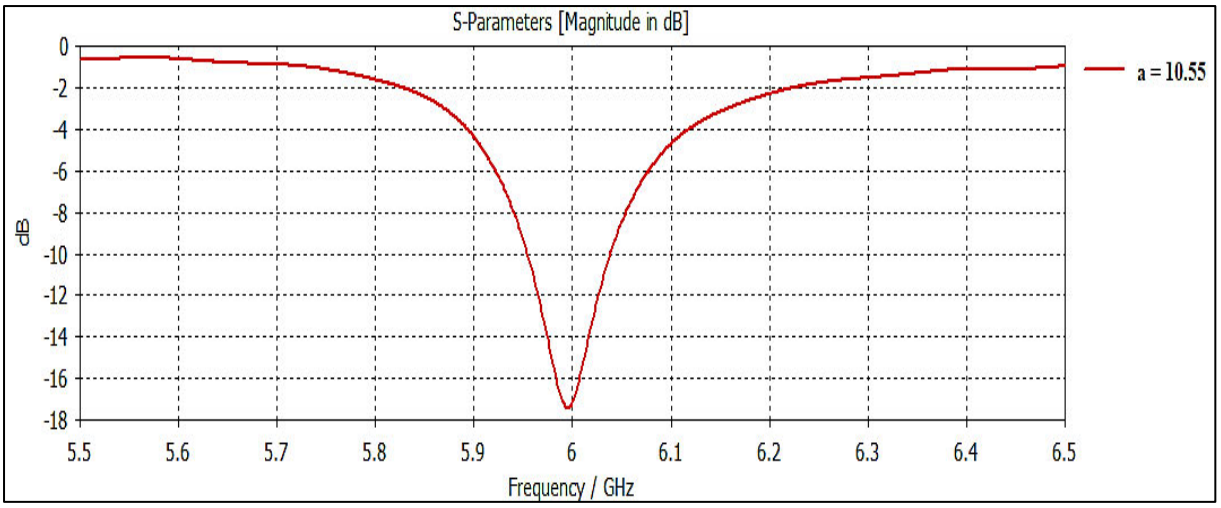

Figure 4:3: Return loss of the triangular m-antenna at a = 10.55mm.

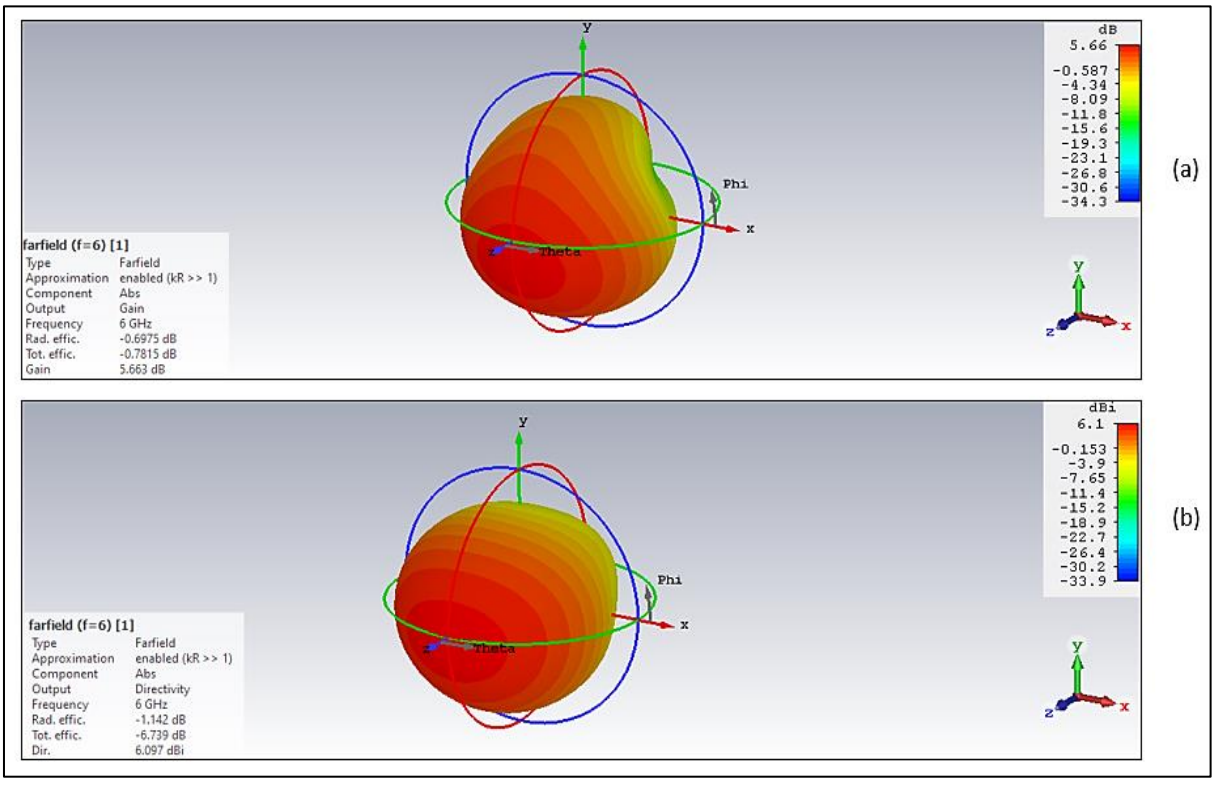

Figure 4:4: Gain and directivity of the triangular m-antenna.

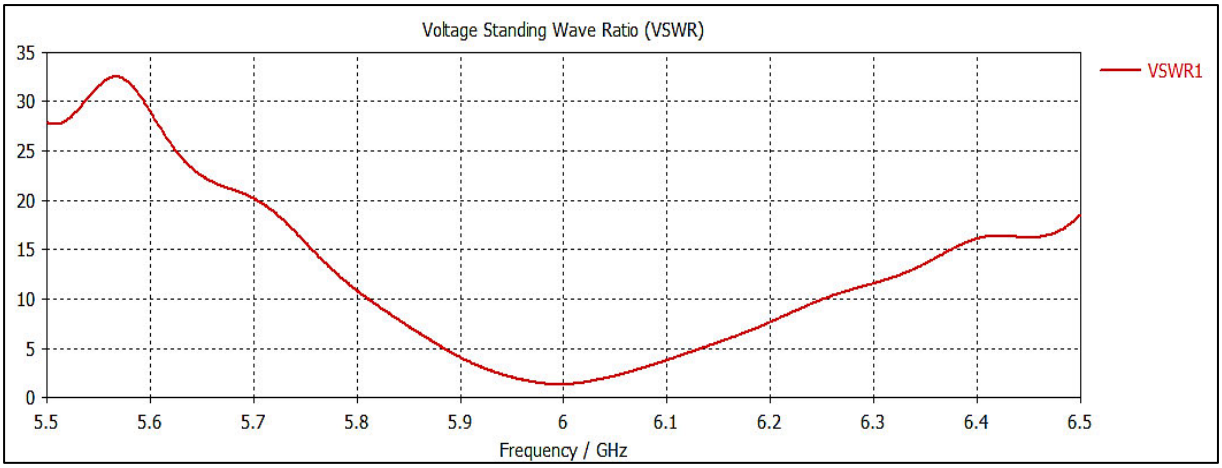

Figure 4:5: VSWR of a triangular microstrip antenna.

4.2.5. Conclusion

In this section, a triangular microstrip antenna was designed. The design parameters that include the side length, ground width, ground length, inset length, inset width, and width of transmission line were first obtained from the equations derived above. These parameters were then optimised using CST microwave studio. From CST microwave studio results such as the return loss, bandwidth, gain, directivity and VSWR were obtained. This design obtained an acceptable return loss of -17.30 *dB*, a narrow bandwidth of 87.7 *MHz* an excellent gain and directivity of 5.66 *dB* and 6.1 *dB* were also obtained, respectively. From this it can be seen that the obtained return loss and bandwidth can still be improved hence, a rectangular microstrip antenna is designed below.

4.3. Rectangular M-Antenna Design

In this section, a rectangular probe fed m-antenna and an inset fed rectangular m-antenna are designed and simulated using CST microwave studio.

4.3.1. Antenna Parameters

This design utilises a resonant frequency (fr) of 6 *GHz*. An FR-4 dielectric substrate with a dielectric constant of 4.4 ($\varepsilon_r = 4.4\ F/m$) and a substrate height of *1.5mm* was selected.

Substituting $C = 3 \times 10^9$, $f_r = 6\ GHz$, $\varepsilon_r = 4.4\ F/m$ into equation (2.8), the width of the rectangular probe fed antenna is obtained to be:

$$W = \frac{3\times10^9}{2(6GHz)}\sqrt{\frac{2}{4.4+1}} = 15.2145\ mm.$$

Substituting $W = 15.2145\ mm$, $\varepsilon_r = 4.4\ F/m$ and $h = 1.5\ mm$ into equation (2.1) the effective dielectric constant is obtained to be:

$$\varepsilon_{reff} = \frac{4.4+1}{2} + \frac{4.4-1}{2}\left[1 + 12\frac{1.5}{15.2145}\right]^{-1/2} = 3.8506F/m.$$

Substituting $\varepsilon_{reff} = 3.8506\ F/m$, $f_r = 6\ GHz$ and $C = 3\times10^9$ to equation (2.4) the effective length of the antenna can be obtained to be:

$$L_{eff} = \frac{3\times10^9}{2(6GHz)\sqrt{3.8506}} = 15.178\ mm.$$

Substituting $\varepsilon_{reff} = 3.8506\ F/m$, $h = 1.5\ mm$, $W = 15.2145\ mm$ into equation (2.2) the change in length can be obtained to be:

$$\Delta L = 0.412(1.5)\frac{(3.85+0.3)\left(\frac{15.2145}{1.5}+0.264\right)}{(3.85-0.258)\left(\frac{15.2145}{1.5}+0.8\right)} = 0.6830\ mm.$$

Substituting $\Delta L = 0.6830\ mm$ and $L_{eff} = 15.78\ mm$ the actual length of the rectangular microstrip antenna is obtained to be:

$L = 15.178 - 2(0.6830) = 13.81mm$.

The design parameters of the rectangular m-antenna are listed Table 4.2.

Table 4.2: Rectangular microstrip antenna design parameters in (mm).

Antenna Parameter	**Value**
Frequency	6 *GHz*
Height	1.5
Polarization	Linear
Feeding Method	Insert and probe feed
Width (W)	15.2145
Effective Dielectric Constant	3.8506

Length (L)	13.812
Length of ground (Lg)	20,382
Width of ground (Wg)	24,2145

4.3.2. Probe Feed M-Antenna

A coaxial probe fed microstrip antenna is designed in this section; its results are then compared to design 1 (triangular microstrip antenna) and design 3 (rectangular inset feed microstrip antenna) The best performing antenna design will be used for 2-port microstrip antenna design. In this m-antenna design, the origin point is at the centre of the patch and the location of feed point is situated at the co-ordinates (W_f, L_f) from the origin. The feed point must be chosen such that, its location corresponds to where the input impedance is 50 ohms for impedance matching purposes. A trial and error technique is utilised to locate a feed point where, the impedance is matched and the return loss is minimal. The feed point will be varied along the width of patch, while the length is kept at -2 i.e. (W_f ,-2). A radius of 0.7 *mm* is selected for the coaxial probe of the m-antenna. Figure 4.6 depicts the CST model of the probe feed microstrip antenna and Table 4.3 lists different feed points with their resonant frequencies and their return loss.

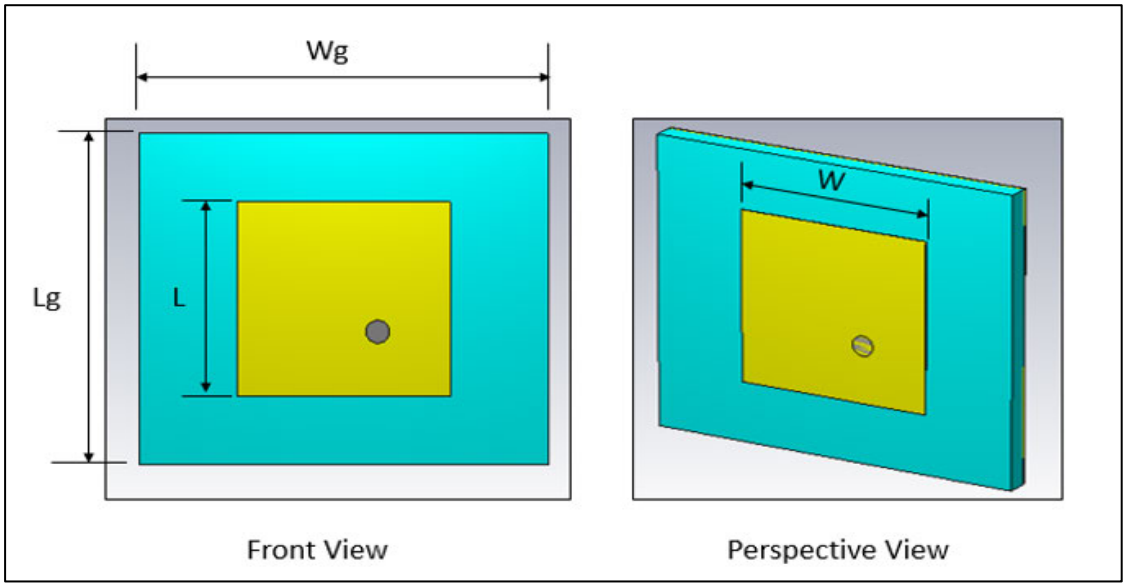

Figure 4:6: Probe feed Rectangular M-Antenna.

Table 4.3: R-frequency, r-loss and bandwidth of the probe fed m-antenna at different feed points.

No.	**Feed Point Location** (W_f, L_f) ***mm***	**Microstrip Width**	**R-Frequency** ***(GHz)***	**R-loss** (dB)	**Bandwidth (-10** dB**)** ***MHz***
1	(1,-2)	15.2145	5,715	-36,39	223,5
2	(2,-2)	15.2145	5,682	-21,9	280,9
3	(3,-2)	15.2145	5,563	-27,8	256
4	(4,-2)	15.2145	5,561	-15,20	185,4
5	(5,-2)	15.2145	5,585	-9,93	-
6	**(1,-2)**	**6,5**	**6**	**-7,72**	-
7	(2,-2)	6,5	6,017	-8,42	-
8	(3,-2)	6,5	6,05	-9,31	-
9	(4,-2)	6,5	5,9	-4	-
10	(5,-2)	6,5	5,924	-	-
11	(6,-2)	6,5	5,922	-	-
12	(7,-2)	6,5	5,913	-	-

From Table 4.3, it can be seen that the calculated width of (15.2145 *mm*) is not suitable for the probe fed microstrip antenna. It is not suitable in a way that it is shifted away from the resonant frequency which is 6 *GHz*. Through extensive numerical simulation a width of 6.5 *mm* was obtained, this width allows the m-antenna to resonate at the anticipated r-frequency as can be seen in No 6 in the table above. Comparing No 1 and No 6 from the above table, it can be observed that a reduction of the microstrip width from 15.2145 to 6.5 resulted in a the bandwidth to be 0 *MHz*, while also decreasing return loss by up to 5 times. Figure 4.7 depicts the return loss of the probe fed microstrip antenna at the optimised width of 6.5 *mm*, at different values of the feed point where W_f is varied from 1 to 7 and L_f is kept constant at -2. It can be observed that the m-antenna resonates at 6 *GHz* at the feed point of (1, -2). The gain and directivity of this m-antenna were obtained to be 6.08 *dB* and 6.41 *dBi*, respectively and they

are depicted in Figure 4.8. The VSWR of this antenna was obtained to be 2.39 and it is depicted in Figure 4.9.

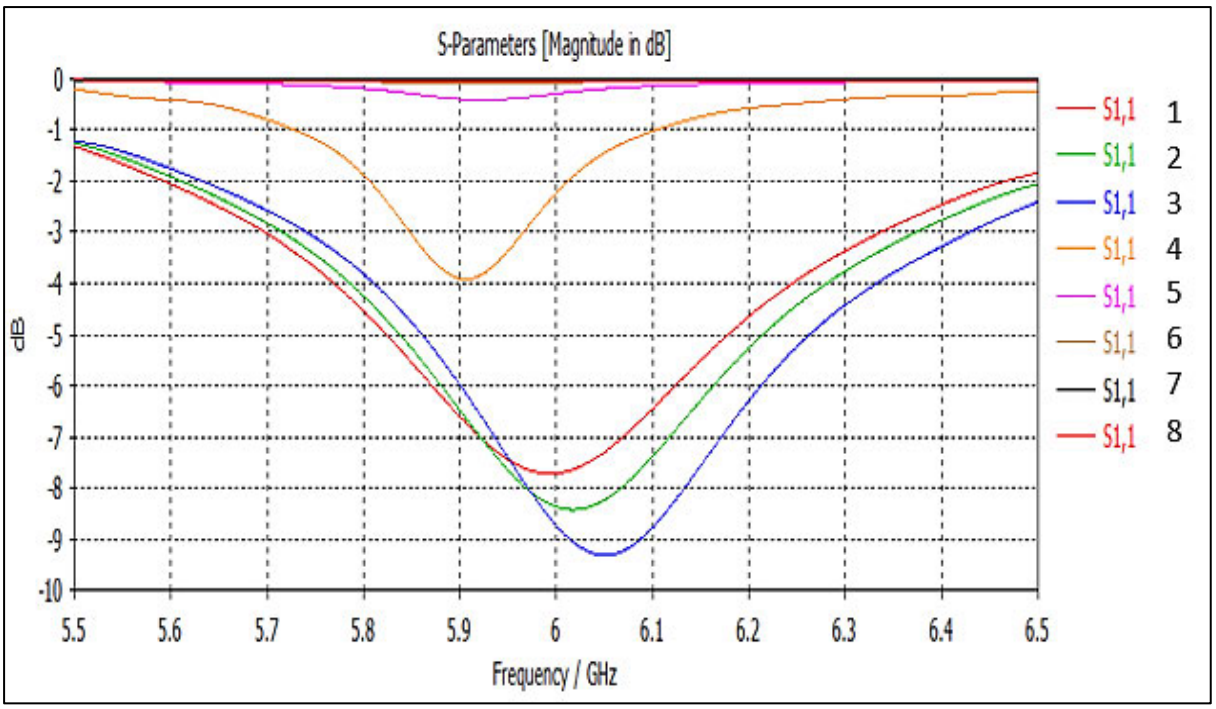

Figure 4:7: Return loss of the probe fed m-antenna at different feed points.

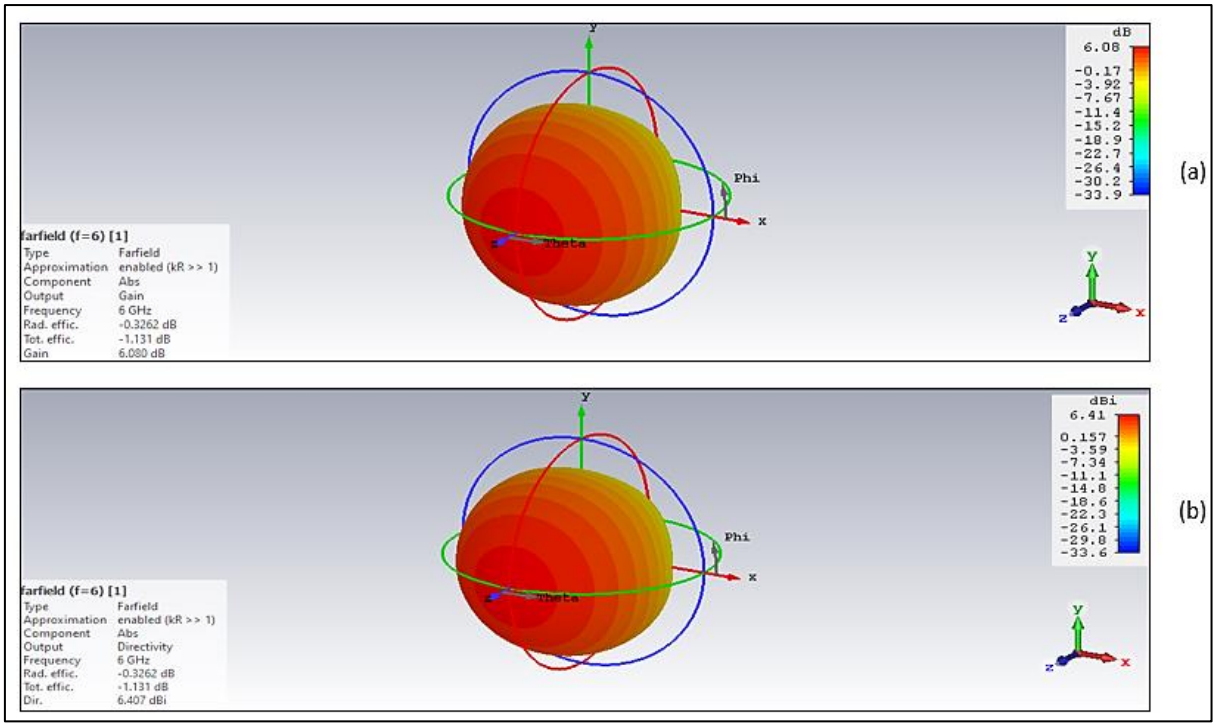

Figure 4:8: Gain and directivity of the probe fed m-antenna.

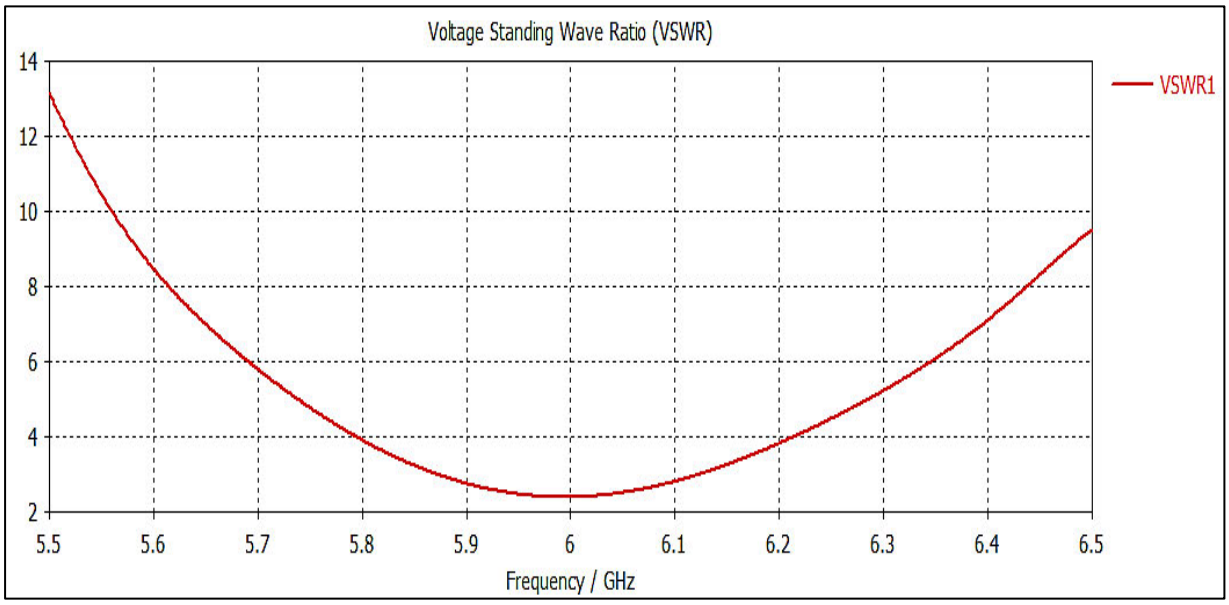

Figure 4:9: VSWR of the probe fed microstrip antenna.

4.3.3. Rectangular Inset Feed

As mentioned in the above chapter, one of the effective ways to achieve impedance matching is by adding an inset feed of distance y_o. The inset width and inset distance can be calculated using the equations below [56].The characteristic impedance of the microstrip line can be calculated from equation (4.6), for this design the chosen impedance is $50\ ohms$ .From this equation one can solve for the width of the microstrip line (W_O).

$$Z_c = \begin{cases} \frac{60}{\sqrt{\varepsilon_{reff}}} \ln\left[\frac{8h}{W_O} + \frac{W_O}{4h}\right] & , \frac{W_O}{h} \leq 1 \\ \sqrt{\varepsilon_{reff}}\left[\frac{W_0}{h} + 1.393 + 0.667 \ln\left(\frac{W_O}{h} + 1.444\right)\right] & , \frac{W_O}{h} > 1 \end{cases} \quad (4.6)$$

Where Z_c is the characteristic impedance of the microstrip line and W_O is the width of the microstrip line.

The inset length y_o can be calculated from equation (4.7) below.

$$R_{in}(y = y_o) = R_{in}(\mathrm{y} = 0) cos^2\left(\frac{\pi}{L} y_o\right) \quad (4.7)$$

Where y_o is the inset length and $R_{in}(y = y_o) = 50\ ohms$.

$R_{in}(\mathrm{y} = 0)$, is the input impedance at edge of the patch. This is where the maximum impedance value occurs, the current is at minimum, voltage is at maximum. Typical values of this impedance occur between 300 – 150 ohms [110]. It can be calculated from equation (4.8) below.

$$R_{in}(\mathrm{y} = 0) = \frac{1}{2\,(G_1 \mp G_{12})} \quad (4.8)$$

The plus sign is for modes with antisymmetric resonant voltages, distributed between the slot and beneath the patch. The minus sign is utilised for is for modes with symmetric resonant voltage distribution. G_1 is the conductance of slot 1 and G_{12} is the mutual conductance between the slots, they are given by equation (4.9) and equation (4.10), respectively [56].

$$G_1 = \begin{cases} \frac{1}{90}\left(\frac{W}{\lambda_O}\right)^2 & W \ll \lambda_O \\ \frac{1}{120}\left(\frac{W}{\lambda_O}\right) & W \gg \lambda_O \end{cases} \quad (4.9)$$

$$G_{12} = \frac{1}{120\,\pi^2}\int_0^{\pi}\left[\frac{\sin(\frac{k_O W}{2}\cos\theta}{\cos\theta}\right]^2 J_O\,(k_O L\sin\theta)\sin^3\theta\,d\theta \qquad (4.10)$$

Where J_O is a Bessel function of the first kind of order zero. Normally $G_{12} \ll G_1$ [111].

The notch gap of the microstrip line is given by equation (4.11) [112].

$$g = \frac{c\times 4.65\times 10^{-12}}{\sqrt{(2\times\varepsilon_{eff})}\,f} \qquad (4.11)$$

Where C is the speed of light in *mm/s* and f is the resonant frequency in *GHz*.

4.3.3.2. Results

The inset fed rectangular m-antenna was simulated and optimised using CST microwave studio suite. Figure 4.10 depicts the CST model of the rectangular microstrip inset feed antenna.

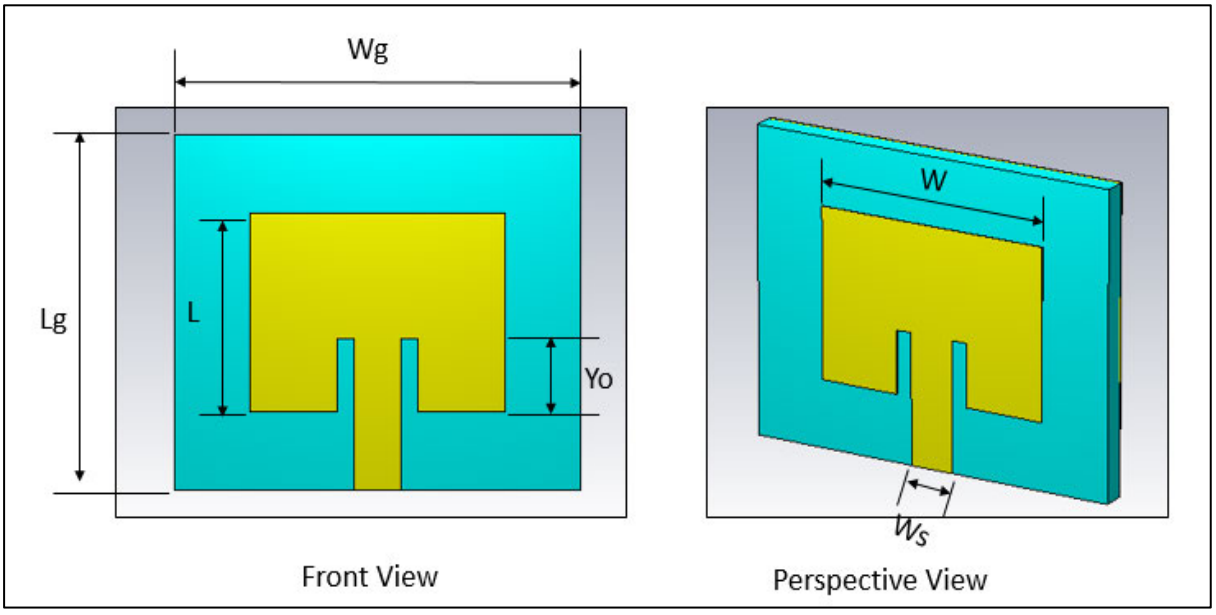

Figure 4:10: Inset feed rectangular microstrip antenna.

Figure 4.11 depicts the r-loss of the rectangular inset feed m-antenna, with two different patch widths. The first width (15.2145 *mm*) being the one obtained from design calculation, with the aid of equation (2.8). The second width (12.58 *mm*) being the one obtained from extensive numeric simulation, using CST microwave studio.

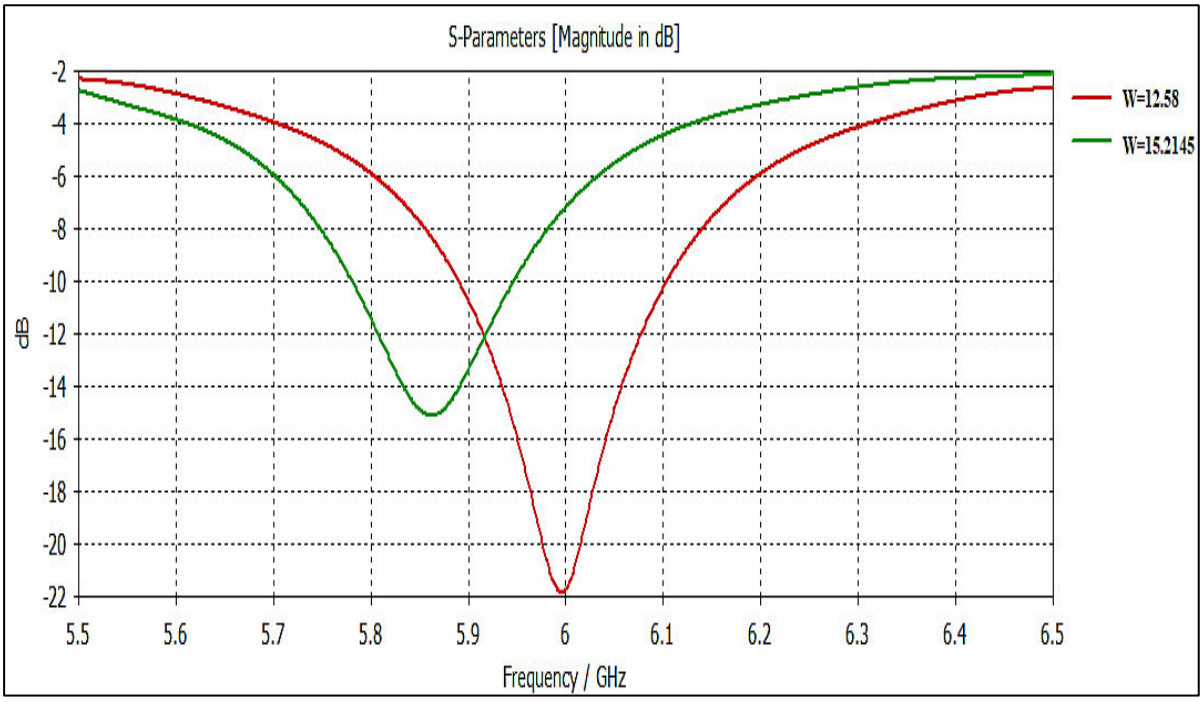

Figure 4:11: R-loss of the rectangular inset fed m-antenna, with the calculated width and the optimised width.

The initial design with the calculated width obtained a return loss of -15.11 *dB* at an undesired r-frequency of 5.85 *GHz*, and a bandwidth of 167.6 *MHz*. The optimised design obtained a return loss of -21.83 *dB*, a resonant frequency shift from 5.85 *GHz* to the desired 6 *GHz*. Additionally a slight increase in bandwidth, from 167.6 *MHz* to 214 *MHz* was also observed. The bandwidth was calculated from the return loss plot. This bandwidth was calculated from the -10 *dB* line. Figure 4.12 depicts the r-loss for different values of inset notch width (Gf). Table 4.4 lists antenna parameters at different values of the inset notch width. Where Gf=0.0837 is the calculated value obtained from equation (6.6). The rest of the values were obtained by taking Gf as the ratio of the width, i.e. $W/_{10}$, $W/_{W}$, $W/_{15}$, $W/_{25}$, $W/_{30}$ to yield an optimised return loss on the selected resonant frequency.

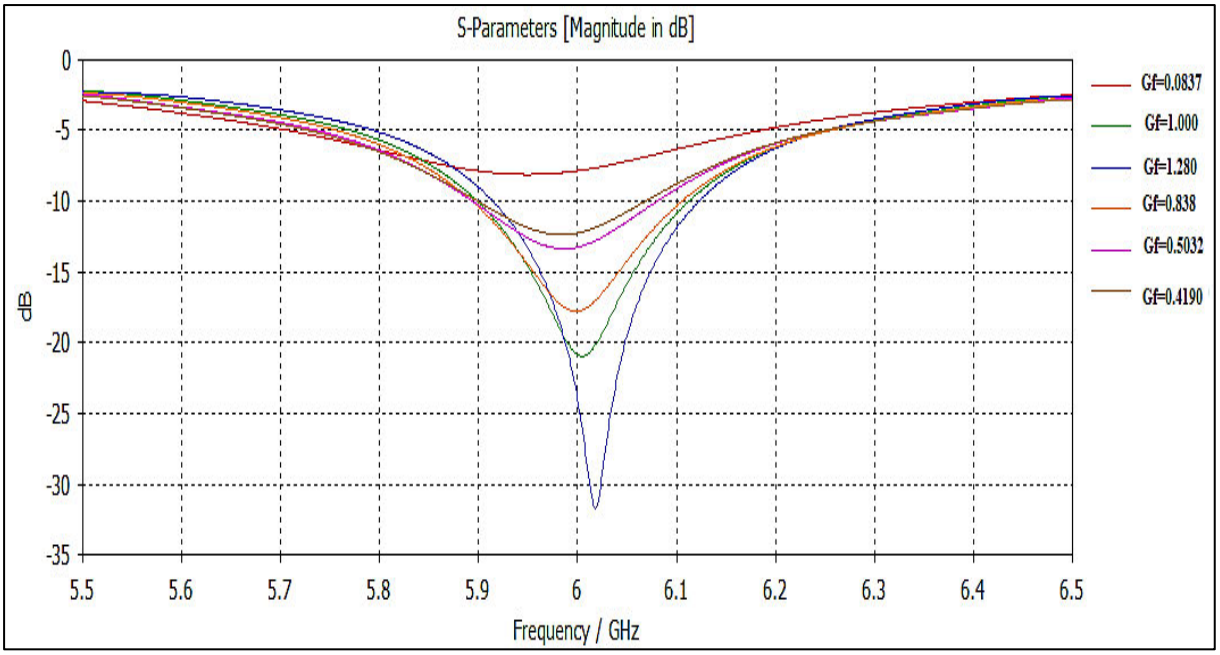

Figure 4:12: R-loss of the rectangular inset fed m-antenna at different values of the Inset Notch width (Gf).

Table 4.4: Different values of the inset notch width (Gf in mm) with their corresponding return loss, resonant frequency and bandwidth.

Antenna Parameters	**Gf=1.280** $(W/10)$	**Gf=1.000** (W/W)	**Gf=0.838** $(W/15)$	**Gf=0.5032** $(W/25)$	**Gf=0.4190** $(W/30)$	**GF=0.0837 (Calculated Value)**
$S_{11}\ (dB)$	-31	-21,82	-17	-13,3	-12,3	-8,11
F (GHz)	6,018	6,005	5,998	5,986	5,983	5,949
Bandwidth MHz $(-10\ dB)$	210,6	214	210,6	187,9	174,6	-

From Figure 4.12 and Table 4.4, it can be observed that the gradual increase of notch the width results in a frequency shift from 5.949 *GHz* towards the resonant frequency of 6 *GHz*. This happens until the W/W point, after which the frequency increases beyond the resonant frequency. The bandwidth can also be observed to, increase with an increase in notch width

until the $^{W}/_{W}$ point, after which it starts decreasing. Finally, the return loss can be seen to decrease with a gradual increase in notch width. The notch width that was selected is *Gf* $=^{W}/_{W} = 1$, this is because it resonates at the desired resonant frequency, it has the highest bandwidth and it has a great return loss of -21.82 dB. Table 4.5 lists the calculated design parameters and optimised design parameters. It can be observed from the table that the width of the patch, inset notch width and the width of transmission line are the only parameters that were optimised from the paper design. These parameters were optimised using CST microwave studio. CST microwave studio has a parameter sweep function that allows one to enter a range of the parameter in question and incremental steps for that parameter. From this, different results like the return loss graph, gain, efficiency are displayed. One can then check for the best results and the value at which they occur.

Table 4.5: Calculated Vs optimised design parameters of the rectangular inset fed microstrip antenna in (mm).

Antenna Parameter	**Calculated Parameter**	**Optimised parameter**
Width	15.2145	12.58
Length	11.3822	11.3822
Inset Length	4.2112	4.2112
Inset Notch Gap	0.083781	1
Width of Transmission line	2.7971	2.89
Ground Width	24.2145	24.2145
Ground Length	20.382	20.382

The figures below depict the results obtained from the optimised design parameters. Figure 4.13 depicts gain and directivity, which was obtained to be 5.64 *dB*, and 6.49 *dBi*, respectively, and Figure 4.14 depicts VSWR, which was obtained to be 1.17 at the resonant frequency.

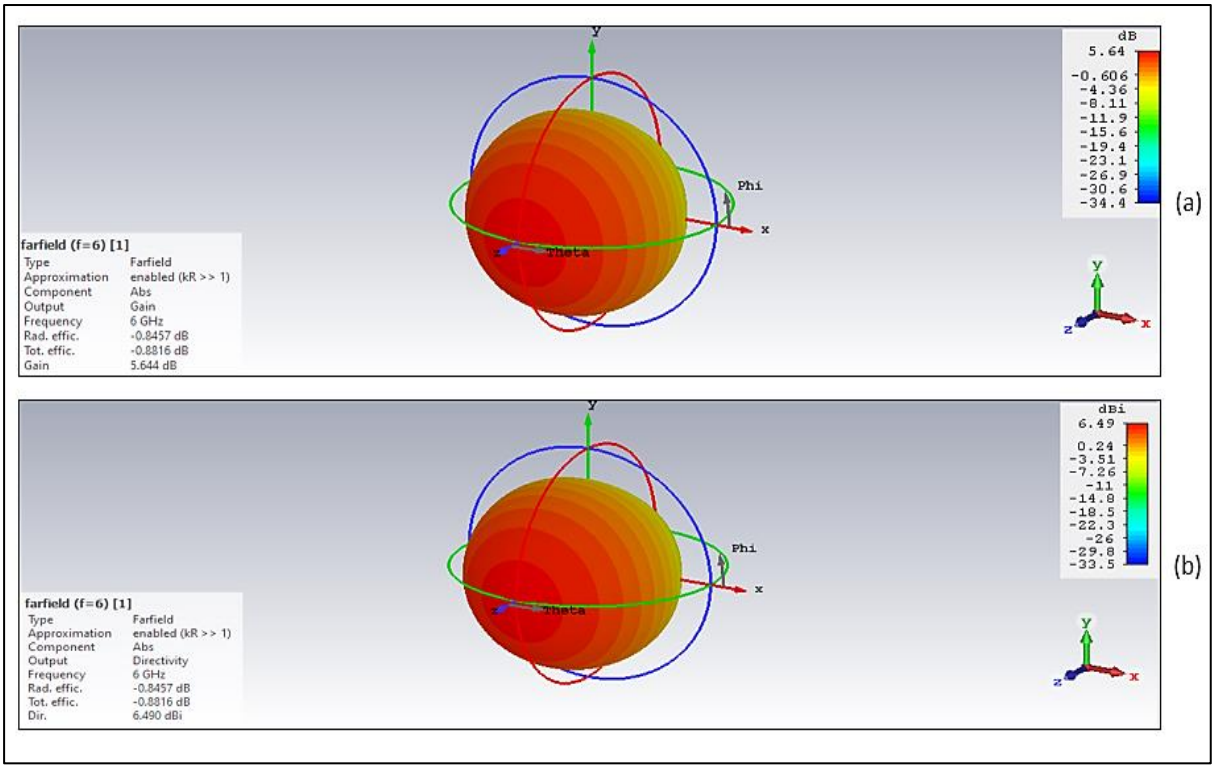

Figure 4:13: Gain and directivity of the rectangular inset fed microstrip antenna.

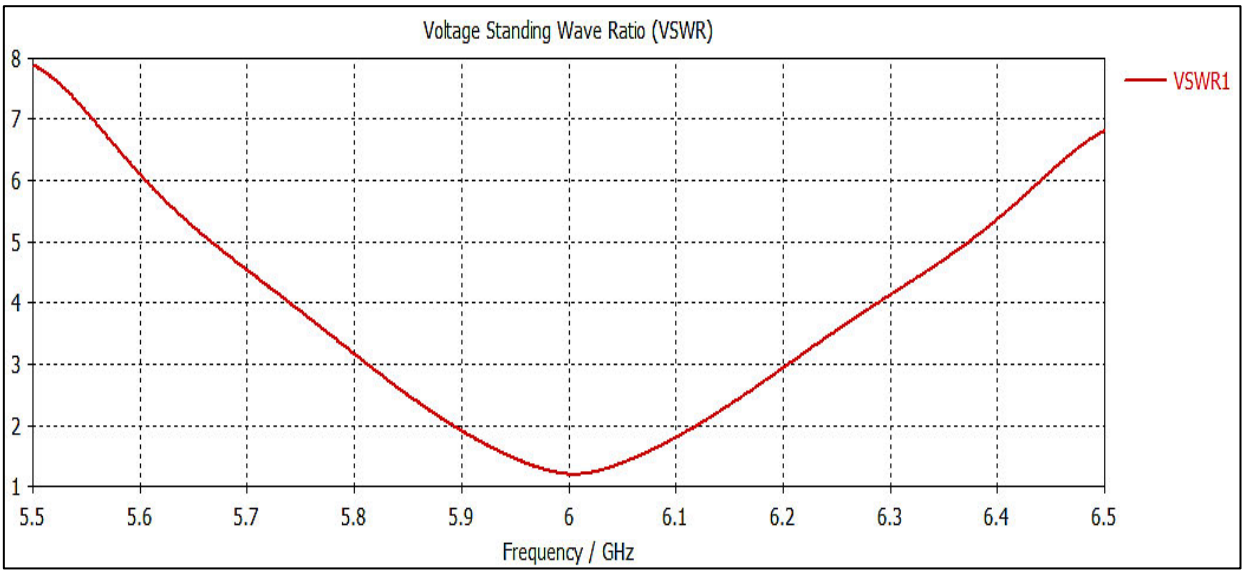

Figure 4:14: VSWR of the inset fed microstrip antenna.

Table 4.6 below compares the perfomance of the three single element microstrip antenna.

Table 4.6: Return loss (in dB), VSWR, bandwidth (in MHz), maximum gain (in dB), maximum directivity (dBi), total efficiency and radiation efficiency.

Parameters	**Triangular inset feed antenna**	**Rectangular probe feed antenna**	**Rectangular inset feed antenna**
Return Loss	-17.30	-7.72	-21.82
VSWR	1.31	2.39	1.17
Bandwidth	87.7	0	214
Maximum Gain	5.66	6.08	5.64
Maximum Directivity	6.1	6.41	6.49
Total Efficieny	83%	76%	80%
Radiation Efficiency	85%	92%	82%

4.4. Chapter Summary

Three different microstrip antenna designs were conducted, where design 1 is the triangular inset fed microstrip antenna (TIA), design 2 is the rectangular probe fed microstrip antenna (RPA) and design 3 is the rectangular insert fed microstrip antenna (RIA). Thier design parameters were calculated using equations derived in chapter 2, they were then simulated and optimised using CST microwave studio. This was done to find the best perfoming antenna system to utilise in the 2-port microstrip antenna design.

The first design parameter of concern is the r-loss which measures the degree of mismatch between the antenna and the transmission line. From Table 4.6 it can be observed that the return loss of design 1 to design 3 was obtained to be -17.30 dB, -7.72 dB and -21.82 dB , respectively. From this it can be observed the RIA (design 3) has the smallest r-loss of -21.82 *dB*, which means that it has very small losses due to the transmission line and antenna coupling. The RIA is then followed by TIA (design 1) with an acceptable return loss of -17.30 *dB*. Lastly the RPA (design 2) follows with an unacceptable return loss of -7.72 *dB*. A well matched antenna has a return loss that is less than -10 *dB*. If the return loss is greater than -10 *dB* it means that the antenna is not well matched and additional matching methods should be

employed. Since RPA has a return less than -10 *dB.* It cannot be consider for further applications.

The next parameter of concern is the VSWR which also measures the degree of mismacth between the feed line and the antenna, the VSWR of design 1 to design 3 was obtained to be 1.31, 2.39 and 1.17, respectivly. From this it can be seen again that RIA is better matched, followed by TIA and lastly RPA which is poorly matched with a VSWR greater than 2. The third parameter of concern is the bandwidth, which measures the range of frequencies over which an antenna perfomes satisfatory. The bandwidth of design 1 to design 3 was obtained to be 87,7 *MHz,* 0 *MHz* and 214 *MHz*, respectively. From this it can be seen that the RIA has the largest bandwith which is 60% more than that of TIA, and the RPA can be seen to be the worst perfomimg with a bandwith of zero.Gain and efficiency of TIA and RIA are quite similar. The gain of TIA can be seen to only be greater by 0.02 *dB* to that of RIA.

The directivity of all three antenna can be seen to be quite similar, with the RIA being more directive than the RPA and TIA. Lastly all three single element microstrip antenna designs can be seen to excellently efficient. From the discustion above it is evident that the best perfomimg single element antenna is the rectangular inset feed microstrip antenna (RIA) becouse it has the lowest return loss,the lowest VSWR, the highest bandwidth which is 60% more than that of the TIA . Hence, this antenna is the one that will be used for a 2-port microstrip antenna design and the rest of design thereof.

Chapter 5 : Metasurface based MIMO Microstrip Antennas

This chapter outlines the design of a 2-port rectangular insert fed m-antenna. Five metasurface-based antenna designs are applied to reduce the m-coupling of the 2-port antenna. The five metasurface-based antenna designs are simulated, analysed and discussed. The metasurface antenna that best reduces the mutual coupling of the 2-port antenna is fabricated and measured.

5.1. Introduction

This chapter proposes using planar metasurface for mutual coupling reduction. As mentioned in the first chapter, metasurface structures are planar in structure and are easy to fabricate. Due to their thin structure and practical implementation, metasurface structures have been getting antenna researcher's attention in recent years. Metasurface structures have been utilized to reduce mutual coupling between antenna elements. However most of these design degrade the antenna matching performance, which then further requires additional antenna matching methods to be employed leading to complex fabrication and improved fabrication costs.

5.2. 2-port Microstrip Antenna Design

When designing a MIMO antenna system, one has to consider parameters that are utilised to measure the performance of a MIMO system. These parameters include but are not limited to m-coupling, envelope correlation coefficient, diversity gain and channel capacity which is the maximum transmission rate of which communication can be achieved and it can be calculated as was seen in chapter 3.

Mutual coupling can be described as electromagnetic interaction between antenna elements in a MIMO system. It is usually a results of two phenomena, the first being radio leakage received through space between antenna elements. The second being signal leakage from currents on the ground surface or surface waves from the substrate. The envelope correlation coefficient is a mutual coupling measuring parameter; it measures the radiation pattern correlation and isolation of MIMO antenna pairs. It ranges from 0 to 1 where 0 represents no correlation between the antenna elements, ideally the envelope correlation between a pair of antennas

should not exceed 0.4 [113]. Envelope correlation coefficient between a pair of antennas can be calculated by equation (5.1) [43].

$$\rho = \frac{|S^*_{11}S_{12}+S^*_{21}S_{22}|^2}{(1-|S_{11}|^2+|S_{21}|^2)(1-|S_{22}|^2+|S_{12}|^2)} \quad (5.1)$$

Where S_{11} and S_{22} are the reflection coefficients of port 1 and port 2, respectively. S_{21} and S_{12} are the mutual couplings between port 1 and port 2 and between port 2 to port 1, respectively. Where port 1 is port on the left and port 2 is the port of the right.

5.2.1. Geometry, Results and Discussion

A 2-port Microstrip rectangular inset fed (Antenna 1) is designed in CST microwave studio, using parameters derived in the single microstrip antenna element designed in chapter 6. Figure 5.1 depicts the CST model of Antenna 1. To validate the theoretical aspect of this design, its prototype is fabricated and measured. Firstly, single layer Gerber files were exported from CST microwave studio. The exported Gerber files were then checked with GerbView to ensure that they were correctly aligned. The Gerber files were then sent to the lab technicians for manufacturing. Figure 5.2 depicts the fabricated prototype of Antenna 1 with the soldered 50 Ω SMA connectors. Table 5.1 lists the optimized design parameters. These parameters were optimised using CST microwave studio. CST microwave studio has a parameter sweep function that allows one to enter a range of the parameter in question and incremental steps for that parameter. From this, different results like the return loss graph, gain, efficiency are displayed. One can then check for the best results and the value at which they occur. Parameters such as resonant frequency, dielectric constant, dielectric substrate height and patch dimensions remain unchanged.

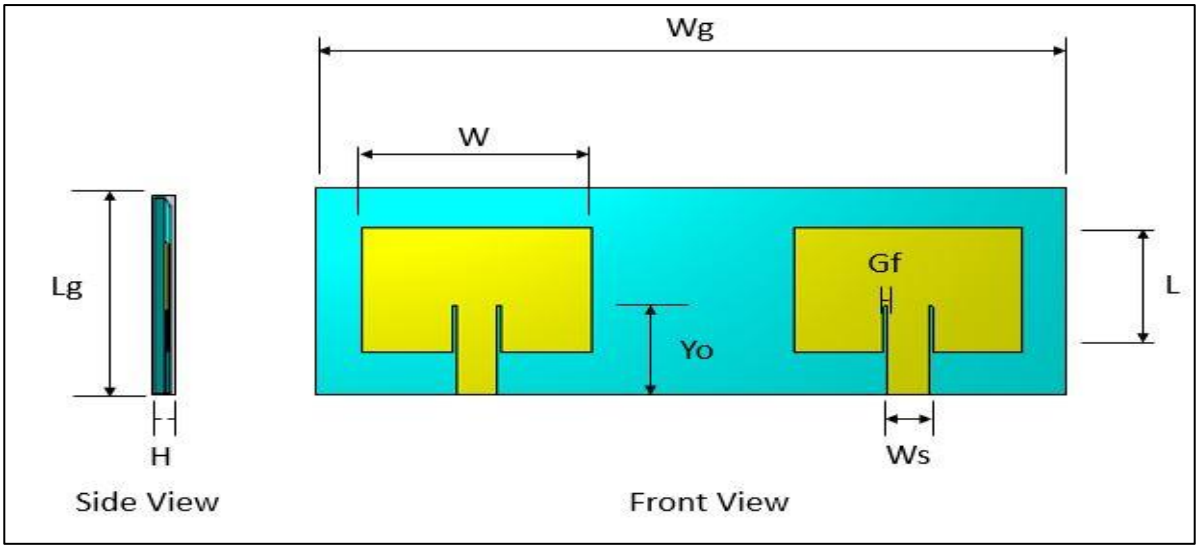

Figure 5:1: CST model of the 2- port MIMO microstrip antenna.

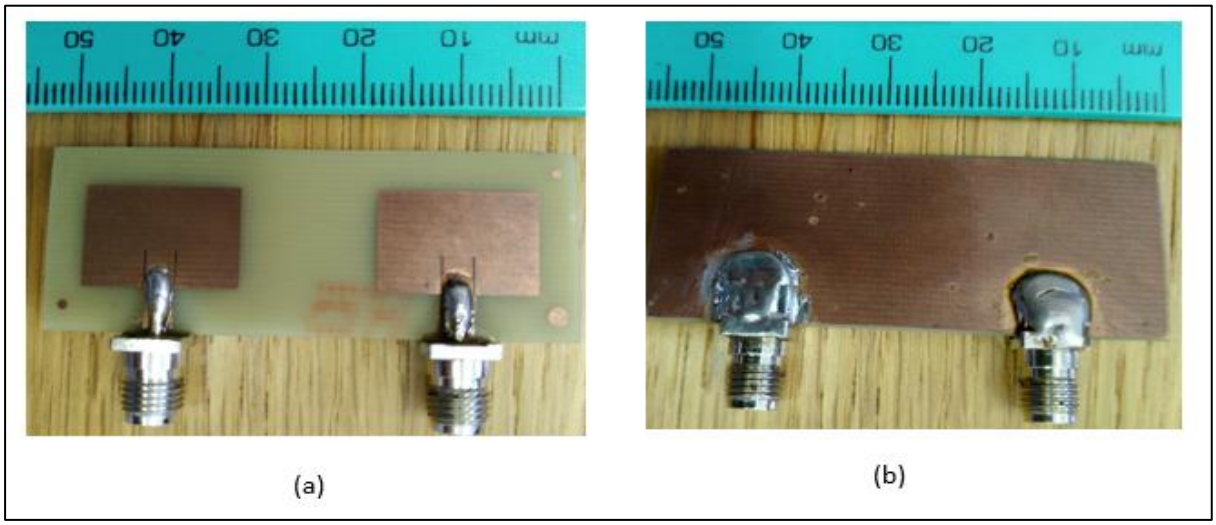

Figure 5:2: (a) Top view, (b) bottom view of fabricated Antenna 1 prototype.

Table 5.1: Optimised design parameters of the 2- port MIMO microstrip antenna (in mm).

Antenna Parameter	**Value**
Width of patch (W)	16.3
Length of patch (L)	11.3822
Inset Length (Yo)	4.2112
Inset Notch Gap (Gf)	0.083781

Width of Transmission line (WS)	2.89
Ground Width (Wg)	55
Ground Length (Lg)	20.382

Figure 5.3 depicts the simulated reflection coefficient and mutual coupling of the of the 2-port microstrip antenna. It can be seen that S1,1 was obtained to be -23,76 dB with bandwidth value of 170,4 *MHz.* S2,2 was obtained to be -31,26 dB with the bandwidth value of 70.2 *MHz*. The mutual coupling between S1,2 was obtained to be -23,06 dB and between S2,1 to be -23,06 dB. The vector network analyzer was used to measure the reflection coefficients and mutual couplings of the fabricated antenna prototype, the obtained results are then compared to the simulated results. Figure 5.4 depicts the simulated and measured S-parameters of Antenna 1. From the figure it can be observed that the that simulated S1,1 parameter is slightly less than the measured S1,1 parameter. A slight shift in resonant frequency towards the right can also be observed for measured the S2,2 parameter, while the measured S2,1 and S1,2 parameters can be seen to be slightly less than the simulated S2,1 and S1,2 parameters, respectively. Minor discrepancies can be seen between the simulated S-parameters and the measured S-parameters, these discrepancies can be attributed to soldering residue, vector network analyzer calibration, fabrication and assembly error.

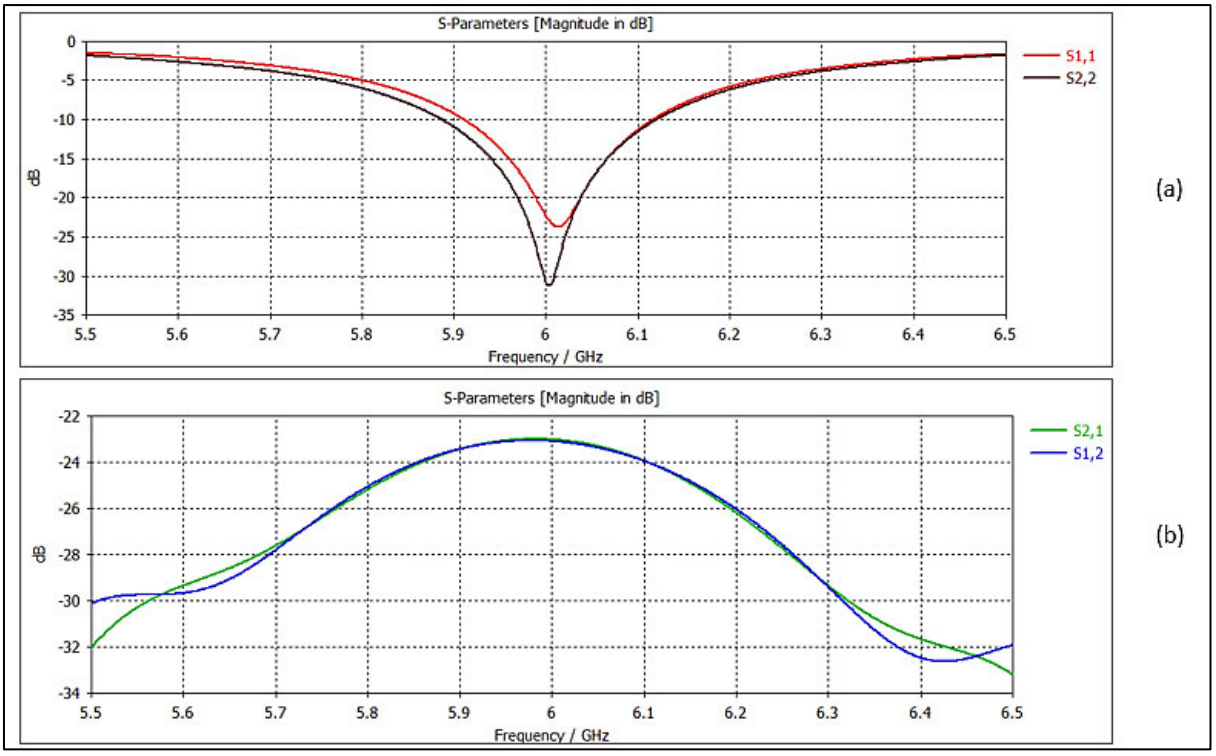

Figure 5:3:(a) Reflection coefficient (b) m-coupling of the 2-port MIMO m-antenna.

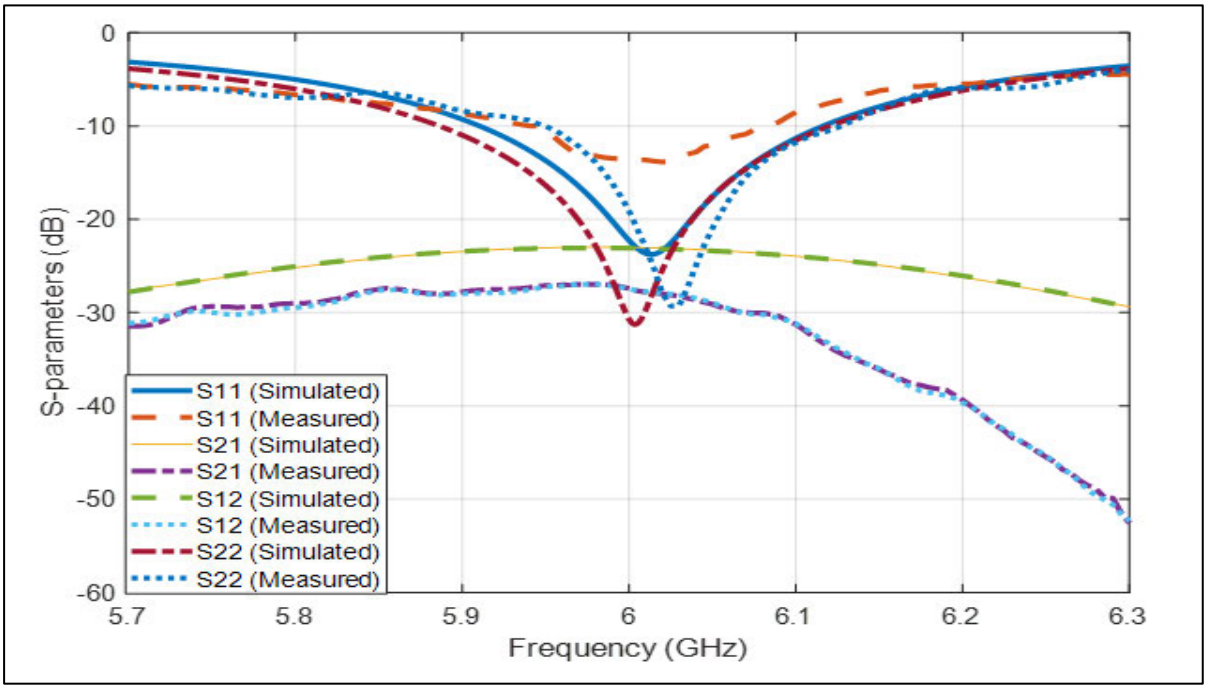

Figure 5:4: Simulated and measured S-parameters of Antenna 1 prototype.

Figure 5.5 depicts the VSWR of the 2-port antenna, the first antenna element obtained a VSWR value of 1.13, while the second antenna elements obtained a VSWR value of 1.05 These results show that this antenna is an exceptional performing antenna but it still has room for improvement in terms of r-loss and m-coupling.

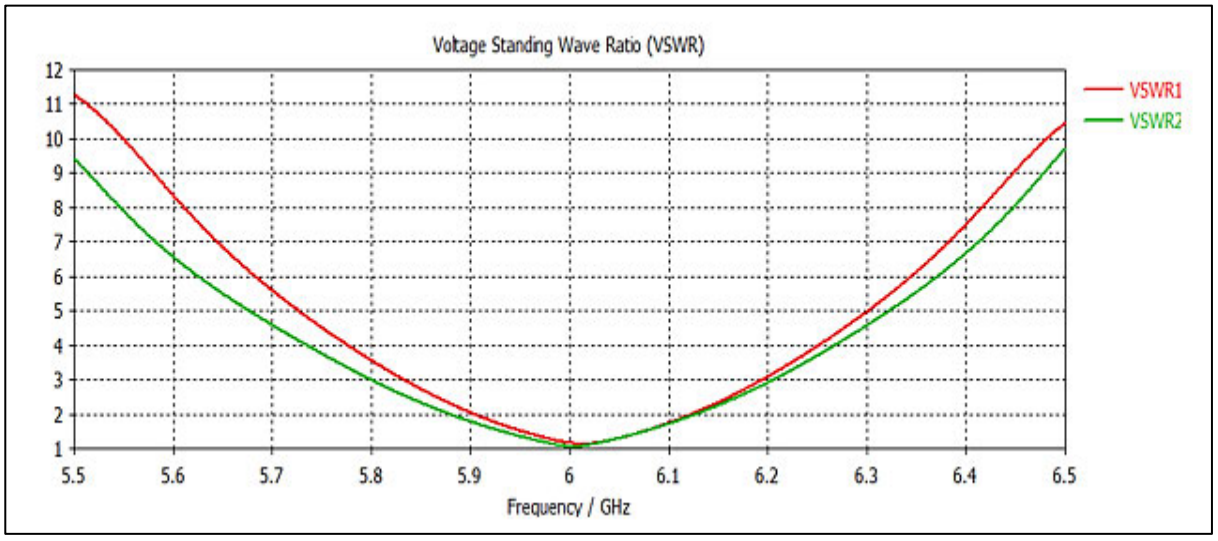

Figure 5:5: VSWR of the 2-port antenna.

Figure 5.6 depicts the gain of the 2-port m-antenna. It can be observed, from the figure that the gain of antenna element 1 was obtained to be 4.71 dB and gain of element 2 was obtained to be 4.88 dB.

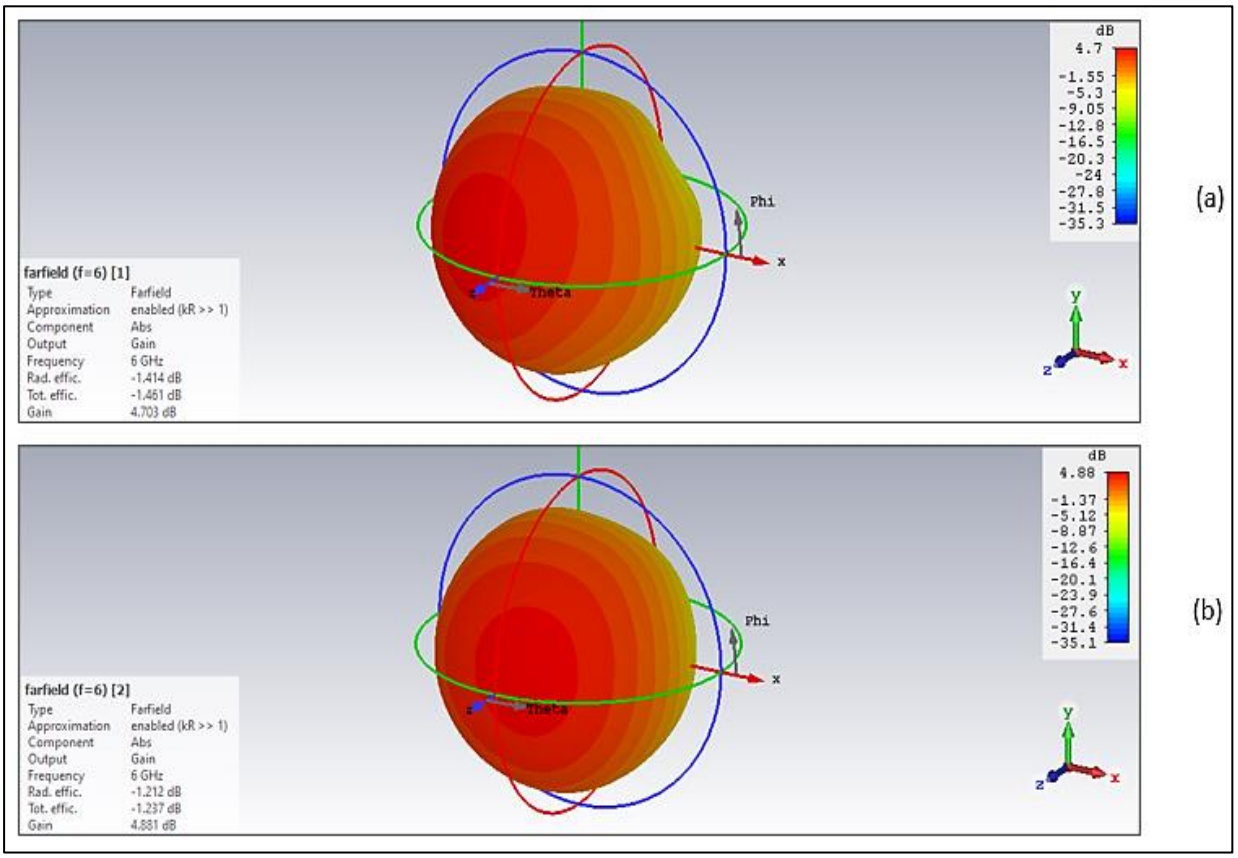

Figure 5:6: Gain of (a) antenna element 1 and (b) antenna element 2.

5.3. Metasurface Design

This section outlines the design of the metasurface unit cell. Where an MNG high impedance metasurface is designed for mutual coupling reduction purposes. An MNG metasurface is a metasurface that is equivalent to negative permeability and positive permittivity medium. This metasurface was selected due to its ability to reject wave propagation in the designed frequency band. The metasurface is formed by a pair of subwavelength split ring resonators (SRR) printed on a dielectric substrate, with splits gaps located 180 degrees from each other. The metal loops of the SRR results in an inductance while the split gaps between the rings results in a capacitance, hence forming an LC circuit. The formed LC circuit is responsible for producing the resonant frequency of the metasurface. This is the frequency where wave propagation will

be rejected, it can be expressed by equation (5.2) below [114]. The induced magnetic field in the SRR is responsible for creating negative permeability.

$$f = \frac{1}{2\pi\sqrt{(LC)}} \tag{5.2}$$

Where L is the inductance and C is the capacitance of the SRR.

The metasurface unit cell is depicted in Figure 5.7 and Table 5.2 lists its design parameters. The values of permittivity and permeability are extracted in CST microwave studio using S-parameters and their depicted in Figure 5.8. This designed metasurface is then used in the unmodified 2-port microstrip antenna, where it introduces a region with positive permittivity and negative permeability. In this region the wave number is given by [1-2].

$$k = k_o.\sqrt{-|\mu_r|.|\varepsilon_r|} = jk_o.\sqrt{|\mu_r|.|\varepsilon_r|} \tag{5.3}$$

Where k is the wave number.

The wave number can be seen to be entirely imaginary, resulting in the electric field of the x-component ($A_o e^{jkx}$) to be written as [1-2]:

$$A_o e^{jkx} \cdot e^{jwt} = A_o e^{j(jk_o.\sqrt{|\mu_r|\cdot|\varepsilon_r|})x} \cdot e^{jwt} \tag{5.4}$$

And

$$A_o e^{j(jk_o.\sqrt{|\mu_r|\cdot|\varepsilon_r|})x} \cdot e^{jwt} = A_o e^{-k_o.\sqrt{|\mu_r|\cdot|\varepsilon_r|}x} \cdot e^{jwt} \tag{5.5}$$

Where A is the electric field.

This demonstrates that the electromagnetic wave propagating in the negative x-component direction is evanescent. This means that the surface waves that cause mutual coupling will be rejected.

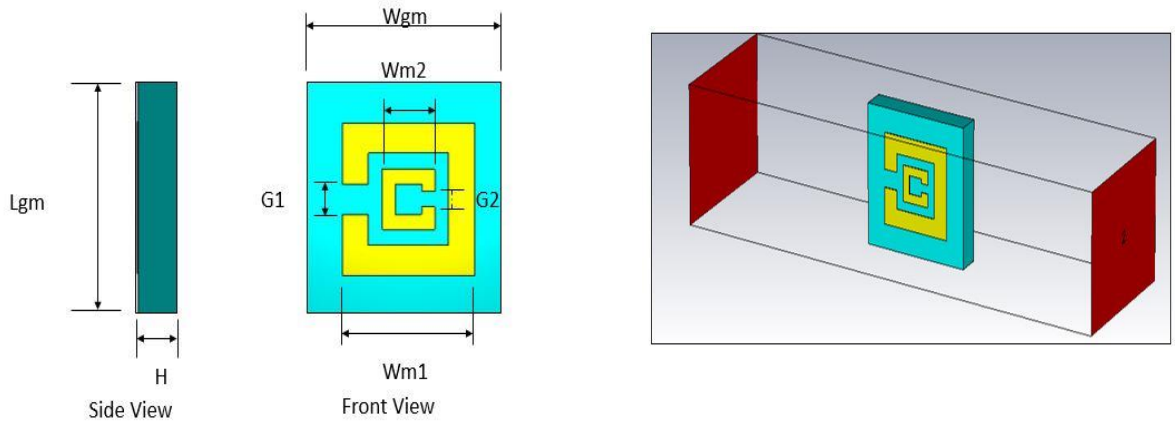

Figure 5:7:(a) Metasurface unit cell structure, (b) metasurface unit cell CST simulation model.

Table 5.2: Design parameters of the metasurface unit cell (in mm).

Parameter	**Value**	**Parameter**	**Value**
Wm2	2	Wgm	7.844
G1	1	Lgm	7.844
G2	0.5	Wm1	5.06
H	1.5	Lm1	5.06

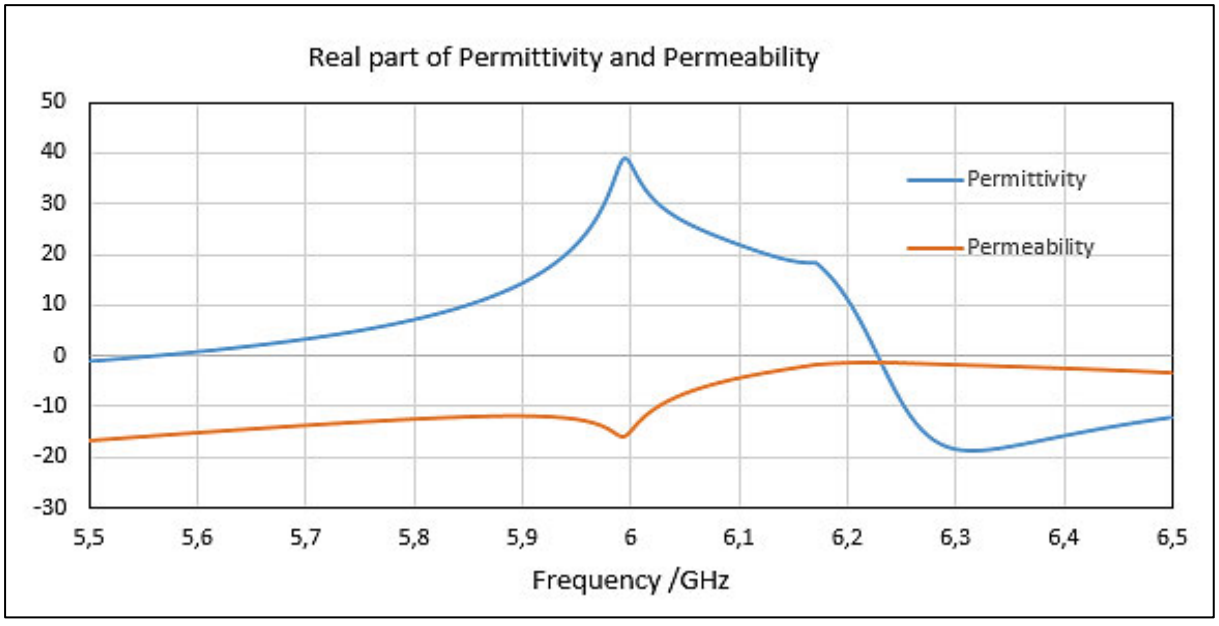

Figure 5:8: Extracted permittivity (ε) and permeability (μ) of the metasurface unit cell.

5.4. Metasurface based Antenna Design

The above designed metasurface unit cell is used to reduce the mutual coupling (m-coupling) of a 2-port microstrip antenna. Five separate metasurface-based antenna designs are conducted in this section. The first three metasurface-based antenna designs are achieved by placing a metasurface wall vertically between the antenna elements. The last two metasurface-based antenna designs are achieved by suspending a metasurface superstrate above the 2-port antenna. Their results are then compared and the best performing design is fabricated and tested further.

5.4.1. Metasurface wall based Antenna Design for M-Coupling Reduction

Three metasurface wall based antenna designs are conducted in this section. The first design places a single metasurface wall in-between the 2-port microstrip antenna. The second and third design place a double and triple metasurface walls in-between the 2-port microstrip antenna, respectively. Their results are simulated, analyzed and compared for the best performing design. The metasurface wall is made up of an FR-4 substrate, with a dielectric constant of 4.4, substrate height of 1.5 *mm* and a $1x3$ SRR unit cells printed on both sides of the FR-4 substrate. Its CST model is depicted in Figure 5.9 and its design parameters are listed in Table 5.3.

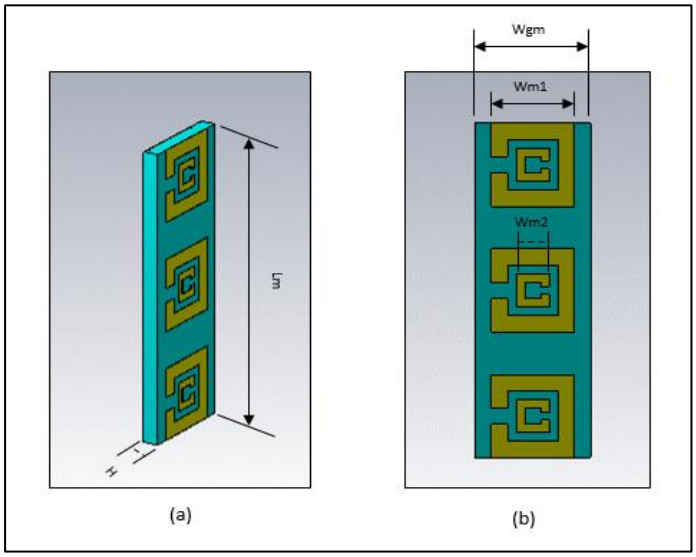

Figure 5:9: 1x3 SRR metasurface wall.

5.4.1.1. Single Metasurface Wall for M-Coupling Reduction (Antenna 2)

This design utilizes a single metasurface wall placed vertically between the two radiating antenna elements. The single metasurface wall is placed at the center of the 2-port microstrip antenna. Its CST model is depicted in Figure 5.10 and its design parameters are listed in Table 5.3.

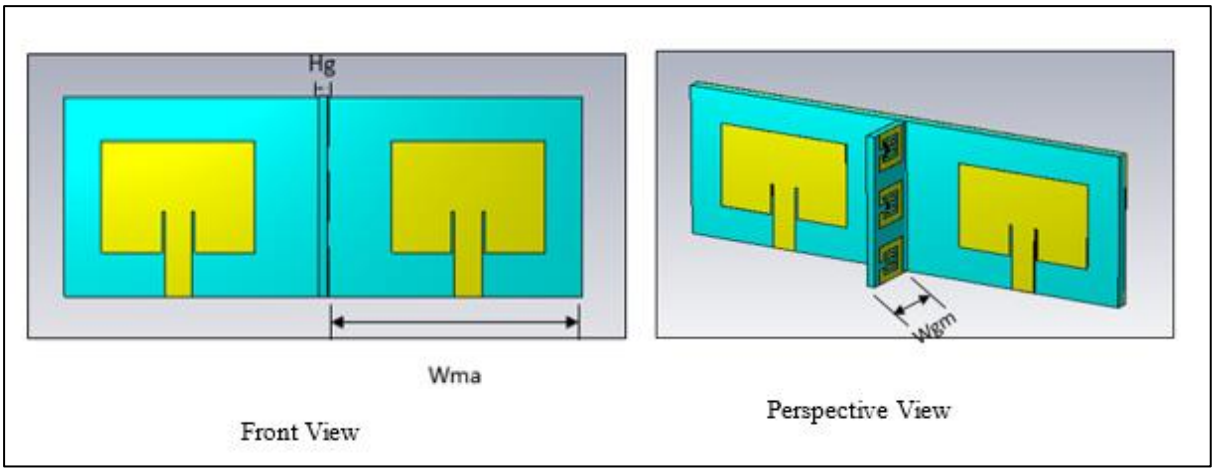

Figure 5:10: Single metasurface wall antenna (Antenna 2).

5.4.1.2. Double Metasurface Wall for M-Coupling Reduction (Antenna 3)

This design is made up of a double wall metasurface also placed vertically between the two radiating antenna elements. The metasurface walls utilized are identical to each other, they are placed at a distance of 5 *mm* from each other and they are at an equidistance of 3.75 *mm* from each antenna element. The distances were obtained based on the optimum results attained, from CST microwave studio. The optimized design parameters of this antenna are listed in Table 5.3 and its CST model is depicted in Figure 5.11.

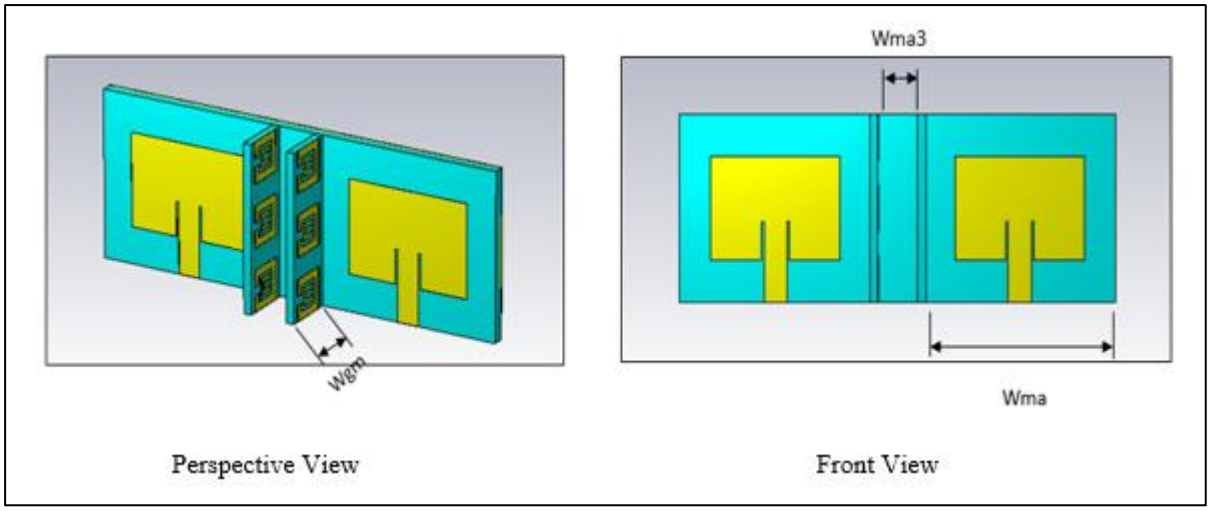

Figure 5:11: Double metasurface wall Antenna (Antenna 3).

5.4.1.3. Triple Metasurface Wall for M-Coupling Reduction (Antenna 4)

This design utilizes a triple metasurface wall placed vertically between the two radiating antenna elements for mutual coupling reduction. All three walls are identical to each other, they are placed at an equivalent distance of 2 *mm* from each other and they are at an equidistance of 3.75 *mm* from each antenna element. The distances were obtained based on the optimum results attained, from CST microwave studio. The optimized dimensions of this design are listed in Table 5.3 and its CST model is depicted in Figure 5.12.

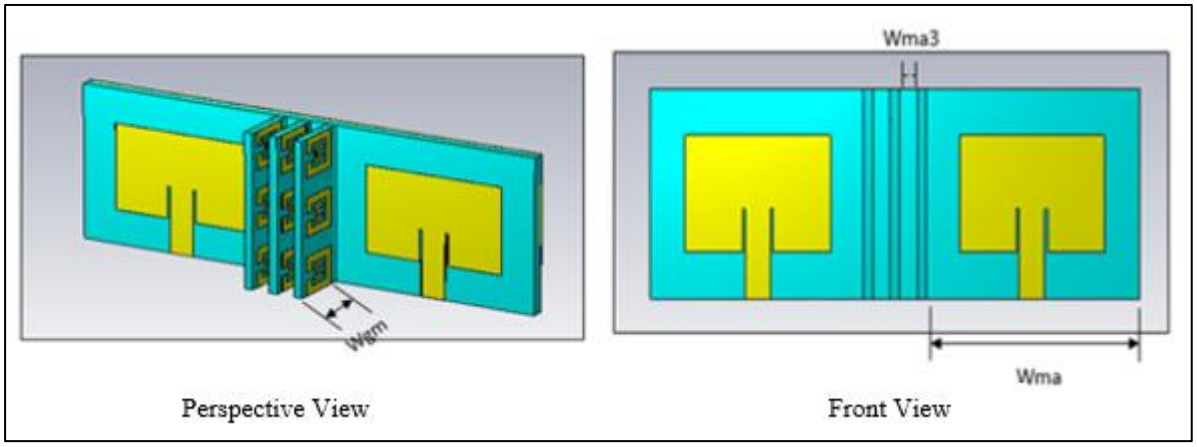

Figure 5:12: Triple metasurface wall antenna (Antenna 4).

Table 5.3: Design parameter of SRR metasurface wall, single metasurface wall antenna, double metasurface wall antenna and triple metasurface wall antenna (in mm).

Parameter	**Value**	**Parameter**	**Value**
Wgm	7.844	Hg	1.0
Wm1	5.06	Wma	24.0
Wm2	2.0	Wma2	2.0
Lm	20.382	Wma3	5.0
H	1.5	-	-

5.4.1.4. Results and Discussion

The single wall based metasurface antenna (Antenna 2), double wall based metasurface antenna (Antenna 3) and the triple wall based metasurface antenna (Antenna 4) are all simulated using CST microwave studio. Their simulation results, which include mutual coupling coefficient, reflection coefficient, gain, radiation pattern, radiation efficiency, directivity and envelope correlation coefficient are assessed, compared and discussed. The reflection coefficients of all four antennas including the reference microstrip antenna (Antenna 1) are depicted in Figure 5.13. From the figure, it can be observed that Antenna 2 and Antenna 3 show a significant reflection coefficient reduction of more than 10 *dB* for both S1,1 and S2,2 parameters. Antenna 4 can be seen to show significant bandwidth enhancement of up to 17% and 8% for S1,1 and S2,2 parameters, respectively in the frequency range (5.86-6.100) *GHz*. Additionally, it can be observed that all four antennas are well matched which means that no additional matching methods are required. Figure 5.14 depicts the mutual coupling coefficients all four antennas, a slight mutual coupling increase of 0.5 *dB* can be seen for Antenna 2. Antenna 3 and Antenna 4 can be observed not to show mutual coupling reduction over the entire bandwidth, but they do show major reduction at the center frequency. Antenna 3 achieves mutual coupling of -34 *dB* from -23 *dB*, which is equivalent to a total mutual coupling reduction of 11 *dB* while Antenna 4 achieves mutual coupling of -48 *dB* from -23 *dB*, which is equivalent to a total mutual coupling reduction of 25 *dB*.

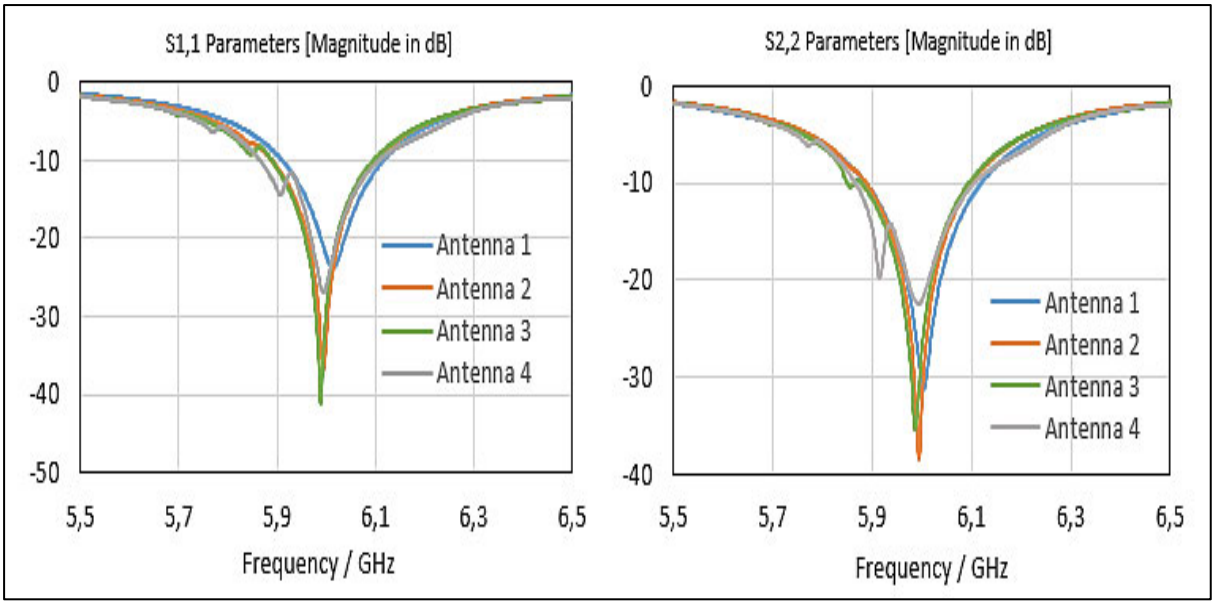

Figure 5:13: Reflection coefficients of reference and proposed antennas.

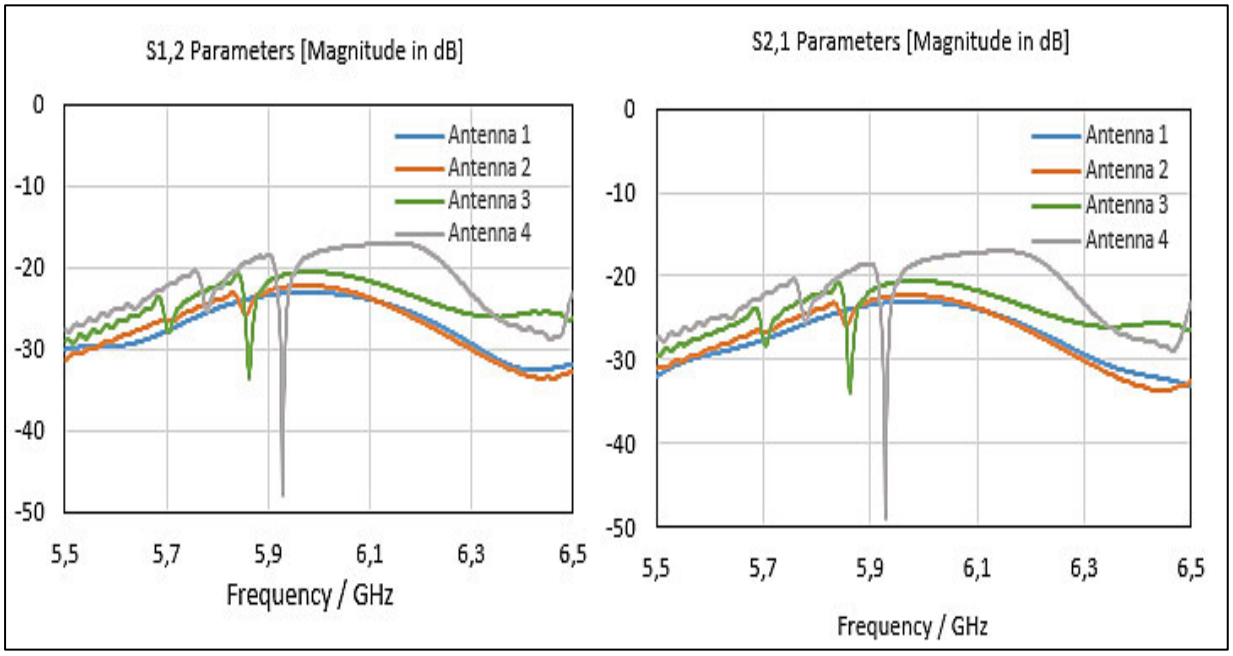

Figure 5:14: Mutual coupling coefficient of the reference and proposed antennas.

Figure 5.15 depicts the normalized radiation patterns of all four antennas, in the E-plane (Phi = 90°) and in the H-plane (Phi=0°) at 6 *GHz*. Table 5.4 lists the radiation parameters of all four antennas, which includes total radiation efficiency, main lobe direction, 3 *dB* beam width, radiation efficiency, maximum gain and maximum directivity. It can be observed from Figure 5.15 that the radiation pattern of all the three proposed antennas is highly maintained in both the E-plane and H-plane. This can be credited to the fact that no changes were made in the original structure of the reference antenna. It can also be observed from Table 5.4, that all the

metasurface wall based antennas show a slight increase in the 3 dB beam width at the H-plane and a slight decrease at the E-plane. A 2% increase in the total efficiency can be seen for Antenna 2 and 3, while the total efficiency of Antenna 4 remains the same as that of the reference antenna. This shows that the proposed designs are well matched. Meanwhile a slight decrease in the antenna's radiation efficiency of less than 5% can be observed for all three proposed antennas. The directivity of Antenna 2 can be seen to remain the same as that of the reference antenna, while a slight decrease and a slight increase can be observed for Antenna 3 and Antenna 4, respectively.

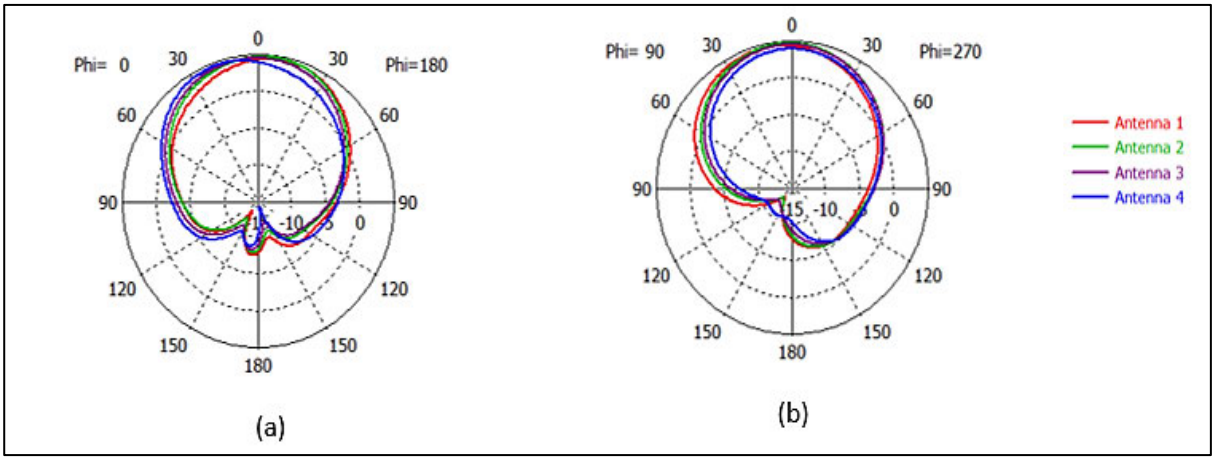

Figure 5:15: Normalized radiation patterns of reference antenna and the proposed antennas (a) in the H-plane (b) in the E-plane.

Table 5.4: Main lobe direction (in degrees), 3 dB beam width (in degrees), total efficiency, radiation efficiency, maximum gain (in dB) and maximum directivity (in dBi).

Antenna Parameter	**Antenna 1**	**Antenna 2**	**Antenna 3**	**Antenna 4**
Main lobe direction (phi = 0)	11	6	2	20
Main lobe direction (phi = 0)	12	4	2	1
3 *dB* Beam width (phi = 0)	93.1	94.3	99.3	94.0
3 *dB* Beam width (phi = 90)	99.1	98.4	97.6	96.3
Total Efficiency	70%	72%	72%	70%
Radiation Efficiency	75%	73%	72%	70%
Maximum Gain	4.7	4.75	4.52	4.7
Maximum Directivity	6.12	6.12	5.93	6.27

The realized gain at 6 *GHz* of all four antennas is depicted in Figure 5.16. It can be observed that Antenna 2 shows a slight increase in the gain value, while Antenna 3 shows a slight

decrease in the gain value. Antenna 4 can be observed to keep the same gain value of 4.7 *dB* at 6 *GHz* as the reference antenna. The envelope correlation coefficient (ECC) of a two-port MIMO antenna can be calculated from S-parameters using the equation (5.1). The envelope correlation coefficients of all four antennas is depicted in Figure 5.17. It can be observed that at 6 *GHz* all four antennas have an envelope correlation coefficient which is less than 0.01, which shows that the mutual coupling of the antennas is well reduced.

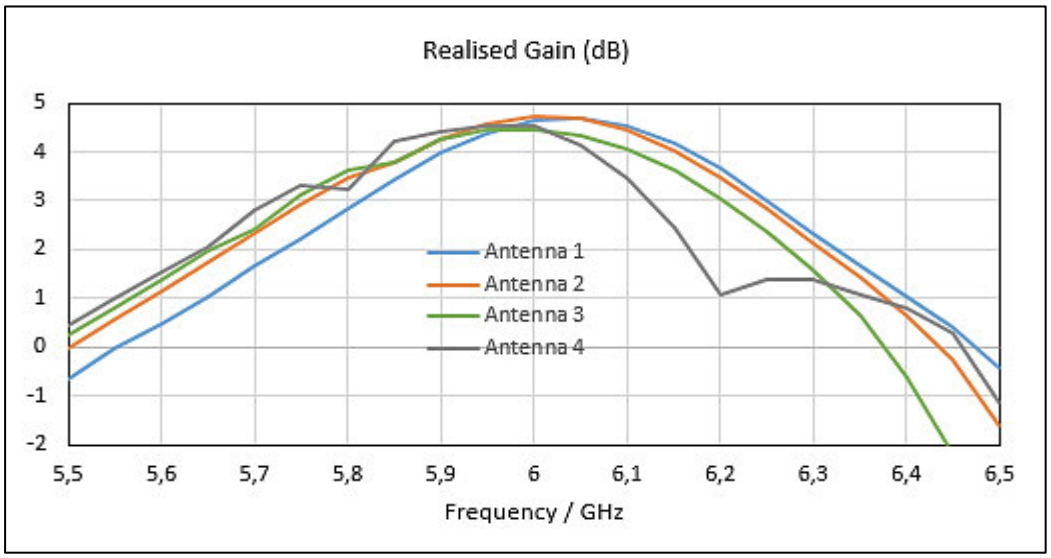

Figure 5:16: Realized gain of the reference and proposed antennas.

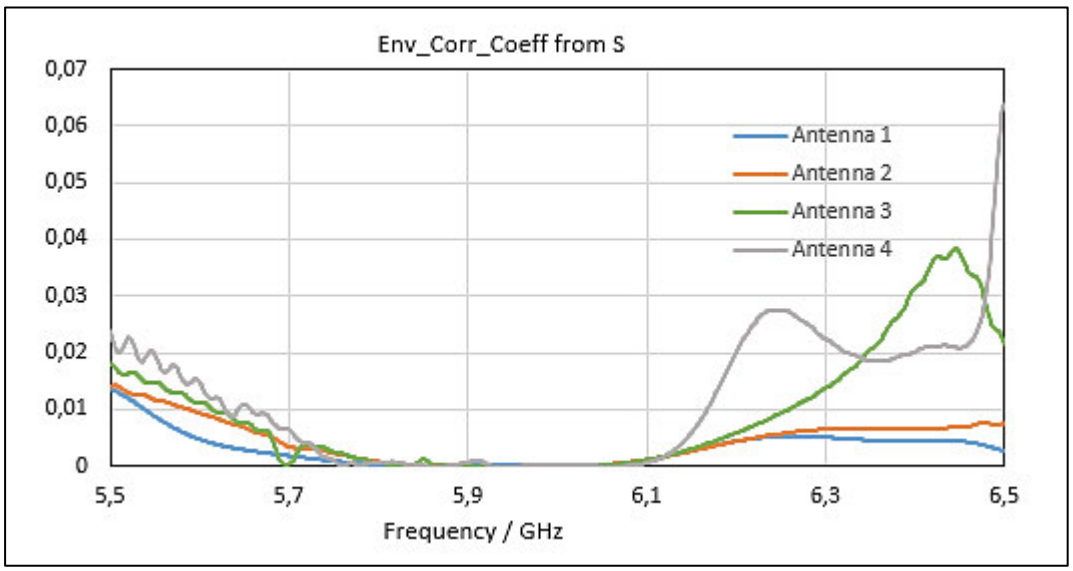

Figure 5:17: Envelope correlation coefficient of the reference and proposed antennas.

5.4.2. Metasurface Superstrate based Antenna for M-Coupling Reduction

Two metasurface superstrate based antenna designs are conducted in this section, their results are analyzed and compared for the best perfoming antenna. Both designs utilize the metasurface superstrate. The superstrate is made up of $4x7$ periodic SRR unit cells prited on one side of an FR-4 substrate , with a dielectric constant of 4.4, substrate height of 1.5 *mm*.The first design suspends a single metasurface superstrate above the two element antenna for m-coupling reduction (Antenna 5). The second design suspends a double metasurface superstrate above the two element antenna (Antenna 6).

5.4.2.1. Single Suspended Metasurface Superstrate for M-Coupling Reduction (Antenna 5)

This design employs a single metasurface superstrate suspended on top of the two-element microstrip antenna for mutual coupling reduction. The metasurface superstrate is suspended by four dielectric posts that are responsible for providing support. It is placed at a height of 6.5 *mm* from the two-element antenna. Its CST model is depicted in Figure 5.18. To validate the theoretical aspect of this design, its prototype is fabricated and measured. Figure 5.19 depicts the fabricated prototype of Antenna 5.The design parameters of this antenna are also listed in Table 5.5.

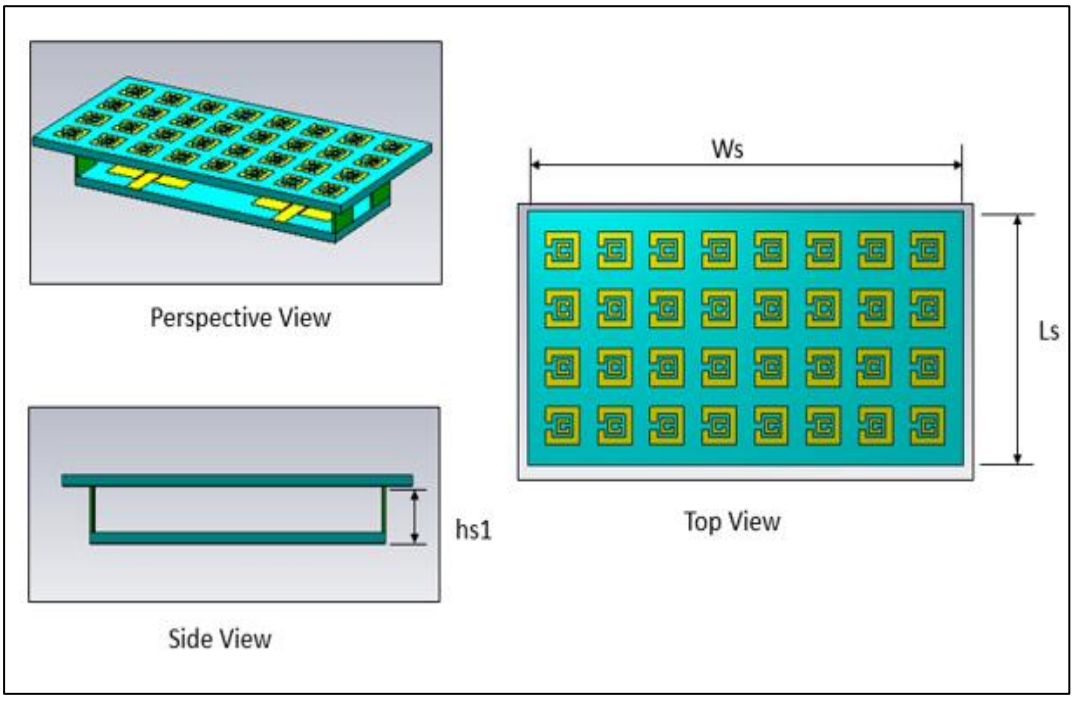

Figure 5:18: Single suspended metasurface antenna (Antenna 5).

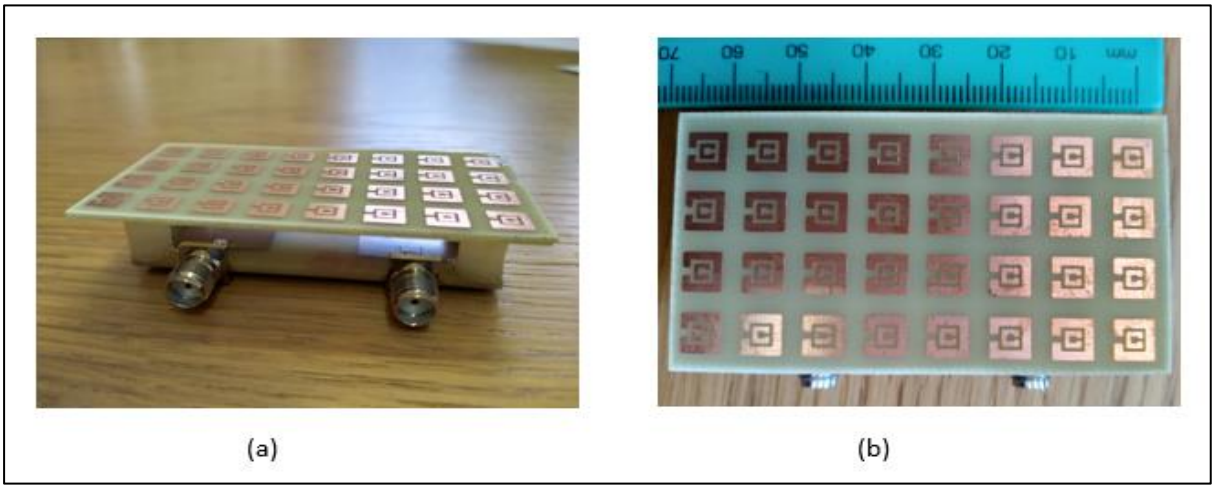

Figure 5:19: (a) Perspective view, (b) top view of fabricated Antenna 5 prototype.

5.4.2.2. Double Suspended Metasurface Superstrate for M-Coupling Reduction (Antenna 6)

This design employs a double metasurface superstrate, suspended above the two-port microstrip antenna for mutual coupling reduction. Both metasurface superstrates are suspended using dielectric posts for providing support. The first metasurface is suspended at a height of 6.5 *mm* from the microstrip antenna, while the second metasurface superstrate is suspended at a height of 3 *mm* from the first metasurface superstrate. Its CST model is depicted in Figure 5.20. To validate the theoretical aspect of this design, its prototype is fabricated and measured. Figure 5.21 depicts the fabricated prototype of Antenna 6. Its design parameters are also listed in Table 5.5.

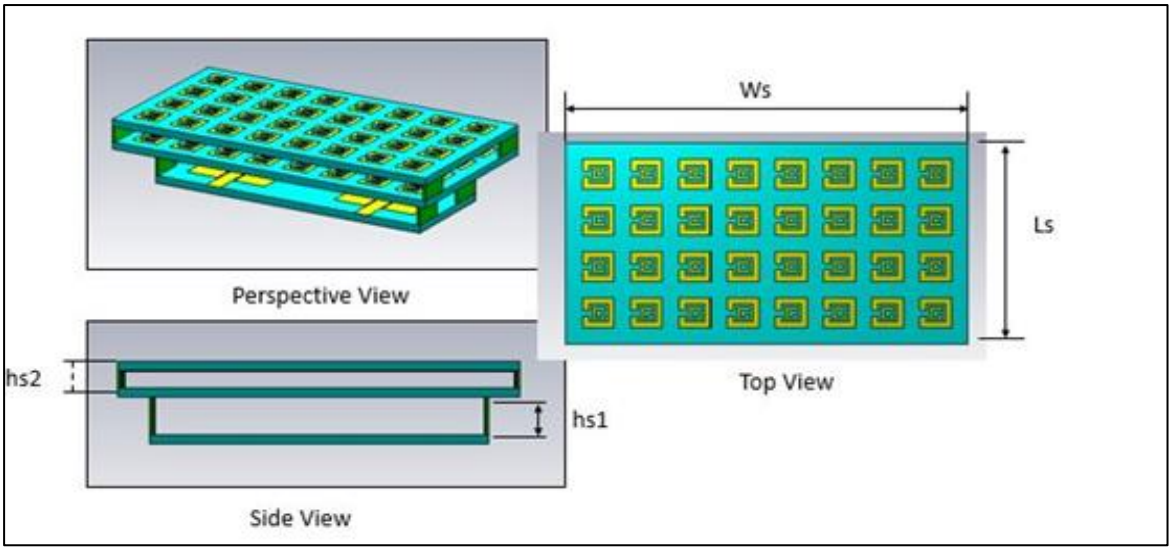

Figure 5:20: CST model of the double suspended metasurface antenna (Antenna 6).

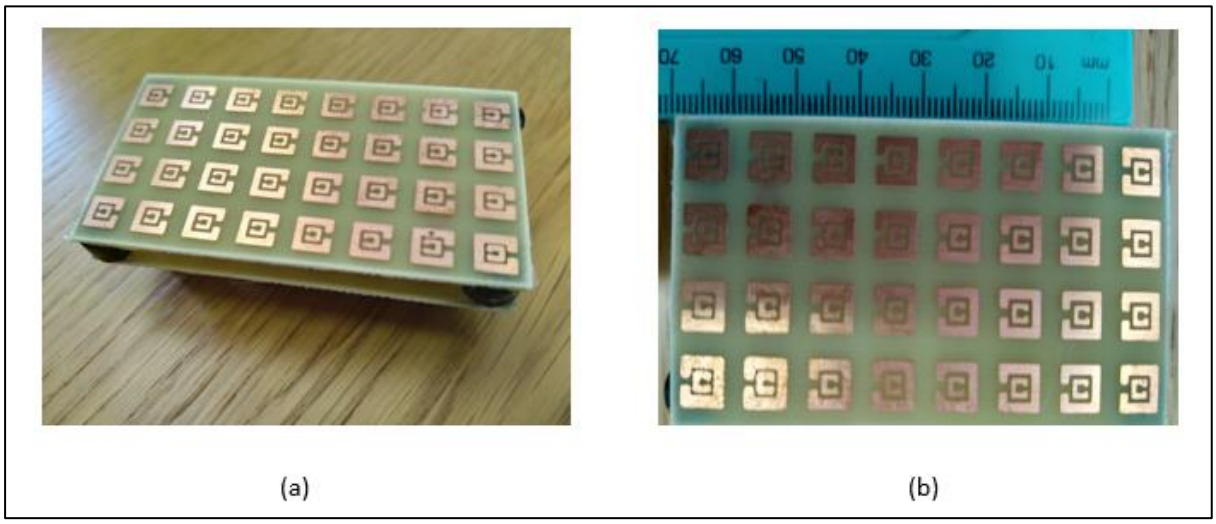

Figure 5:21: (a) Perspective view, (b) Side view of fabricated Antenna 6 prototype.

Table 5.5: Design parameters of Antenna 2 and Antenna 3 (in mm).

Parameter	**Value**
Ws	65
Ls	33.862
Hs1	6.5
Hs2	3

5.4.2.3. Results and Discussion

The single suspended metasurface superstrate based antenna (Antenna 5) and the double suspended metasurface superstrate based antenna (Antenna 6) are simulated using CST microwave studio. Their simulation results, which include the mutual coupling coefficient, reflection coefficient, radiation pattern, gain, directivity, radiation efficiency, and envelope correlation coefficient, are assessed, compared and discussed. Antenna 5 and Antenna 6 were fabricated and a vector network analyzer was used to measure the reflection coefficients and mutual couplings of the fabricated antenna prototypes, the obtained results are then compared to the simulated results.

The simulated reflection coefficients of the reference microstrip antenna (Antenna 1), Antenna 5 and Antenna 6 are depicted in Figure 5.22. It can be observed from the figure that Antenna 5 is not well matched and requires additional matching methods when compared to the reference antenna. This is because its reflection coefficients show a significant increase of 10 *dB* from -24 *dB* to -14 *dB*. Moreover, a 49% bandwidth reduction for S1,1 parameter and a

43% bandwidth reduction for S2,2 can be seen in the frequency range of (6.05-6.15) *GHz*. However, Antenna 6 can be seen to be well matched with a 38% bandwidth enhancement for S1,1 parameter and a 17% bandwidth enhancement for S2,2 parameters in the frequency range of (5.92-6.2) *GHz*.

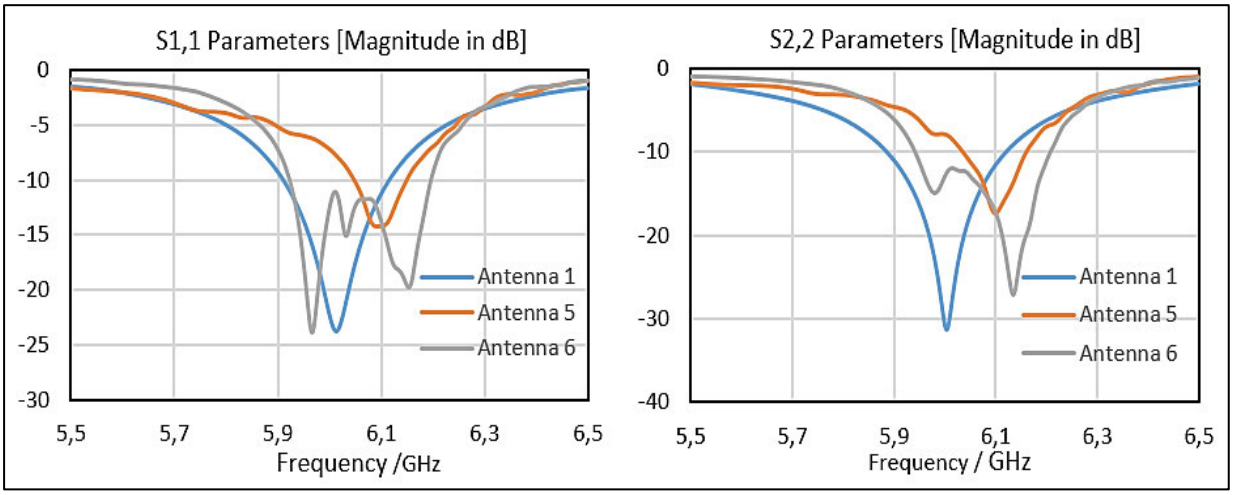

Figure 5:22: Simulated reflection coefficients of the reference antenna and proposed antennas.

Figure 5.23 depicts the m-coupling of Antenna 1, Antenna 5 and Antenna 6. It can be observed that both metasurface based antennas, drastically reduces the mutual coupling of Antenna 1 over the entire bandwidth. Antenna 5 shows m-coupling reduction from -29 *dB* to -60.6 *dB*, which equates to a total mutual coupling reduction of 31.6 *dB*. Antenna 6 shows maximum mutual coupling reduction from -24 *dB* to -46 *dB*, which equates to a total mutual coupling reduction of 22 *dB*.

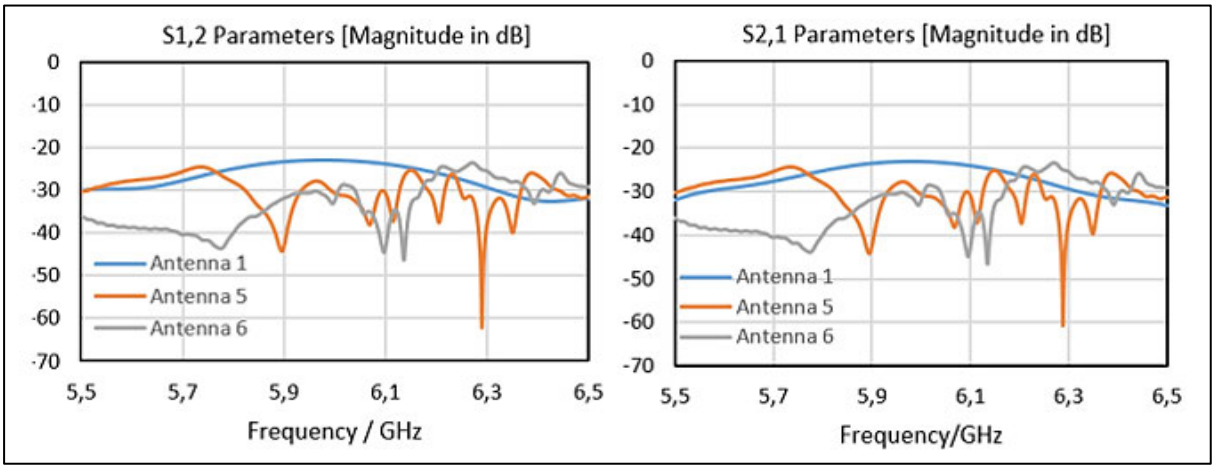

Figure 5:23: Mutual coupling coefficients of the reference antenna and proposed antennas.

Figure 5.24 depicts the simulated and measured S-parameters of Antenna 5. From the figure, the measured and simulated reflection coefficients can be observed to be quite similar, while the measured mutual coupling S-parameters can be observed to be slightly less than the simulated mutual coupling S-parameters. Figure 5.25 depicts the simulated and measured S-parameters of Antenna 6. From the figure it can be seen that the simulated and measured reflection coefficients are quite similar, while the measured mutual coupling S-parameters can be observed to be slightly less than the simulated mutual coupling S-parameters. Minor discrepancies can be seen between the simulated S-parameters and the measured S-parameters in all three-antenna prototypes, these discrepancies can be attributed to soldering residue, vector network analyzer calibration, fabrication and assembly error.

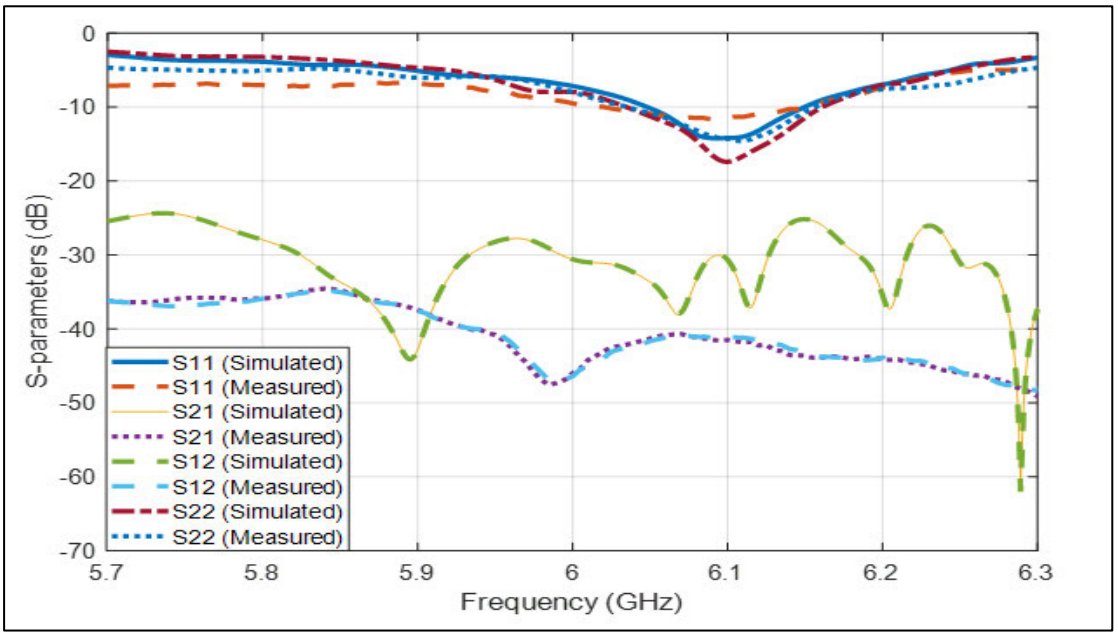

Figure 5:24: Simulated and measured S-parameters of Antenna 5.

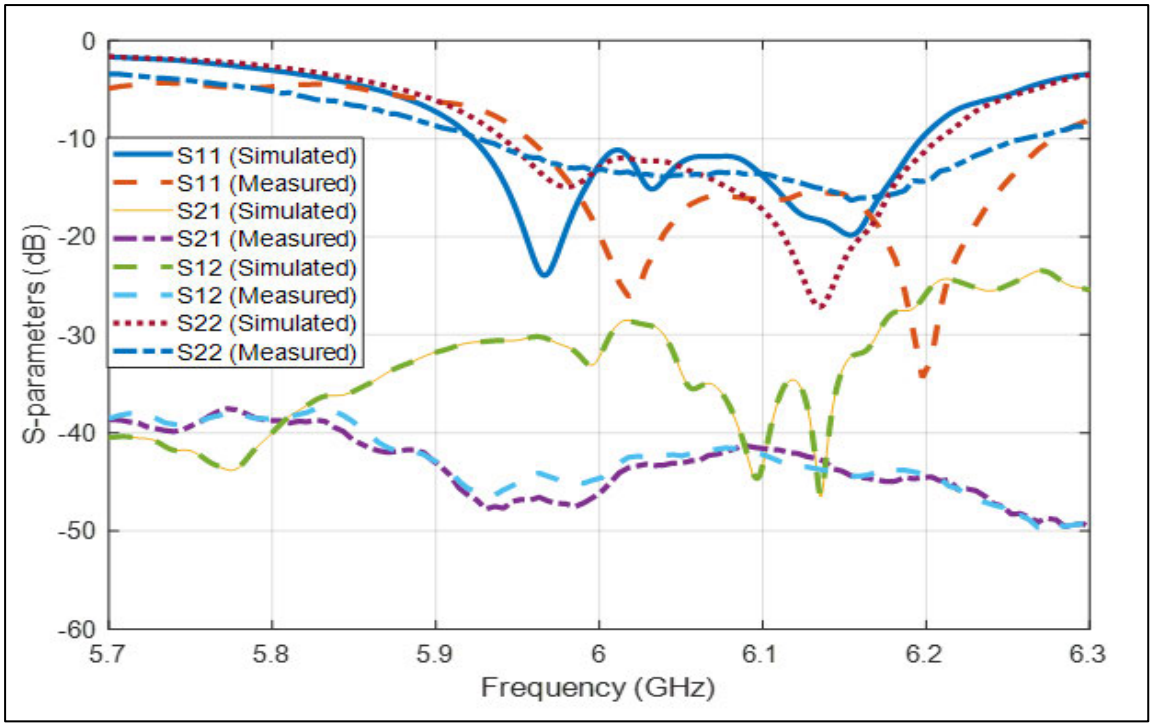

Figure 5:25:Simulated and measured S-parameters of Antenna 6.

Figure 5.26 depicts the normalized radiation pattern of Antenna 1, Antenna 5 and Antenna 6 in the H-plane (Phi = 0°) and E-plane (Phi = 90°) at 6 *GHz*. The radiation parameters of the three antennas, which include the 3 *dB* beam width, main lobe direction, radiation efficiency, total radiation efficiency, maximum directivity and maximum gain, are listed in Table 5.6. It can be observed from Figure 5.26 that the radiation pattern of Antenna 5 in the E-plane is highly distorted, while, the radiation pattern of Antenna 6 is more directive compared to that of the reference antenna. This increase in directivity can also be seen by a major gain enhancement of up to 2.09 *dB*, an increase in maximum directivity and a slight 3 *dB* beam width reduction. However, the H-plane radiation pattern of both metasurface superstrate based antenna can be seen to be highly maintained.

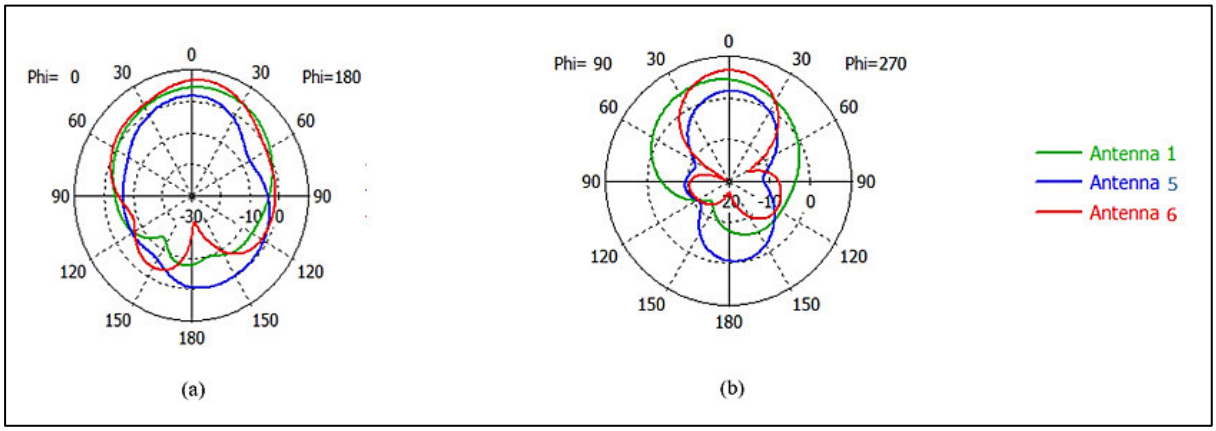

Figure 5:26: Normalized radiation patterns of reference antenna and the proposed antennas (a) in the H- plane (b) In the E-plane.

From Table 5.6 a significant decrease in fifth antenna's total efficiency from 70% to 26% can be seen, this again highlights that Antenna 5 is poorly matched. Antenna 6 also shows a 15% reduction in antenna's total efficiency from 70% to 55%. However, this is still acceptable because the antenna's efficiency is greater than 50%.

Table 5.6: Main lobe direction (in degrees), 3dB beam width (in degrees), total efficiency, radiation efficiency, maximum gain (in dB) and maximum directivity (in dBi).

Antenna Parameters	**Antenna 1**	**Antenna 2**	**Antenna 3**
Main lobe direction (phi= 0)	11	1	6
Main lobe direction (phi= 90)	12	3	0
3 *dB* Beam Width (phi= 0)	93.1	65.4	53.9
3 *dB* Beam Width (phi= 90)	99.1	61.9	50.1
Total Efficiency	70%	26%	55%
Radiation Efficiency	75%	32%	55%
Maximum Gain	4,7	1.69	6.79
Maximum Directivity	6.12	6.6	9.24

The realized gain of Antenna 1, Antenna 5 and Antenna 6 is depicted in Figure 5.27. From the figure, a significant gain reduction in Antenna 5 can be seen over the entire bandwidth when compared to the reference antenna. At 6 *GHz* a gain reduction of 3.01 *dB*, from 4.7 *dB* to 1.69 *dB* can be seen. However, Antenna 6 shows a significant gain enhancement from 4.7 *dB* to 6.79 *dB*. This is equivalent to a gain enhancement of 2.09 *dB*, when compared to the reference microstrip antenna. This also highlights the effectiveness of the mutual coupling reduction method applied. The envelope correlation coefficients of Antenna 1, Antenna 5 and Antenna 6 are depicted in Figure 5.28. It can be observed that at 6 *GHz* the envelope correlation

coefficient of all three antennas is less than 0.01. This validates that the two employed metasurface superstrate based microstrip antennas are effective and significantly reduce mutual coupling.

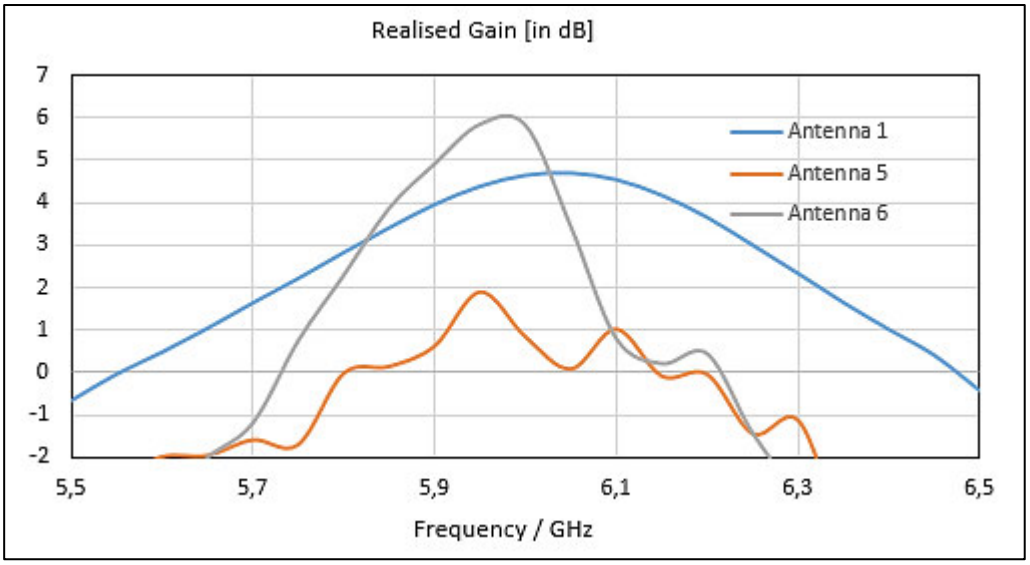

Figure 5:27: Realized gain of the reference antenna and the proposed antenna.

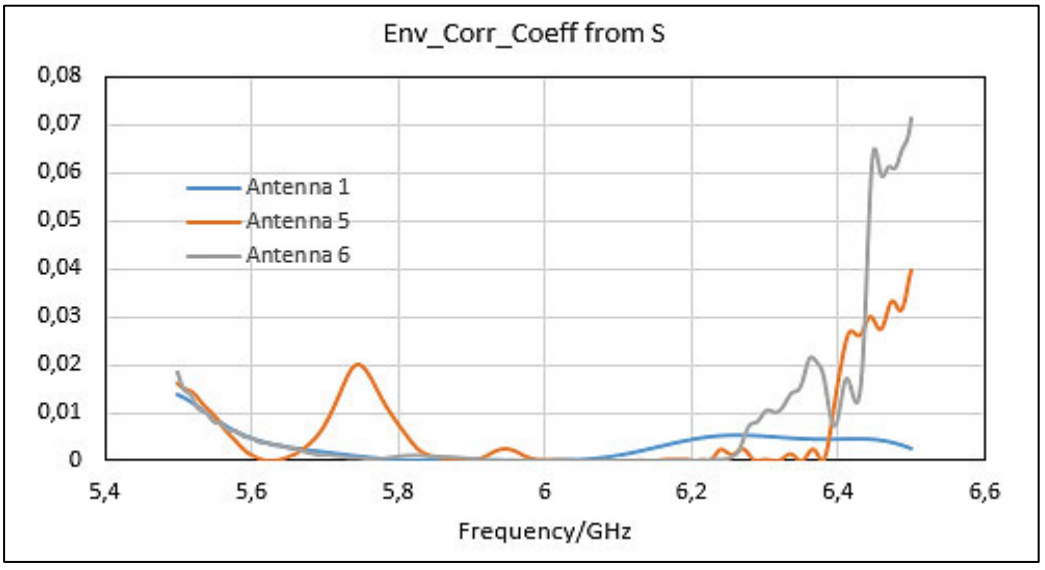

Figure 5:28:Envelope correlation coefficient of the reference antenna and the proposed antennas.

Table 5.7 below, compares the performance of all five metasurface-based antenna designs.

Table 5.7: Lists the performance of the five metasurface based antenna designs.

Parameter	**Antenna 2**	**Antenna 3**	**Antenna 4**	**Antenna 5**	**Antenna 6**
M-coupling Reduction	-	11 *dB*	25 *dB*	31.6 *dB*	22 *dB*
Gain Enhancement	-	-	-	-	2.09 *dB*
Bandwidth Enhancement	-	-	17%	-49%	38%
Total Efficiency	72%	72%	70%	26%	55%
Maximum Directivity	6.12 *dBi*	5.93 *dBi*	6.27 *dBi*	6.6 *dBi*	9.24 *dBi*

Table 5.8 compares the proposed metasurface-based antenna design (Antenna 6) with other decoupling methods. These methods are the recent mutual decoupling works and they include defected ground structures (DGS), defected ground structures (DGS) and metamaterials structures (MTM).

Table 5.8: Comparison of the proposed antenna with related works.

Case	**[10]**	**[15]**	**[27]**	**Proposed Antenna**
Method Used	EBG	DGS	MTM	MTS
Edge to edge separation	$0.75\lambda_o$	$0.116\lambda_o$	$0.13\lambda_o$	$0.29\lambda_o$
Mutual coupling reduction	6 *dB*	10 *dB*	18 *dB*	22 *dB*
Gain enhancement	-	-	-	2.09 *dB*

5.4.3. Chapter Summary

Five metasurface-based antenna designs were conducted for the purpose of reducing mutual coupling between a 2-port rectangular microstrip antenna. The first three antenna designs utilized a metasurface wall placed vertically between the two antenna elements, while the last two antenna designs utilized a metasurface superstrate suspended above the 2-port antenna. The first metasurface wall based antenna design (Antenna 2) was achieved by, placing a single metasurface wall vertically in between the two antenna elements. The second (Antenna 3) and third (Antenna 4) metasurface wall based antenna designs. Are achieved by placing double and triple metasurface walls vertically between the two radiating antenna elements, respectively.

The first metasurface superstrate based antenna design (Antenna 5) was achieved by suspending a single metasurface superstrate above the two radiating antenna elements. Lastly, the second metasurface superstrate based antenna design (Antenna 6) was achieved by suspending a double metasurface superstrate above the two-element antenna. The metasurface wall and the metasurface superstrate are made up of, periodic split ring resonators printed on a FR-4 dielectric substrate. The metasurface is responsible for introducing a negative permeability medium. The medium converts the propagating electromagnetic waves into evanescent, hence rejecting mutual coupling between the radiating antenna elements.

From Table 5.7 it can be seen that the single metasurface wall based antenna design (Antenna 2) does not reduce mutual coupling. Instead, it increases it by 0.5 *dB* hence proving to be inefficient for this application. The double metasurface wall based design (Antenna 3) and the triple metasurface wall based design (Antenna 4) displayed, significant mutual coupling reduction at the center frequency. Antenna 3 reduced mutual coupling from -23 *dB* to -34 *dB*, which is equivalent to a total mutual coupling reduction of 11 *dB*. Antenna 4 displayed mutual coupling reduction from -23 *dB* to -48 *dB*, which is equivalent to a total mutual coupling reduction of 25 *dB*. Additional to that Antenna 4 also displayed a bandwidth enhancement of up to 17%. Unfortunately, Antenna 3 and Antenna 4 do not display mutual coupling reduction over the entire bandwidth, but only at the center frequency.

Antenna 5 and Antenna 6 achieve significant m-coupling reduction over the entire bandwidth. Antenna 5 achieved an m-coupling reduction of 31.6 *dB*. However, it also displayed a 10 *dB* increase in the reflection coefficient, a 49% reduction in bandwidth and a 3.01 *dB* reduction in gain. This clearly shows that this design is not suitable for this application; the antenna is not well matched. It requires additional matching methods to achieve the required results. Unfortunately, additional matching methods are undesired because they increase fabrication costs and complexities. Antenna 6 achieved an m-coupling reduction of 22 *dB*, a 38% increase in bandwidth and a 2.09 *dB* increase in gain. It reduces the m-coupling between the two microstrip antenna elements and achieves enhancements on both the antenna bandwidth and gain, without a need of any additional matching methods. Hence proving to be less complex in terms of fabrication and costs. Antenna 1, Antenna 5 and Antenna 6 were fabricated and measured using a vector network analyzer. The measured results are quite similar to the simulated resulted. Minor discrepancies were observed, which are mainly because of the soldering residue between Antenna and the SMA connector and fabrication and assembly error

It can be seen from table 5.8 that the proposed antenna, is quite effective in reducing mutual coupling when compared to the other decoupling methods. Moreover, the proposed work also shows some major advantages when compared to other works i.e. significant gain improvement.

Chapter 6 : Conclusion and Future Work

This chapter concludes on the overall work conducted in this thesis. It also recommends work that can be further researched in the future.

6.1. Conclusion

In this thesis, five metasurface-based antenna designs were conducted for the purpose of reducing mutual coupling between a 2-port MIMO microstrip antenna. These designs were then compared for the best performing antenna. Three single element microstrip antennas with different geometries and feeding methods were first designed. This was done to get the best performing single element antenna to use in the 2-port MIMO microstrip antenna design. The first single element antenna design conducted was the rectangular inset fed microstrip antenna (RIA). The second design was the rectangular probe fed microstrip antenna (RPA). Finally, the last design was the triangular inset fed microstrip antenna (TIA). The first design (RIA) was found to be the best performing antenna with the smallest return loss of -21.82 *dB*, Followed by the third design (TIA) with the return loss of -17.30 *dB*. The second design (RPA) came in last with an unacceptable return loss of -7.72 *dB*. The first design, which is the rectangular inset fed microstrip antenna, was then used for the 2-port MIMO microstrip antenna design. The 2-port rectangular microstrip antenna obtained mutual coupling parameters of -23.06 *dB*. The metasurface-based antenna designs were then employed to reduce the mutual coupling of the 2-port antenna.

Firstly, a high impedance, MNG (negative permeability and positive permittivity) metasurface was designed. This type of metasurface was designed because of its ability to reject wave propagation in certain frequency bands, hence reducing mutual coupling between the radiating antenna elements. This metasurface was then applied in the metasurface-based antenna designs. The first three metasurface-based antenna designs were formulated by inserting a metasurface wall in between the two antenna elements, while the last two metasurface based antenna designs were formulated by suspending a metasurface superstrate above the two-port antenna. The metasurface wall based antenna designs achieved acceptable results in terms of mutual

coupling reduction. The second (Antenna 3) and third (Antenna 4) metasurface wall based antenna designs achieved mutual coupling reduction of 11 *dB* and 25 *dB,* respectively. However, they did not show mutual coupling reduction over the entire bandwidth. Hence, they are not highly preferred for this application. The double suspended metasurface superstrate based antenna design (Antenna 6) obtained a mutual coupling reduction of 22 *dB* over the entire bandwidth. Additional to that it also obtained a 38% bandwidth increase and a 2.09 *dB* gain increase, without a need of additional matching methods. Hence, proving to be the best performing antenna when compared to the other four metasurface-based antenna designs. It also shows great performance when compared to other recent mutual coupling works because it is well matched with a highly maintained radiation pattern. This eliminates the need of any additional matching methods, which are undesired because they increase fabrication costs and complexities. Additionally, it also enhances the overall performance of the antenna i.e. significantly increases bandwidth and gain.

6.2. Future Works

For future research one can look at, the limit of metasurface walls and metasurface superstrate one can fit before they stop reducing mutual coupling. This will obviously depend on the available surface area between the radiating antenna elements and the available height above the antenna. These designs utilized an SRR metasurface for mutual coupling reduction because it is a 2D structure, hence it is less complicated to fabricate and it costs less. If costs and fabrication complexities are not a limiting factor, one can look at combining other mutual coupling reduction methods with this type of design. Mutual coupling methods that do not change the original structure of the antenna would be recommended. This is because the radiation pattern of the antenna is not affected, and the design can be implemented on already existing antennas without changing the whole antenna design i.e. 1D EBG structure, MTM-EBG decoupling slabs.

References

[1] M. Rouse, “What is MIMO,” pp. 4–7, 2020, [Online]. Available: https://searchmobilecomputing.techtarget.com/definition/MIMO.

[2] Hong-Chuan Yang, “Multipath fading,” *Introd. to Digit. Wirel. Commun.*, pp. 33–54, 2017, doi: 10.1049/pbte072e_ch3.

[3] E. Munoz and R. Murch, “‘ 2 . 4 GHz MIMO Antenna on Microstrip Technology ’ 2 . 4 GHz MIMO Antenna on Microstrip Technology,” 2009.

[4] E. Ghayoula, A. Bouallegue, and R. Ghayoula, “Capacity and Perfomance of MIMO system for wireless Communications,” vol. 7, no. 3, pp. 108–111, 2014

[5] F. DeFlaviis, L. Jofre, J. Romeu, and A. Grau, *Multi-Antenna Systems for MIMO Communications*. .

[6] “Design of Microstrip Antennas for 2 × 2 Mimo Systems,” pp. 40–92.

[7] Q. Wang, N. Mu, LingLi Wang, S. Safavi, and JingPin, “5G Confrormal Antenna,” vol. 2020, pp. 1–17, 2020.

[8] Electronics Notes, “what is MIMO Wireless Technology O -Multiple Input Multiple Output basics,” pp. 3–5, 2020, [Online]. Available: https://www.electronics-notes.com/articles/antennas-propagation/mimo/what-is-mimo-multiple-input-multiple-output-wireless-technology.php

[9] D. Gesbert and J. Akhtar, “Breaking the barriers of Shannon’s capacity: An overview of MIMO wireless systems,” *Signal Processing*, pp. 1–9, 2002, [Online]. Available: http://citeseerx.ist.psu.edu/viewdoc/download?doi=10.1.1.18.3414&rep=rep1&type=pdf.

[10] F. DeFlaviis, L. Jofre, J. Romeu, and A. Grau, *Multi-Antenna Systems for MIMO Communications*. .

[11] A. Sibille, C. Oestges, and A. Zabella, *From theory to implementation*, vol. 105, no. 28. 2008.

[12] A. EL Zooghby, *Smart Antenna Engineering*, vol. 53, no. 9. 2008.

[13] Z. Wang, L. Zhao, Y. Cai, S. Zheng, and Y. Yin, “A Meta-Surface Antenna Array Decoupling (MAAD) Method for Mutual Coupling Reduction in a MIMO Antenna System,” *Sci. Rep.*, no. September 2017, pp. 1–9, 2018, doi: 10.1038/s41598-018-21619-z.

[14] J. Tang *et al.*, “A Metasurface Superstrate for Mutual Coupling Reduction of Large Antenna Arrays,” *IEEE Access*, vol. 8, pp. 126859–126867, 2020, doi: 10.1109/ACCESS.2020.3008162..

[15] H. Luan, C. Chen, W. Chen, L. Zhou, H. Zhang, and Z. Zhang, “Mutual coupling reduction of closely E/H-Plane coupled antennas through metasurfaces*,” IEEE Antennas Wirel. Propag. Lett., vol. 18, no. 10, pp. 1996–2000, 2019, doi: 10.1109/LAWP.2019.2936096.*

[16] Kubacki, R., Lamari, S., Czyhewski, M., Laskowski, D., “A broadband left-handed metamaterial microstrip antenna with double-fractal layers”, *International Journal of Antennas and Propagation, vol. 2017, pp. 1-6, 2017.*

[17] M. Alibakhshikenari *et al.*, “Meta-surface wall suppression of mutual coupling between microstrip patch antenna arrays for THz-band applications,” *Prog. Electromagn. Res. Lett.*, vol. 75, pp. 105–111, 2018, doi: 10.2528/pierl18021908.

[18] X. M. Yang, X. G. Liu, X. Y. Zhou, and T. J. Cui, “Reduction of mutual coupling between closely packed patch antennas using waveguided metamaterials,” *IEEE Antennas Wirel. Propag. Lett.*, vol. 11, pp. 389–391, 2012, doi: 10.1109/LAWP.2012.2193111.

[19] F. Yang and Y. Rahmat-Samii, “Microstrip Antennas Integrated with Electromagnetic

Band-Gap (EBG) Structures: A Low Mutual Coupling Design for Array Applications," *IEEE Trans. Antennas Propag.*, vol. 51, no. 10 II, pp. 2936–2946, 2003, doi: 10.1109/TAP.2003.817983.
[20] M. M. and J. Kelly, "in N Ovations in Labor Mar Ket in Formation an D Thei R Ap P L I Cati on," vol. 7, no. 6, p. 16, 2012.
[21] P. S. Kildal, "Metasurfaces for Antennas," no. October, pp. 5–9, 2015.
[22] F. Ding, A. Pors, and S. I. Bozhevolnyi, "Gradient metasurfaces: A review of fundamentals and applications," *Reports Prog. Phys.*, vol. 81, no. 2, 2018, doi: 10.1088/1361-6633/aa8732.
[23] S. S. Bukhari, J. Vardaxoglou, and W. Whittow, "A metasurfaces review: Definitions and applications," *Appl. Sci.*, vol. 9, no. 13, 2019, doi: 10.3390/app9132727.
[24] H. T. Chen, A. J. Taylor, and N. Yu, "A review of metasurfaces: Physics and applications," *Reports Prog. Phys.*, vol. 79, no. 7, 2016, doi: 10.1088/0034-4885/79/7/076401.
[25] A. P. Feresidis, G. Goussetis, S. Wang, and J. C. Vardaxoglou, "Artificial magnetic conductor surfaces and their application to low-profile high-gain planar antennas," *IEEE Trans. Antennas Propag.*, vol. 53, no. 1 I, pp. 209–215, 2005, doi: 10.1109/TAP.2004.840528.
[26] G. Expósito-Domínguez, J. M. Fernández-González, P. Padilla, and M. Sierra-Castañer, "EBG size reduction for low permittivity substrates," *Int. J. Antennas Propag.*, vol. 2012, 2012, doi: 10.1155/2012/106296.
[27] I. Mohamed and M. Abdalla, "Reduced Size Mushroom Like EBG for Antenna Mutual Coupling Reduction," *32nd Natl. RADIO Sci. Conf.*, vol. 32, no. Nrsc, pp. 57–64, 2015.
[28] V. Ionescu, M. Hnatiuc, and A. TopalĂ, "Optimal design of mushroom-like EBG structures for antenna mutual coupling reduction in 2.4 GHz ISM band," *2015 E-Health Bioeng. Conf. EHB 2015*, pp. 19–22, 2016, doi: 10.1109/EHB.2015.7391559.
[29] F. Benykhlef and N. Boukli, "EBG structures for reduction of mutual coupling in patch antennas arrays," *J. Commun. Softw. Syst.*, vol. 13, no. 1, pp. 9–14, 2017, doi: 10.24138/jcomss.v13i1.242.
[30] B. Yin, X. Feng, and J. Gu, "A Metasurface Wall for Isolation Enhancement," *IEEE Antennas Propag. Mag.*, no. February, pp. 14–22, 2020, doi: 10.1109/MAP.2019.2943299.
[31] D. Guha, S. Biswas, M. Biswas, J. Y. Siddiqui, and Y. M. M. Antar, "Concentric ring-shaped defected ground structures for microstrip applications," *IEEE Antennas Wirel. Propag. Lett.*, vol. 5, no. 1, pp. 402–405, 2006, doi: 10.1109/LAWP.2006.880691.
[32] F. Zulkifli, E. Rahardjo, and D. Hartanto, "Mutual coupling reduction using dumbbell defected ground structure for multiband microstrip antenna array," *Prog. Electromagn. Res. Lett.*, vol. 13, pp. 29–40, 2010.
[33] Q. C. Zhang, J. D. Zhang, and W. Wu, "Reduction of mutual couing between cavity-backed slot antenna elements," *Prog. Electromagn. Res. C*, vol. 53, no. 6, pp. 27–34, 2014, doi: 10.2528/PIERC14052908.
[34] M. I. Ahmed, A. Sebak, E. A. Abdallah, and H. Elhennawy, "Mutual coupling reduction using defected ground structure (DGS) for array applications," *2012 15th Int. Symp. Antenna Technol. Appl. Electromagn. ANTEM 2012*, 2012, doi: 10.1109/ANTEM.2012.6262354
[35] G. Dadashzadeh, A. Dadgarpour, F. Jolani, and B. S. Virdee, "Mutual coupling suppression in closely spaced antennas," *IET Microwaves, Antennas Propag.*, vol. 5, no. 1, pp. 113–125, 2011, doi: 10.1049/iet-map.2009.0564.
[36] F. G. Zhu, J. Xu, and Q. Xu, "Reduction of mutual coupling between closely-packed antenna elements using defected ground structure," *Proc. - 2009 3rd IEEE Int. Symp.*

Microwave, Antenna, Propag. EMC Technol. Wirel. Commun. MAPE 2009, pp. 1–4, 2009, doi: 10.1109/MAPE.2009.5355659.
[37] L. Zhao and K. Wu, "A Decoupling Technique for Four-Element Symmetric Arrays With Reactively Loaded Dummy Elements," *IEEE Trans. Antennas Propag.*, vol. 62, no. 8, pp. 4416–4421, 2014.
[38] L. Zhao and K. Wu, "A Dual-Band Coupled Resonator Decoupling Network for Two Coupled Antennas," *IEEE Antennas Propag. Mag.*, vol. 63, no. 7, pp. 2843–2850, 2015..
[39] M. M. Antenna, C. F. Ding, X. Y. Zhang, S. Member, and C. Xue, "Novel Pattern-Diversity-Based Decoupling Method and Its Application to," vol. 66, no. 10, pp. 4976–4985, 2018.
[40] W. Chen and H. Lin, "LTE700 / WWAN MIMO Antenna System Integrated with Decoupling Structure for Isolation Improvement," *IEEE*, pp. 689–690, 2014.
[41] M. S. Khan, A. Capobianco, A. I. Najam, I. Shoaib, E. Autizi, and M. Farhan, "Compact ultra-wideband diversity antenna with a floating parasitic digitated decoupling structure," *IET Microwaves, Antennas Propag.*, no. January, pp. 747–753, 2014, doi: 10.1049/iet-map.2013.0672...
[42] R. Xia, S. Qu, S. Member, P. Li, Q. Jiang, and Z. Nie, "An Efficient Decoupling Feeding Network for Microstrip Antenna Array," *IEEE Antennas Wirel. Propag. Lett.*, vol. 14, pp. 871–874, 2015.
[43] B. C. Pan, W. X. Tang, M. Q. Qi, H. F. Ma, Z. Tao, and T. J. Cui, "Reduction of the spatially mutual coupling between dual-polarized patch antennas using coupled metamaterial slabs," *Sci. Rep.*, vol. 6, no. 4, pp. 1–8, 2016, doi: 10.1038/srep30288.
[44] Q. Le Zhang, Y. T. Jin, J. Q. Feng, X. Lv, and L. M. Si, "Mutual coupling reduction of microstrip antenna array using metamaterial absorber," *2015 IEEE MTT-S Int. Microw. Work. Ser. Adv. Mater. Process. RF THz Appl. IEEE MTT-S IMWS-AMP 2015 - Proc.*, 2015, doi: 10.1109/IMWS-AMP.2015.7324947.
[45] H. Kondori, M. A. Mansouri-birjandi, and S. Tavakoli, "Reducing Mutual Coupling in Microstrip Array Antenna Using Metamaterial Spiral Resonator," *Int. J. Comput. Sci. Issues*, vol. 9, no. 3, pp. 51–56, 2012.
[46] A. A. Odhekar, "Mutual Coupling Reduction using Metamaterial Structure for Closely Spaced Microstrip Antennas," pp. 9–11, 2013.
[47] M. M. Bait-Suwailam, O. F. Siddiqui, and O. M. Ramahi, "Mutual coupling reduction between microstrip patch antennas using slotted-complementary split-ring resonators," *IEEE Antennas Wirel. Propag. Lett.*, vol. 9, pp. 876–878, 2010, doi: 10.1109/LAWP.2010.2074175.
[48] S. Luo and Y. Li, "A Dual-Band Antenna Array with Mutual Coupling Reduction Using 3D Metamaterial Structures," *ISAP 2018 - 2018 Int. Symp. Antennas Propag.*, pp. 5–6, 2019.
[49] K. Yu, Y. Li, and X. Liu, "Mutual coupling reduction of a MIMO antenna array using 3-D novel meta-material structures," *Appl. Comput. Electromagn. Soc. J.*, vol. 33, no. 7, pp. 758–763, 2018
[50] A. Habashi, J. Nourina, and C. Ghobadi, "Mutual Coupling Reduction Between Very Closely Spaced Patch Antennas Using Low-Profi le Folded Split Ring Resonators," *IEEE Antennas Wirel. Propag. Lett.*, vol. 10, pp. 862–865, 2011, doi: 10.1109/LAWP.2011.2165931.
[51] H. Lihao, Z. Huiling, H. Zhang, and C. Quanming, "Reduction of Mutual Coupling between Closely-Packed Antenna Elements with Split Ring Resonator (SRR)," *2010 Int. Conf. Microw. Millim. Wave Technol.*, pp. 1873–1875, 2010, doi: 10.1109/ICMMT.2010.5524882.
[52] J. Y. Lee, S. H. Kim, and J. H. Jang, "Reduction of Mutual Coupling in Planar Multiple

Antenna by Using 1-D EBG and SRR Structures," *IEEE Trans. Antennas Propag.*, vol. 63, no. 9, pp. 4194–4198, 2015, doi: 10.1109/TAP.2015.2447052.
[53] P. Fernandes da Silva Junior *et al.*, "Fractal and Polar Microstrip Antennas and Arrays for Wireless Communications," *Wirel. Mesh Networks - Secur. Archit. Protoc.*, pp. 1–24, 2020, doi: 10.5772/intechopen.83401.
[54] R. Mishra, "An Overview of Microstrip," vol. 21, no. 2, pp. 1–17, 2016.
[55] V. L. Subrahmanya, "Pattern Analysis of ' The Rectangular Microstrip Patch Antenna ,'" 2009.
[56] C. A. Balanis, *Antenna Theroy Analysis and Design*. 2005.
[57] J. Wang, "Antenna Theory and Design," pp. 115–133.
[58] R. DR Mishra, "An Overview of Microstrip," vol. 21, no. 2, pp. 1–17, 2016.
[59] T. U.-C. S. and I. Technology, "Chapter 2. Microstrip patch antennas and modeling techniques," pp. 12–47.
[60] V. Faizan, S. Mohammed, K. Aftab, K. T. Campus, and N. E. W. Panvel, "Dual Frequency Rectangular," 2015.
[61] H. Subhi, S. M. Juma, and M. Office, "Cavity model analysis of rectangular microstrip antenna opera TM03 mode," vol. 2020, pp. 1–13, 2020.
[62] V. L. Subrahmanya, "Pattern Analysis of ' The Rectangular Microstrip Patch Antenna ,'" 2009.
[63] P. David and J. Voge, "Propagation of Waves," *Phys. Today*, vol. 24, no. 4, pp. 53–55, 1971, doi: 10.1063/1.3022693.
[64] G. Kumar and K. P. Ray, *Broadband microstrip antenna array*, vol. 26, no. 6. 1998.
[65] Nikolova, "Lecture 21: Microstrip Antennas - PartII," pp. 1–25.
[66] Pasquale Dottorato, "Analysis and Design of the Rectangular Microstrip Patch Antennas for TM0n0 Operating Mode," *Microw. J.*, vol. 53,10, no. October, p. 6, 2010.
[67] G. Y. Lee, J. Sung, and B. Lee, "Recent advances in metasurface hologram technologies," *ETRI J.*, vol. 41, no. 1, pp. 10–22, 2019, doi: 10.4218/etrij.2018-0532.
[68] B. Bahaa and N. Qas, "Analysis of Different Structures of Patch Antennas," *East. Mediterr. Univ.*, no. January, pp. 1–121, 2014.
[69] I. Hamieh, "Scholarship at UWindsor A 77 GHz Reconfigurable Micromachined Microstrip Antenna Array A 77 GHz Reconfigurable Micromachined Microstrip Antenna Array by," 2012.
[70] R. O. E. Mohamed, "Design of Efficient Millimeter Waves Planar Antennas for 5G Communication Systems," *Proc. 2020 Int. Conf. Comput. Control. Electr. Electron. Eng. ICCCEEE 2020*, 2021, doi: 10.1109/ICCCEEE49695.2021.9429596.
[71] H. Light and G. Back, "Classification of Polarization Circular Polarization," pp. 1–5, 2008.
[72] F. O. F. Engineering, "FACULTY OF ENGINEERING AND SUSTAINABLE DEVELOPMENT . Antenna Design for Portable Applications in LTE Band September 2011," no. September, 2011.
[73] E. Munoz and R. Murch, "' 2 . 4 GHz MIMO Antenna on Microstrip Technology ' 2 . 4 GHz MIMO Antenna on Microstrip Technology," 2009.
[74] I. Park, "Application of metasurfaces in the design of performance- enhanced low-pro le antennas," pp. 1–16, 2020.
[75] N. H. Savaliya and P. A. Nandurbarkar, "Metamaterial Incorporated Planar Antenna for Improving Parameters," pp. 1896–1899, 2018.
[76] D. R. S. Group, "Metamaterials Metamaterial Projects in Our Group , Past and Present Centers," pp. 1–2, 2020.
[77] S. E. Mendhe and Y. P. Kosta, "Metamaterial properties and applications," *Int. J. Inf. Technol. Knowl. Manag.*, vol. 4, no. 1, pp. 85–89, 2011.

[78] K. Gangwar, Paras, and R. P. S. Gangwar, “Metamaterials: Characteristics, Process and Applications,” *Adv. Electron. Electr. Eng.*, vol. 4, no. 1, pp. 97–106, 2014, [Online]. Available: http://www.ripublication.com/aeee_spl/aeeev4n1spl_14.pdf.
[79] C. M. Soukoulis and M. Wegener, “Past achievements and future challenges in the development of three-dimensional photonic metamaterials,” *Nat. Photonics*, vol. 5, no. 9, pp. 523–530, 2011, doi: 10.1038/nphoton.2011.154.
[80] W. Jan Krzysztofik and T. Nghia Cao, “Metamaterials in Application to Improve Antenna Parameters,” *Metamaterials and Metasurfaces*, pp. 1–19, 2019, doi: 10.5772/intechopen.80636
[81] O. Souihli, “Capacity Enhancements to Wireless MIMO Systems: Channel Feedback,Keyhole Mitigation and Multi-User Support,” no. August, 2011.
[82] N. H. Savaliya and P. A. Nandurbarkar, “Metamaterial Incorporated Planar Antenna for Improving Parameters,” pp. 1896–1899, 2018.
[83] M. Teniou and U. Pierre, “Metasurface antennas for space applications To cite this version : HAL Id : tel-02336550 Université Pierre et Marie Curie Metasurface Antennas for Space Applications,” 2019.
[84] S. E. Mendhe and Y. P. Kosta, “Metamaterial properties and applications,” *Int. J. Inf. Technol. Knowl. Manag.*, vol. 4, no. 1, pp. 85–89, 2011.
[85] C. Craeye, S. Glybovski, and C. Simovski, “Comparative study of metasurfaces stressed on MRI application WP4 Report : Deliverable 4 . 1,” 2017.
[86] M. M. and J. Kelly, “in N Ovations in Labor Mar Ket in Formation an D Thei R Ap P L I Cati on,” vol. 7, no. 6, p. 16, 2012.
[87] P. S. Kildal, “Metasurfaces for Antennas,” no. October, pp. 5–9, 2015.
[88] F. Ding, A. Pors, and S. I. Bozhevolnyi, “Gradient metasurfaces: A review of fundamentals and applications,” *Reports Prog. Phys.*, vol. 81, no. 2, 2018, doi: 10.1088/1361-6633/aa8732.
[89] S. S. Bukhari, J. Vardaxoglou, and W. Whittow, “A metasurfaces review: Definitions and applications,” *Appl. Sci.*, vol. 9, no. 13, 2019, doi: 10.3390/app9132727.
[90] H. T. Chen, A. J. Taylor, and N. Yu, “A review of metasurfaces: Physics and applications,” *Reports Prog. Phys.*, vol. 79, no. 7, 2016, doi: 10.1088/0034-4885/79/7/076401.
[91] A. P. Feresidis, G. Goussetis, S. Wang, and J. C. Vardaxoglou, “Artificial magnetic conductor surfaces and their application to low-profile high-gain planar antennas,” *IEEE Trans. Antennas Propag.*, vol. 53, no. 1 I, pp. 209–215, 2005, doi: 10.1109/TAP.2004.840528.
[92] E. G. Turitsyna and S. Webb, “Simple design of FBG-based VSB filters for ultra-dense WDM transmission ELECTRONICS LETTERS 20th January 2005,” *Electron. Lett.*, vol. 41, no. 2, pp. 40–41, 2005, doi: 10.1049/el.
[93] K. N. Rozanov, “Ultimate thickness to bandwidth ratio of radar absorbers,” *IEEE Trans. Antennas Propag.*, vol. 48, no. 8, pp. 1230–1234, 2000, doi: 10.1109/8.884491.
[94] S. Kim, A. Li, and D. F. Sievenpiper, “Reconfigurable impedance ground plane for broadband antenna systems,” *2017 IEEE Antennas Propag. Soc. Int. Symp. Proc.*, vol. 2017-January, pp. 1503–1504, 2017, doi: 10.1109/APUSNCURSINRSM.2017.8072794.
[95] C. Pfeiffer and A. Grbic, “Metamaterial Huygens’ surfaces: Tailoring wave fronts with reflectionless sheets,” *Phys. Rev. Lett.*, vol. 110, no. 19, pp. 1–5, 2013, doi: 10.1103/PhysRevLett.110.197401.
[96] O. Quevedo-Teruel *et al.*, “Roadmap on metasurfaces,” *J. Opt. (United Kingdom)*, vol. 21, no. 7, p. 73002, 2019, doi: 10.1088/2040-8986/ab161d.
[97] M. Chen, M. Kim, A. M. H. Wong, and G. V. Eleftheriades, “Huygens’ metasurfaces

from microwaves to optics: A review," *Nanophotonics*, vol. 7, no. 6, pp. 1207–1231, 2018, doi: 10.1515/nanoph-2017-0117.
[98] S. B. Glybovski, S. A. Tretyakov, P. A. Belov, Y. S. Kivshar, and C. R. Simovski, *Metasurfaces: From microwaves to visible*, vol. 634. 2016.
[99] Z. Chen, "Physica B : Condensed Matter Metamaterials-based enhanced energy harvesting : A review," 2020
[100] A. Y. Modi, C. A. Balanis, C. R. Birtcher, and H. N. Shaman, "Novel Design of Ultrabroadband Radar Cross Section Reduction Surfaces Using Artificial Magnetic Conductors," *IEEE Trans. Antennas Propag.*, vol. 65, no. 10, pp. 5406–5417, 2017, doi: 10.1109/TAP.2017.2734069.
[101] A. M. Hawkes, A. R. Katko, and S. A. Cummer, "A microwave metamaterial with integrated power harvesting functionality," *Appl. Phys. Lett.*, vol. 103, no. 16, pp. 101–103, 2013, doi: 10.1063/1.4824473.
[102] F. C. Commission, "Unlinced use of the 6GHz Band, (report and order futher notice of propsed rulemaking ET Docket N0. 18-295, GN Docket No. 17-1823)," Washington, D.C 20554, 2020.
[103] HUAWEI, "5G Spectrum public policy position," 2016. [Online]. Available: https://www.gsma.com/spectrum/wp-content/uploads/2016/06/GSMA-5G-Spectrum-PPP.pdf
[104] E. Notes, "5G Frequency Bands, Channels for FR1 & FR2," 2021. https://www.electronics-notes.com/articles/connectivity/5g-mobile-wireless-cellular/frequency-bands-channels-fr1-fr2.ph
[105] D. Rowell, "The 6 GHz network : Bigger channels , stronger signal , faster data," 2020. https://www.hpe.com/us/en/insights/articles/the-6-ghz-network--bigger-channels--stronger-signal--faster-data-2007.html.
[106] T. Lee, "What you should know about Wi-Fi 6 and the 6-GHz band," 2019. https://www.testandmeasurementtips.com/what-you-should-know-about-wi-fi-6-and-the-6-ghz-band/.
[107] P. Knott, "Patch Antenna Design using MICROWAVE STUDIO What is CST MICROWAVE STUDIO ? Simulation Workflow," *Design*, pp. 11–16, 2020.
[108] M. Olaimat, "Comparison between rectangular and triangular patch antennas array," vol. 2020, no. 20, pp. 1–23, 2020, doi: 10.1007/s12206-011-0709-0.
[109] J. Siddiqui and D. Guha, "Applications Of Triangular Microstrip Patch: Circuit Elements To Modern Wireless Antennas," *Microw. Rev.*, vol. 13, no. 1, pp. 8–11, 2007.
[110] F. Breu, S. Guggenbichler, and J. Wollmann, "Chapter 3 Microstrip Patch Antenna," *Vasa*, pp. 31–47, 2008, [Online]. Available: http://medcontent.metapress.com/index/A65RM03P4874243N.pdf
[111] Balanis, "Microstrip Antennas - Rectangular Patch Transmission line model," pp. 1–16.
[112] M. A. Matin and A. I. Sayeed, "A design rule for inset-fed rectangular microstrip patch antenna," *WSEAS Trans. Commun.*, vol. 9, no. 1, pp. 63–72, 2010.
[113] T. Prabhu and S. C. Pandian, "Design and development of planar antenna array for mimo application," *Wirel. Networks*, vol. 27, no. 2, pp. 939–946, 2021, doi: 10.1007/s11276-020-02253-y.
[114] M. R. Islam, M. T. Islam, M. Moniruzzaman, M. Samsuzzaman, and H. Arshad, "Penta band single negative meta-atom absorber designed on square enclosed star-shaped modified split ring resonator for S-, C-, X- and Ku- bands microwave applications," *Sci. Rep.*, vol. 11, no. 1, 2021, doi: 10.1038/s41598-021-87958-6.